Implementation of a ply inclination in the Classical Laminate Theory

S. Lambregts

Implementation of a ply inclination in the Classical Laminate Theory

by

S. Lambregts

to obtain the degree of Master of Science
at the Delft University of Technology,
to be defended publicly on Friday July 5, 2019 at 10:00.

Student number:	4309189	
Project duration:	September 3, 2018 – July 5, 2019	
Thesis committee:	Dr. ir. F. P. van der Meer,	TU Delft, chair
	Prof. dr. ir. L. J. Sluys,	TU Delft
	Dr. M. Pavlovic,	TU Delft
	Ir. K. van Cann,	Wagemaker B.V.

An electronic version of this thesis is available at `http://repository.tudelft.nl/`.

Cover: InfraCore bicycle and pedestrian bridge Exercitiesingel, Rotterdam. Source: `FiberCore Europe`.

TU Delft

wagemaker

Preface

This report contains the thesis that concludes my Master of Science degree in Civil Engineering at the Delft University of Technology. For the past ten months I have been working on this project in collaboration with my supervisors in the Structural Mechanics department and with my supervisor at Wagemaker B.V., an engineering firm in Rosmalen. Throughout my study, I have always been interested the most in the fundamental aspects in the field of structural engineering. Therefore, I am glad Wagemaker B.V. suggested a subject that fitted my wishes and was suitable for a Master Thesis subject in the Structural Mechanics department.

First of all, I would like to thank the chair of my committee, Frans van der Meer, for the theoretical feedback and providing the answer to virtually all my questions. Koen van Cann from Wagemaker B.V. helped me a lot by finding the right direction of the different parts of my research and gave me great feedback on my report. Furthermore, Bert Sluys and Marko Pavlovic provided many useful suggestions during the progress meetings. I am also thankful to Jan Peeters of FiberCore Europe for the enthusiastic response to my research results.

I would also like to thank my fellow student assistants in Structural Mechanics for the many coffee breaks in room 6.68. It was the most comfortable and most fun office in the complete faculty. They also helped me with my programming issues, which saved me a lot of time with processing my results.

Finally, I am grateful to all my friends and family who supported me the whole time. I am very proud of the obtained results and I am pleased to present them in this Master Thesis report.

S. Lambregts
Delft, June 2019

Abstract

In civil engineering, Fibre Reinforced Polymer (FRP) structures are on the rise. The high strength-to-weight ratio of FRP material makes it a good alternative for traditional building materials, such as steel and concrete, in certain designs. The material consist of fibres embedded in a matrix material. The fibres provide strength and stiffness to the FRP material and the matrix keeps the fibres in place. When fibres are oriented in the same direction, a unidirectional (UD) ply is created. Several UD plies stacked together create a laminate, where every ply can have a different fibre orientation. The Classical Laminate Theory (CLT) can be used to derive the elastic behaviour of a laminate, which uses the lay-up, material properties and the ply thickness as input parameters.

The use of the CLT is limited to laminates where all the fibres in a ply are oriented in the plane of the laminate. In some applications, it is possible that the plies will start at the bottom of a laminate and end at the top of the laminate. This means an inclination is added to the plies, which creates an extra rotation in the fibre direction with respect to the plane of the laminate. Such a laminate with inclined plies is found for example in the skin of InfraCore panels. In the regular CLT, this extra rotation cannot be taken into account, thus the elastic behaviour of a laminate with inclined plies cannot be described properly.

The main goal of this research is to determine the influence of the inclination in the plies on the elastic behaviour of a laminate. The extra rotation that occurs in a laminate with inclined plies has analytically been implemented in the regular CLT to obtain a modified CLT. The regular CLT makes use of plane stress conditions, meaning a reduced stiffness matrix per ply could be used. Since stresses perpendicular to the plane of the ply could occur in a laminate with inclined plies, plane stress conditions are not applicable in the derivation of the modified CLT. This means the reduction of the stiffness matrix of each ply is not possible. Furthermore, the transformation equations used to transfer the ply stiffness matrix from the local coordinate system of each ply to the global coordinate system of the complete laminate must include both the fibre orientation of a ply and the ply inclination angle. Due to the inclination in the plies, an out-of-plane shear deformation could occur due to the difference between the out-of-plane elastic modulus perpendicular and the elastic modulus along the fibre direction. This means the Kirchhoff assumption that straight lines perpendicular to the mid-surface remain perpendicular to the mid-surface after deformation, which is used in the regular CLT, must be rejected in the modified CLT. Therefore, the constitutive equations that derive the resulting elastic behaviour of a laminate with inclined plies need to take all the strain components into account, where the regular CLT only required in-plane strains.

Finite Element (FE) analyses have been used to verify the modified CLT. The strains and curvatures of several axially loaded laminates have been compared with modified CLT results. The results of individual plies with inclined material properties matched perfectly, where the results of a non-balanced and non-symmetric four-ply laminate differed 2% on average. These differences could be assigned to limitations of the FE model, and are assumed to be small enough to conclude that the modified CLT has been derived correctly.

Using the modified CLT, a reduction in equivalent stiffness can be observed for a single UD-ply with an inclination in the fibre direction. For a complete laminate the reduction in equivalent stiffness is also found, which increases as the inclination angle increases. The exact value of stiffness reduction strongly depends on the material properties and the lay-up of the laminate. For InfraCore skins, the stiffness reduction is very small (0.15%).

Due to the inclination in the plies, the lay-up of the laminate differs along the length of the plate. As a result, the output of the modified CLT is only applicable to one location along the plate. Due to the lay-up differences, the equivalent stiffness will also differ along the inclination direction. The in-plane equivalent stiffnesses will be the highest for symmetric laminates, where the flexural equivalent stiffness will be the highest when the plies with the stiffest fibre direction are located on the outside of a laminate.

The modified CLT can be used to determine the elastic behaviour of laminates with inclined plies. Failure of FRP is beyond the scope of this report. However, with the modified CLT it is possible to determine the stresses within a laminate that are relevant for delamination of that laminate, which is not possible with the regular CLT. In future research, the modified CLT could be used to determine the sensitivity to delamination, which is an important failure mode for FRP structures.

Contents

List of symbols

Symbol	Description	Unit
$\mathbf{A}$	Extensional stiffness matrix	kN/m
$\mathbf{B}$	Coupling stiffness matrix	kN
$\mathbf{C}$	Stiffness matrix in the global coordinate system	GPa
$\overline{\mathbf{C}}$	Stiffness matrix in the local coordinate system	GPa
$\mathbf{D}$	Bending stiffness matrix	kNm
$\boldsymbol{e}$	Unit vector in the global coordinate system	-
$\overline{\boldsymbol{e}}$	Unit vector in the local coordinate system	-
E_1	Elastic modulus of a UD-ply in the fibre direction	GPa
E_2	Elastic modulus of a UD-ply perpendicular to the fibre direction and in the plane of the ply	GPa
E_3	Elastic modulus of a UD-ply perpendicular to the plane of the ply	GPa
$E_{x,\mathrm{ip}}$	In-plane engineering constant of the elastic modulus in x-direction	GPa
$E_{x,\mathrm{f}}$	Flexural engineering constant of the elastic modulus in x-direction	GPa
$E_{y,\mathrm{ip}}$	In-plane engineering constant of the elastic modulus in y-direction	GPa
$E_{y,\mathrm{f}}$	Flexural engineering constant of the elastic modulus in y-direction	GPa
$f_k(\alpha)$	Parabola fit to the relative equivalent stiffness	-
f_u	Tensile strength	MPa
g	Gravitational acceleration	m/s^2
G_{23}	Out-of-plane shear modulus of a UD-ply	GPa
G_{13}	Out-of-plane shear modulus of a UD-ply	GPa
G_{12}	In-plane shear modulus of a UD-ply	GPa
$G_{xy,\mathrm{ip}}$	In-plane engineering constant for the shear modulus in the xy-plane	GPa
$G_{xy,\mathrm{f}}$	Flexural engineering constant for the shear modulus in the xy-plane	GPa
k	Number of points used to evaluate the original equivalent stiffness	-
l_x	Plate dimension in x-direction	m
l_y	Plate dimension in y-direction	m
$\mathbf{L}$	Total rotation matrix	-
$\mathbf{L}_x$	Rotation matrix for a rotation about the x-axis	-
$\mathbf{L}_y$	Rotation matrix for a rotation about the y-axis	-
$\mathbf{L}_z$	Rotation matrix for a rotation about the z-axis	-
$\mathrm{M}_{i,j}$	Minor of the element on the i^{th} row and j^{th} column of a matrix	-
M_{xx}	Bending moment in x-direction on a plate	kNm/m
M_{yy}	Bending moment in y-direction on a plate	kNm/m
M_{zz}	Bending moment in z-direction on a plate	kNm/m
M_{yz}	Torsional moment in the yz-plane of a plate	kNm/m
M_{xz}	Torsional moment in the xz-plane of a plate	kNm/m
M_{xy}	Torsional moment in the xy-plane of a plate	kNm/m
n	Number of plies	-
N	Number of repetition in an InfraCore skin	-
N_{xx}	Axial force in x-direction on a plate	kN/m
N_{yy}	Axial force in y-direction on a plate	kN/m
N_{zz}	Axial force in z-direction on a plate	kN/m
N_{yz}	Shear force in the yz-plane of a plate	kN/m
N_{xz}	Shear force in the xz-plane of a plate	kN/m
N_{xy}	Shear force in the xy-plane of a plate	kN/m

Symbol	Description	Unit
q_x	Distributed load in x-direction on the FE model	N/m^2
q_y	Distributed load in y-direction on the FE model	N/m^2
$\mathbf{Q}$	Reduced stiffness matrix in the global coordinate system	GPa
$\overline{\mathbf{Q}}$	Reduced stiffness matrix in the local coordinate system	GPa
$\mathbf{S}$	Compliance matrix in the global coordinate system	GPa^{-1}
$\overline{\mathbf{S}}$	Compliance matrix in the local coordinate system	GPa^{-1}
t_{ply}	Ply thickness perpendicular to the plane of the ply	m
t_α	Ply thickness perpendicular to the plane of the laminate	m
$t_{\text{tot},\alpha}$	Total laminate thickness for a laminate with an inclination	m
$t_{\text{tot},0}$	Total laminate thickness for a laminate without an inclination	m
$\mathbf{T}$	Transformation matrix for the regular CLT	-
$\mathbf{T}_{\text{r}}$	Reduced transformation matrix	-
$\mathbf{T}_{\theta\alpha}$	Transformation matrix for the modified CLT	-
U_x	Displacement in x-direction from the FE results	m
U_y	Displacement in y-direction from the FE results	m
U_z	Displacement in z-direction from the FE results	m
y_{ply}	Ply width	m
α	Rotation about the x-axis	° or rad
β	Rotation about the y-axis	° or rad
γ_{yz}	Out-of-plane engineering shear strain of the yz-plane	-
γ_{xz}	Out-of-plane engineering shear strain of the xz-plane	-
γ_{xy}	In-plane engineering shear strain of the xy-plane	-
$\boldsymbol{\varepsilon}$	Strain vector in the global coordinate system	-
$\boldsymbol{\varepsilon}^0$	Strain vector of the mid-surface	-
$\overline{\boldsymbol{\varepsilon}}$	Strain vector in the local coordinate system	-
ε_{xx}	In-plane axial strain in x-direction	-
ε_{yy}	In-plane axial strain in y-direction	-
ε_{zz}	Out-of-plane axial strain in z-direction	-
ε_{xy}, ε_{yx}	Tensorial shear strain	-
θ	Rotation about the z-axis	° or rad
$\boldsymbol{\kappa}$	Curvature vector	m^{-1}
κ_{xx}	Out-of-plane bending curvature in x-direction	m^{-1}
κ_{yy}	Out-of-plane bending curvature in y-direction	m^{-1}
κ_{zz}	In-plane bending curvature in z-direction	m^{-1}
κ_{yz}	In-plane torsional curvature of the yz-plane	m^{-1}
κ_{xz}	In-plane torsional curvature of the xz-plane	m^{-1}
κ_{xy}	Out-of-plane torsional curvature of the xy-plane	m^{-1}
ν_{12}	In-plane Poisson's ratio of a UD-ply	-
ν_{13}	Out-of-plane Poisson's ratio of a UD-ply	-
ν_{23}	Out-of-plane Poisson's ratio of a UD-ply	-
$\nu_{xy,\text{ip}}$	In-plane engineering constant for the Poisson's ratio	-
$\nu_{xy,\text{f}}$	Flexural engineering constant for the Poisson's ratio	-
ρ	Density	kg/m^3
σ_{ij}	Second order stress tensor in the global coordinate system	MPa
$\overline{\sigma}_{ij}$	Second order stress tensor in the local coordinate system	MPa
$\boldsymbol{\sigma}$	Stress vector in the global coordinate system	MPa
$\overline{\boldsymbol{\sigma}}$	Stress vector in the local coordinate system	MPa
σ_{xx}	In-plane axial stress in x-direction	MPa
σ_{yy}	In-plane axial stress in y-direction	MPa
σ_{zz}	Out-of-plane axial stress in z-direction	MPa
τ_{yz}	Out-of-plane shear stress in the yz-plane	MPa
τ_{xz}	Out-of-plane shear stress in the xz-plane	MPa
τ_{xy}	In-plane shear stress in the xy-plane	MPa
Φ_x	Rotation about the x-axis from the FE results	-
Φ_y	Rotation about the y-axis from the FE results	-
Φ_z	Rotation about the z-axis from the FE results	-

1 Introduction

1.1. Problem definition

Fibre Reinforced Polymer (FRP) materials are widely used in aviation, racing bicycle manufacturing, car manufacturing and many other applications. In civil engineering applications, FRP as a construction material is on the rise. This material has several great advantages. For example, FRP has a high strength-to-weight ratio compared to traditional construction materials, such as steel and concrete. This makes it a good alternative for structures with a slender design, for example pedestrian bridges.

FRP is a composite material which consists of fibres and a matrix material. The fibres have high strength and stiffness and are bonded together by the matrix material. In general, the fibres are the main load-carrying elements and the matrix keeps the fibres in the desired direction and protects them from environmental damage [12]. Furthermore, the matrix acts as a load transfer medium between the fibres. When fibres are oriented in the same direction in a plane, a unidirectional (UD) ply is created. Several UD plies together create a laminate, where the individual plies can have different fibre orientations compared to each other. Figure 1.1 shows an example of a laminate where all four plies have a different fibre orientation.

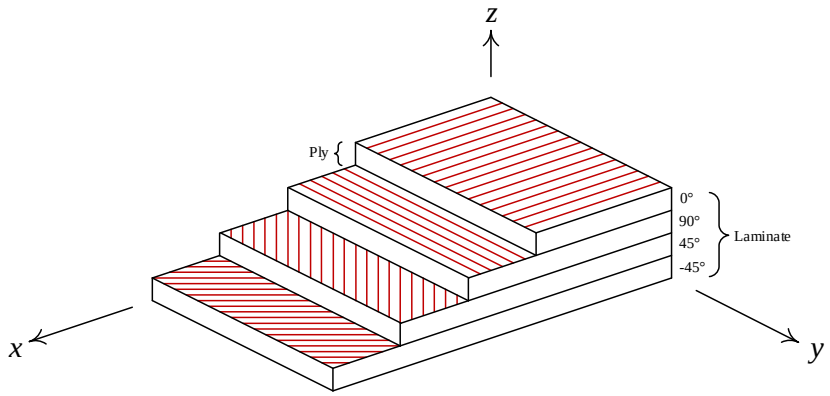

Figure 1.1: Overview of a laminate with four plies.

In civil engineering applications, sandwich panels are often used. Sandwich panels consist of two laminate skins connected by a lightweight core. The main weakness of such panels is skin-core debonding, which may occur after an impact or as a consequence of fatigue loading [4]. A special type of sandwich panel has been developed by FiberCore Europe, which contains webs that connect the two skins. The plies in the bottom skin continue in the web and end in the top skin. This special type of sandwich panel is called an InfraCore panel and is more robust compared to traditional sandwich panels. The continuous plies running from the web into the skins make skin-core debonding less likely to occur. Figure 1.2 schematically shows a cross section of such a panel. The plies continue from top to bottom in the panel, so Z-shaped profiles are created. These are stacked next to each other with the core material as spacer. This creates an overlap in the plies in the skin of an InfraCore panel. Due

to this overlap, an inclination in the plies occurs, with respect to the complete skin. The value of this inclination depends on the design of the panel, but is usually around 2° [5].

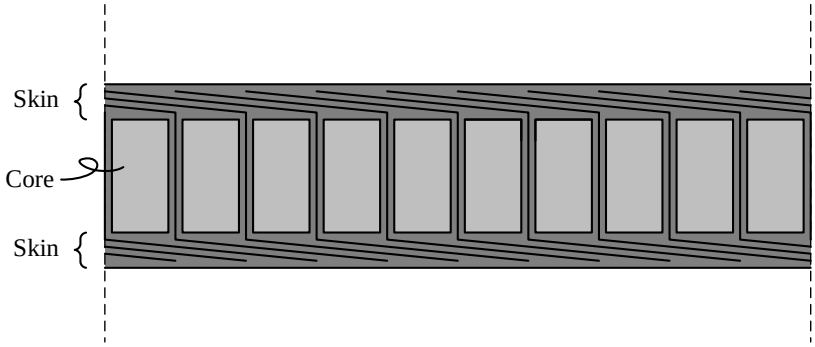

Figure 1.2: Cross section of an InfraCore panel (not to scale).

The elastic behaviour of a laminate is described using the Classical Laminate Theory (CLT). This theory makes use of the linear elastic properties in the local coordinate system of an individual UD-ply and translates these properties to the global coordinate system of the complete laminate. When all the plies are stacked, a total stiffness matrix is obtained for the laminate. This stiffness matrix is referred to as the ABD-matrix and relates strains and curvatures to forces and moments. In the CLT, it is assumed that all the plies are in the same plane as the complete laminate. Therefore, the extra rotation of the fibres that occurs in the skin of an InfraCore panel is not taken into account in the CLT. This means the InfraCore skin is not fully described by the CLT. In general, the elastic behaviour of any laminate with inclined plies cannot be described properly by the CLT.

1.2. Research objectives

The main objective of this thesis is to determine the influence of the inclination in the plies on the elastic behaviour of a laminate. It is therefore necessary to analytically implement the ply inclination in a laminate in the CLT. The main research question is formulated as follows:

In what way does an inclination in the plies of a laminate affect the elastic behaviour of that laminate?

The modified CLT can be used to determine the influence of the inclination on the elastic behaviour of a laminate. For example, the equivalent stiffnesses of a laminate will differ when the inclination angle changes. The modified CLT will be derived by adjusting the regular CLT where necessary. The assumptions that are applicable to the regular CLT, such as the plane stress conditions and Kirchhoff assumptions, must be revised. The modified CLT should include an extra input parameter that defines the inclination angle. In the modified CLT, the transformation that translates the local coordinate system of each individual ply to the global coordinate system of the laminate will not only depend on the fibre orientation of the ply in the plane of the laminate, but also on the inclination angle of the plies.

Before the dependence on the inclination angle can be checked analytically, the modified CLT must be verified. Results from Finite Element (FE) analyses will be compared with modified CLT results. Differences need to be quantified and if the differences are small enough and can be explained, it can be assumed that the derived modified CLT will be correct.

1.3. Research scope

This thesis focusses on the elastic behaviour of composite materials. The following items are relevant for the scope of this research:

- Laminates are considered on mesoscale, meaning no individual fibres can be distinguished but individual plies can be distinguished and are simplified using transversely isotropic material properties. The fibre-matrix interaction on microlevel is beyond the scope of this research.
- Linear elastic material behaviour is assumed to be applicable to the FRP material. Non-linear effects and plastic behaviour are not taken into account.

- Failure of laminates is beyond the scope of this research, meaning the strength of laminates is not considered.
- Temperature variations could cause out-of-plane deformations in a laminate due to the difference in thermal loads on each ply. These thermal differences can be taken into account in the regular CLT [9]. However, thermal differences are not within the scope of this research, thus they are not taken into account in the derivation of the modified CLT.

1.4. Thesis outline

The literature research is covered by two chapters. Chapter 2 gives more background information on FRP. Here, the structure of FRP elements is further elaborated, as well as the properties of fibres, matrix material and plies. Furthermore, information regarding InfraCore panels will be provided. Chapter 3 will explain the regular CLT. First, the elastic behaviour of individual plies is elaborated. Next, the transformation equations that translate the ply properties from a local coordinate system to a global coordinate system are derived. The ABD-matrix is derived using the laminate constitutive equations that stack all the plies. Finally, the derivation of engineering constants is given. These engineering constants can be used to determine material properties of a single-layer simplification of a laminate.

The alterations made to the regular CLT in order to obtain the modified CLT are given in chapter 4. Here, all the necessary modifications on the elastic behaviour, transformation equations and laminate constitutive equations are given. The assumptions and limitations of the modified CLT are also discussed. Chapter 5 contains the verification of the modified CLT using FE analyses.

Chapter 6 gives the influence of the inclination of the plies on the elastic behaviour of a laminate. Distinction is made between strains and equivalent stiffnesses of laminates with a certain chosen lay-up. Due to the inclination in the plies, lay-up differences can occur along a certain direction. The influence of these lay-up differences is elaborated in chapter 7. Finally, the modified CLT is applied to an InfraCore skin in chapter 8, where both the influence of the inclination angle and the influence of the lay-up differences are dealt with.

Chapter 9 gives all the relevant conclusions and provides recommendations for further research.

2

Fibre Reinforced Polymers

Fibre Reinforced Polymers (FRP) are a type of composite material. Fibres are used to reinforce the polymer matrix. This cooperation between the two ingredients creates a high strength material with relatively low self weight. In this section, some basic background information is given on FRP.

2.1. Structure of FRP elements

Elements of FRP consist of high strength fibres that are bonded together by a matrix. The fibres are the main elements to transfer loads and the matrix keeps the fibres in place. The fibres and the matrix have different material properties. There are several ways for the fibres to be oriented in the matrix. First of all, unidirectional (UD) continuous fibres could be used, resulting in high strength and stiffness in only one direction. Secondly, bidirectional continuous fibres provide strength and stiffness in multiple directions. Besides continuous fibres, discontinuous fibres could be used. These short fibres in the matrix result in lower strength. When the discontinuous fibres are used in a random manner, a more homogeneous material is created.

The main function of the matrix is to keep the fibres in place. The matrix also protects the fibres from external factors, such as moisture, chemicals and superficial damage. The matrix is also used to transfer the stresses between the fibres. The compressive strength, interlaminar and in-plane shear properties depend predominantly on the matrix material properties. However, the tensile load-carrying capacity of an FRP structure is mainly determined by the fibres [12].

Depending on the manufacturing technique, the fibres can be arranged in such a way that a ply is created. Usually, the plies contain UD fibres. When plies are bonded together, a laminate is created. The fibre orientation, fibre content and thickness of the plies may vary per laminate, as well as the number of plies in a laminate. Since there are many different kinds of laminates, a specific notation is introduced. This notation indicates how many plies are present and how they are oriented in the laminate. The orientation is denoted in degrees (°). Numbers between +90° and -90° compared to a reference direction (e.g. a beam axis) are used. Both + and -90° indicate the same orientation, since they both indicate a right angle, so only a positive notation for a right angle is used. For example, the laminate in figure 1.1 could be denoted as $[0/90/45/-45]$.

Several simplifications are used in laminate notation. If the same direction is used for adjacent plies, a subscript can be used to indicate the number of plies in that direction. For example, if one extra 0°-ply is placed on top of the laminate in figure 1.1, the laminate could be indicated as $[0_2/90/45/-45]$. A subscript can also be used if the whole laminate is used n times on top of each other: $[0/90/45/-45]_n$ (for example: $[0/90/0/90] = [0/90]_2$). A subscript s is used when a symmetric laminate is concerned (e.g.: $[0/90/90/0] = [0/90]_s$). A laminate is balanced if for every $+\theta$-ply a $-\theta$-ply is also present.

2.2. Properties

FRP objects have specific material properties, due to the combination of high strength fibres and a resin based matrix. Due to the alignment of the fibres and the use of multiple materials, the strength and stiffness properties are not the same in all directions. This means FRP is an anisotropic material. FRP with fibres in multiple directions shows orthotropic material properties, meaning material properties differ along three orthogonal axes.

Figure 2.1 shows a bundle of UD fibres, which could represent a part of an FRP ply with UD fibres. In the local coordinate system, it is assumed that the (1)-direction coincides with the fibre direction. The properties perpendicular to the fibres will be equal in every direction, meaning the (2)- and (3)-direction span a plane of isotropy. A material with a plane of isotropy is referred to as a transversely isotropic material.

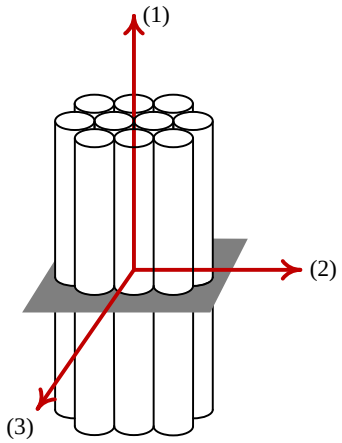

Figure 2.1: Transverse isotropy. The fibre direction (1) is perpendicular to the plane of isotropy (gray plane).

2.2.1. Fibres

There are several fibre types that can be used in an FRP object. The most common fibre type used as reinforcement is glass fibre [12]. Carbon fibres are also applied in several applications. Other fibre types include aramid fibres and natural fibres (such as hemp and wood).

Glass fibres

Compared to other fibre types, glass fibres have several advantages, such as low cost, high tensile strength, chemical resistance and good insulation properties. Some disadvantages of glass fibres are low elastic modulus, high density and low fatigue resistance.

The most common type of glass fibre is E-glass. Compared to other glass fibre types, such as C-glass and S-glass, E-glass fibres have the lowest cost, which makes them preferable in FRP structures. The main ingredient for E-glass fibres is silica (SiO_2), among other oxides [12]. The raw materials are mixed and melted at high temperature before the molten glass is separated through a number of apertures. This process creates very thin filaments with a thickness of approximately 10 µm. These filaments are used to create strands, which consist of many parallel filaments bound together. These strands can be used to create for example a woven roving or chopped strand mats.

Carbon fibres

In comparison to other fibre types, carbon fibres have very high tensile strength and tensile elastic modulus compared to their self weight. There is a wide variety in properties of carbon fibres. Usually, carbon fibres with a low elastic modulus have a lower density, lower cost and higher strength (both tensile and compressive).

For the production of carbon fibres, raw material with a high carbon atom content is needed. Polyacrylonitrile (PAN) is the most common raw material. This semi-finished product has more consistent properties compared to other raw materials which have a natural origin, such as pitch. This makes PAN preferable when a high quality of the FRP product must be guaranteed. Thin filaments are spun, which are then oxidised at a temperature between 200 and 300 °C [12]. Next, the filaments are heated at a temperature between 1000 and 2000 °C, which makes carbonisation possible. This means redundant substances, such as nitrogen atoms, are removed. Finally, the filaments are heated again, this time at a temperature above 2000 °C, to initiate graphitisation. In this final stage, the fibres obtain their definite structure by aligning the carbon chains parallel to each other.

Fibre properties

Since there are different manufacturing techniques of fibres, the properties vary significantly. Also, when natural resources are used, for example in some carbon fibres, the material properties differ per raw material type used.

Many sources provide different values for the density, elastic modulus and tensile strength. Table 2.1 provides rough boundary values for these material properties.

Table 2.1: Properties of common used fibre types [15].

Fibre type	Density (kg/m^3)	Elastic modulus (GPa)	Tensile strength (MPa)
Glass	2500-2600	70-80	2400
Carbon	1800-2000	160-440	2000-5300

Compared to steel, the fibres have a lower density and elastic modulus. The tensile strength proves to be higher compared to very high strength steel S1100, which has a tensile strength between 1250 MPa and 1550 MPa [21]. The high strength-to-weight ratio of FRP is confirmed by the breaking length of fibres, which is an indication for the specific strength of a material. The breaking length is defined as the maximum length of a suspended vertical element of a material, when that element is only supported at the top. The breaking length is related to the tensile strength (f_u), the density (ρ) and the gravitational acceleration (g):

$$L = \frac{f_u}{\rho g} \tag{2.1}$$

When the upper limits from table 2.1 are used, E-glass has a breaking length of 94.1 km and carbon fibres have a breaking length of 270 km. When high strength steel properties (ρ =7850 kg/m^3 and $f_u \approx$ 1550 MPa) are used, the breaking length of very high strength steel results in 20.1 km. This significant difference confirms the exceptional qualities of the fibres used in FRP. Note that these values only relate to the fibres and not to the whole FRP element. The matrix material also affects the FRP properties. Moreover, in multidirectional laminates, only fibres aligned with the direction of loading contribute to their full capacity.

2.2.2. Matrix

Two types of matrix materials can be distinguished: thermoset- and thermoplastic polymers. Thermoplastic polymers melt when heated. Thermoset polymers will not melt, but will burn eventually when heated. Thermoset polymers are mostly used as matrix material for structural FRP elements. They are often referred to as resin.

The three resin types used most often are polyester, vinyl ester and epoxy. The properties strongly depend on the exact chemical composition of the resin, as well as the curing circumstances. Table 2.2 shows relevant properties of some resin types when cured.

Table 2.2: Properties of common used resin types [15].

Resin type	Density (kg/m^3)	Elastic modulus (GPa)	Tensile strength (MPa)
Polyester	1150-1250	2.4-4.6	40-85
Vinyl ester	1150-1250	3-3.5	50-80
Epoxy	1150-1200	3.5	60-80

When the values in the tables 2.1 and 2.2 are compared, it can clearly be seen that the strength and stiffness are predominantly provided by the fibres in an FRP element, which means the higher the fibre content in a ply, the higher the strength and stiffness of that ply. However, the matrix is of the utmost importance to bind the individual fibres together and prevent the individual fibres to buckle. A typical fibre volume fraction is in the order of 55% [2]. Figure 2.2 schematically shows a cross section of a UD-ply.

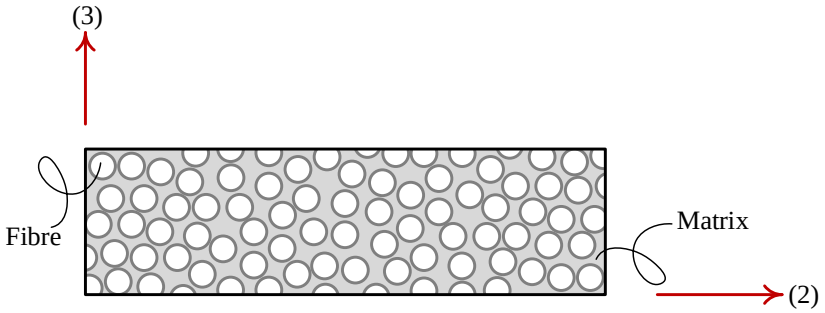

Figure 2.2: Cross section of a UD-ply.

2.2.3. Plies

The properties of the fibres and the matrix are often combined and translated to transversely isotropic material properties for a complete ply. This can be done using rules of mixture to obtain for example the effective transverse and longitudinal elastic moduli of a ply. These rules of mixture assume a perfect bond between matrix and fibre and do not take any defects or damage into account [15]. This especially affects the reliability of the shear modulus derived by the rule of mixture, since it highly depends on the interaction between fibre and matrix. Improved models have been derived to determine the effective material parameters of plies. For example the Halpin-Tsai relationships, which makes use of semi-empirical formulas combining elasticity models with experimental results, show better results for the effective shear moduli [2].

Both the rules of mixture and the Halpin-Tsai relationships will not be discussed in detail here. Transversely isotropic material properties of a unidirectional E-glass/epoxy ply will be chosen and will be used for all the calculations. The values for the five independent material parameters can be found in table 2.3.

Table 2.3: Transversely isotropic material properties of a unidirectional E-glass/epoxy ply [2, 20].

Property	Value
E_1	39 GPa
E_2	8.6 GPa
G_{12}	3.8 GPa
ν_{12}	0.28
ν_{23}	0.4

2.3. Types of 2D FRP elements

2.3.1. Sandwich panels

Sandwich panels consist of a core material that is covered by two skins. The core is made of a lightweight material, such as polyurethane foam, metal foam or balsawood. These provide a homogeneous support to the two skins. It is also possible to implement non-homogeneous support of the skins, such as a honeycomb structure as core material. This honeycomb structure could be manufactured from several materials, for example phenolic reinforced aramid paper [19]. When a homogeneous support of the two skins is used (e.g. a foam), the structure depicted in figure 2.3 remains the same, but the honeycomb core is replaced by the foam. The skins and adhesives are still present on both sides of the panel.

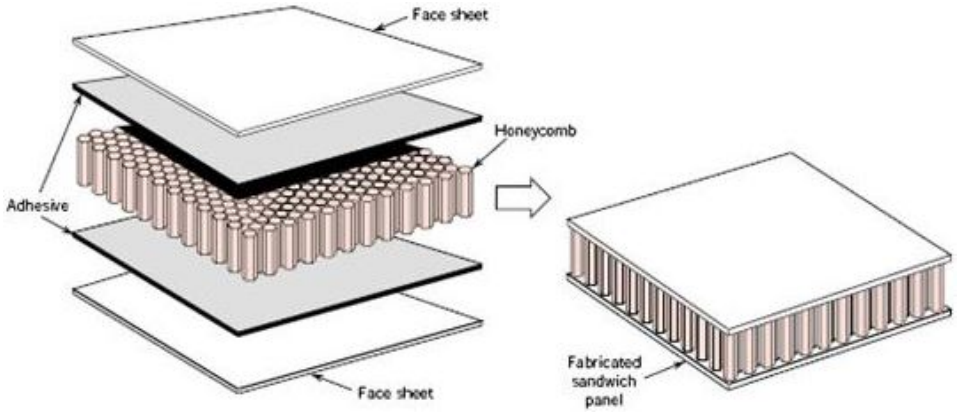

Figure 2.3: Sandwich structure with a honeycomb core [1].

The great advantage of a sandwich panel is the significant increase of stiffness, without adding much weight. This makes sandwich panels very lightweight compared to steel or concrete structures and gives them very high mass specific properties. The increase in bending stiffness and strength can be assigned to the increase of area moment of inertia due to the increased distance between the FRP skins. It is important that a decent connection between the skins and the core is achieved, because the core material has to transfer shear stresses, so the core has an important structural function.

Several manufacturing techniques of sandwich panels are known, which all include the use of a mould. Adhesive bonding is used when pre-produced FRP skins are bonded separately to the core material. Adhesive layers are applied to the faces of the core and the FRP skins are applied with pressure (for example with a hydraulic press). When the adhesive is cured, the sandwich panel is complete [11]. A similar manufacturing technique to adhesive bonding is wet lay-up, where dry fibres for the top and bottom skin are impregnated with resin and bonded to the core material. Both hand lay-up of layers and spray-up could be used for the skins. Compared to other methods, wet lay-up is a very labour intensive manufacturing technique.

Resin Transfer Moulding (RTM) uses a two sided mould to create sandwich panels. A bottom mould is covered by the bottom skin (dry fibres), and the core material is placed on top together with the dry fibres of the top skin. Finally, a top mould is placed on the raw materials. Next, resin is injected through apertures in the mould. Smooth surfaces of both the top and bottom skin are a great advantage of RTM compared to other methods. Vacuum-Assisted Resin Transfer Moulding (VARTM) is similar to RTM. However, VARTM makes use of only a bottom mould, the top mould is replaced by a vacuum bag. When the raw materials (dry fibres and core) are placed on the mould, the vacuum bag is sealed on top of the sandwich panel. Resin is injected through apertures in the vacuum bag. A vacuum pump is used to transfer the resin until it is equally spread throughout the whole sandwich panel. A great advantage of VARTM compared to RTM is that the process of resin transfer can visually be checked through the transparent vacuum bag. A disadvantage is the coarse structure of skin on the bag side of the sandwich panel. The mould side of the sandwich panel has a smooth structure. For this reason, sandwich panels are often produced upside down.

Failure of sandwich panels

The main weakness of regular sandwich panels is the debonding of skin and core. When a high impact load is performed on the skin, the skin deforms and crushes the core of the sandwich panel (see figure 2.4). Due to its high strength and elastic properties, the FRP skin returns to its original shape. However, the core is permanently damaged and locally debonded from the skin. The danger of this damage, is that it is not visible from the outside of the panel.

The reduced bond length between the skin and core affects the distribution of shear stresses. The same amount of total shear stress must be able to be transferred between skin and core. Since the contact surface between skin and core is reduced, the shear stress is redistributed and will increase over the full span of the sandwich panel. The shear force is largest near the supports, consequently the shear stresses too. This means debonding of skin and core will initiate near the supports. Due to extra fatigue loading, the debonding will continue and will lead to failure of the sandwich panel.

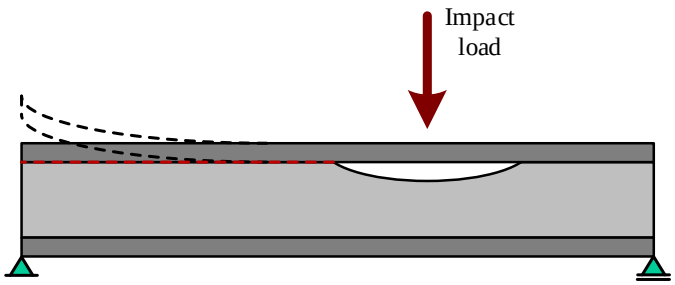

Figure 2.4: Debonding of skin and core due to an impact load.

Another possible failure mode is local buckling of the skin. Besides increasing the area moment of inertia of the cross section, the core of a sandwich panel functions as support for the skins. When that support disappears, for example due to an impact load, extra deformations are possible, making buckling of the skin an issue.

2.3.2. InfraCore panels

Robustness being the main weakness of regular sandwich panels, FiberCore Europe developed a special type of sandwich panel that should provide better damage resistance, namely the InfraCore panels. These panels contain, besides a core and two skins, also webs of FRP material. The core is made of polyurethane foam blocks. These blocks are wrapped in dry glass fibre fabric with fibres in the +45° direction and the -45° direction. For the assembly of an InfraCore panel, a mould is used. This mould consists of a steel plate that can be bent in the desired shape, for example a curvature in the span direction of a pedestrian bridge. The blocks are placed on the mould, with their wrapped sides parallel to the span direction of the final product. The glass fibre fabric is unwrapped in such a manner that they overlap the fabric belonging to the adjacent block. This creates several Z-profiles placed next to each other. When the plane perpendicular to the span direction is considered, box profiles with a foam core are observed (see figure 2.5). Between the two layers of unwrapped glass fibre fabric, an extra UD-0° dry ply is inserted (fibre direction parallel to the span direction). The panel is finished with an extra cover layer on both skins to account for increased delamination risk due to the inclined plies.

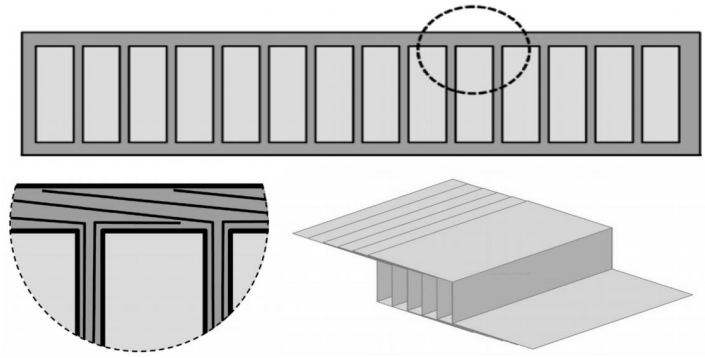

Figure 2.5: Principle of the InfraCore panels [5].

The great advantage of InfraCore panels is that skin-core debonding due to an impact load is not relevant. When damage is done to an InfraCore panel due to an impact load, the core is crushed and the skin debonds locally from the core. A resin-dominated crack could propagate through the skin to the surface (dashed red line in figure 2.6). Due to the inclined laminates, debonding will not take place over the full cross section. It is possible that the crack also propagates in the span direction, which is not shown in figure 2.6. However, below and above the crack the laminate bonds will remain intact and account for the extra shear stress.

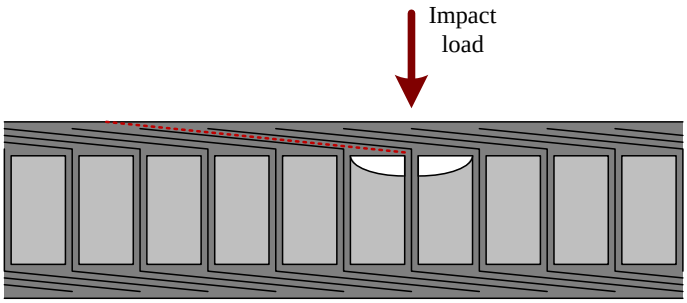

Figure 2.6: Debonding of skin and core due to an impact load of an InfraCore panel. This is not the span direction, but a cross section, so the supports are not shown.

When an impact load occurs right above a web of the panel, it is possible that the web is crushed together with a part of the core. The crack that occurs would propagate along the red dashed line in figure 2.7. However, since both +45° and -45° plies are used in the web and continue in the skins, as indicated with the red fibre directions in figure 2.7, the crushed part of the web cannot expand. This result in robust panel, where resin dominated cracks are reduced to a minimum.

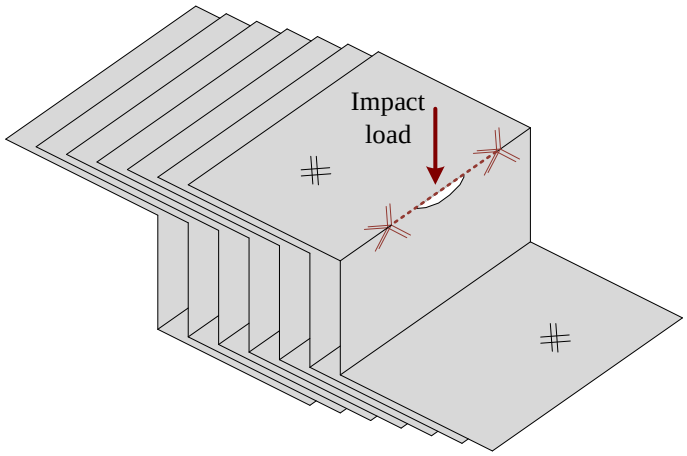

Figure 2.7: Crack propagation after an impact load. The core material has not been shown in this figure.

A consequence of the overlapping Z-profiles is the inclination in the plies in the top and bottom skin of an InfraCore panel, which can be seen from figure 2.6. The inclination angle depends on the ply thickness and the core dimension and is usually around 2° [5]. This extra rotation in the plies is not taken into account in the current theory for laminates, the Classical Laminate Theory, which will be dealt with in the next chapter.

3

Classical Laminate Theory

Due to the orthotropic properties of FRP material, the elastic behaviour of a laminate depends on the number of plies, the ply properties and the fibre orientation of the plies. The Classical Laminate Theory (CLT) combines the different ply properties to create a single stress-strain relation for a complete laminate. In order to do so, the (elastic) behaviour of the individual plies must be known, as well as the transformation formulae that translate properties from the local coordinate system each ply to the global coordinate system of the laminate.

3.1. Elastic behaviour

Any general material could be referred to as an anisotropic material. Due to the fact the properties of an anisotropic material are different in every direction, an anisotropic materials must be evaluated in 3D, which means six different kinds of deformations are possible. Three normal strains (ε_{xx}, ε_{yy} and ε_{zz}) and three shear strains (γ_{xy}, γ_{yz} and γ_{zx}) can be distinguished (see figure 3.1).

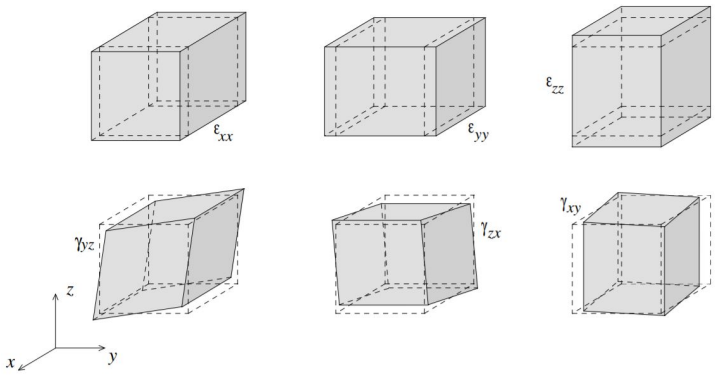

Figure 3.1: Deformations of a 3D-element [8].

When a single stress (e.g. σ_{xx}) is applied on an anisotropic material, all six deformations could be observed. Consequently six different stiffness parameters are needed to describe the full deformation when only one stress type is applied on an anisotropic material. The former holds for all six stress components: σ_{xx}, σ_{yy}, σ_{zz}, τ_{yz}, τ_{xz} and τ_{xy}. This means the full elastic behaviour of anisotropic material requires 36 stiffness parameters. These can all be displayed in a 6×6 stiffness matrix:

$$\boldsymbol{\sigma} = \mathbf{C}\boldsymbol{\varepsilon} \tag{3.1}$$

$$\begin{bmatrix} \sigma_{xx} \\ \sigma_{yy} \\ \sigma_{zz} \\ \tau_{yz} \\ \tau_{xz} \\ \tau_{xy} \end{bmatrix} = \begin{bmatrix} C_{11} & C_{12} & C_{13} & C_{14} & C_{15} & C_{16} \\ C_{21} & C_{22} & C_{23} & C_{24} & C_{25} & C_{26} \\ C_{31} & C_{32} & C_{33} & C_{34} & C_{35} & C_{36} \\ C_{41} & C_{42} & C_{43} & C_{44} & C_{45} & C_{46} \\ C_{51} & C_{52} & C_{53} & C_{54} & C_{55} & C_{56} \\ C_{61} & C_{62} & C_{63} & C_{64} & C_{65} & C_{66} \end{bmatrix} \begin{bmatrix} \varepsilon_{xx} \\ \varepsilon_{yy} \\ \varepsilon_{zz} \\ \gamma_{yz} \\ \gamma_{xz} \\ \gamma_{xy} \end{bmatrix} \tag{3.2}$$

Material properties are often not expressed in a global coordinate system, but in a local coordinate system. Since both the stiffness and strain vector are changed to the local coordinate system, it is not necessary to apply any transformation formulae. It should however be noted that the stiffness parameters in the local coordinate system do differ from the stiffness parameters in the global coordinate system (i.e. $C_{ij} \neq \overline{C}_{ij}$). The material properties in the local coordinate system are shown with a bar in equation 3.4. For continuity, all stresses in the local coordinate system are shown with a σ symbol.

$$\overline{\boldsymbol{\sigma}} = \overline{\mathbf{C}}\overline{\boldsymbol{\varepsilon}} \tag{3.3}$$

$$\begin{bmatrix} \sigma_{11} \\ \sigma_{22} \\ \sigma_{33} \\ \sigma_{23} \\ \sigma_{13} \\ \sigma_{12} \end{bmatrix} = \begin{bmatrix} \overline{C}_{11} & \overline{C}_{12} & \overline{C}_{13} & \overline{C}_{14} & \overline{C}_{15} & \overline{C}_{16} \\ \overline{C}_{21} & \overline{C}_{22} & \overline{C}_{23} & \overline{C}_{24} & \overline{C}_{25} & \overline{C}_{26} \\ \overline{C}_{31} & \overline{C}_{32} & \overline{C}_{33} & \overline{C}_{34} & \overline{C}_{35} & \overline{C}_{36} \\ \overline{C}_{41} & \overline{C}_{42} & \overline{C}_{43} & \overline{C}_{44} & \overline{C}_{45} & \overline{C}_{46} \\ \overline{C}_{51} & \overline{C}_{52} & \overline{C}_{53} & \overline{C}_{54} & \overline{C}_{55} & \overline{C}_{56} \\ \overline{C}_{61} & \overline{C}_{62} & \overline{C}_{63} & \overline{C}_{64} & \overline{C}_{65} & \overline{C}_{66} \end{bmatrix} \begin{bmatrix} \varepsilon_{11} \\ \varepsilon_{22} \\ \varepsilon_{33} \\ \gamma_{23} \\ \gamma_{13} \\ \gamma_{12} \end{bmatrix} \tag{3.4}$$

The inverse of the stiffness matrix is called the compliance matrix:

$$\mathbf{S} = \mathbf{C}^{-1} \qquad \text{and} \qquad \overline{\mathbf{S}} = \overline{\mathbf{C}}^{-1} \tag{3.5}$$

It is more common to use the strain-stress relation instead of the stress-strain relation, due to the fact that the elements of the compliance matrix are easier to determine than the elements of the stiffness matrix. The strain-stress relation is shown below:

$$\overline{\boldsymbol{\varepsilon}} = \overline{\mathbf{S}}\overline{\boldsymbol{\sigma}} \tag{3.6}$$

$$\begin{bmatrix} \varepsilon_{11} \\ \varepsilon_{22} \\ \varepsilon_{33} \\ \gamma_{23} \\ \gamma_{13} \\ \gamma_{12} \end{bmatrix} = \begin{bmatrix} \overline{S}_{11} & \overline{S}_{12} & \overline{S}_{13} & \overline{S}_{14} & \overline{S}_{15} & \overline{S}_{16} \\ \overline{S}_{21} & \overline{S}_{22} & \overline{S}_{23} & \overline{S}_{24} & \overline{S}_{25} & \overline{S}_{26} \\ \overline{S}_{31} & \overline{S}_{32} & \overline{S}_{33} & \overline{S}_{34} & \overline{S}_{35} & \overline{S}_{36} \\ \overline{S}_{41} & \overline{S}_{42} & \overline{S}_{43} & \overline{S}_{44} & \overline{S}_{45} & \overline{S}_{46} \\ \overline{S}_{51} & \overline{S}_{52} & \overline{S}_{53} & \overline{S}_{54} & \overline{S}_{55} & \overline{S}_{56} \\ \overline{S}_{61} & \overline{S}_{62} & \overline{S}_{63} & \overline{S}_{64} & \overline{S}_{65} & \overline{S}_{66} \end{bmatrix} \begin{bmatrix} \sigma_{11} \\ \sigma_{22} \\ \sigma_{33} \\ \sigma_{23} \\ \sigma_{13} \\ \sigma_{12} \end{bmatrix} \tag{3.7}$$

When virtual work of applied stresses is investigated, it can be shown that both the stiffness matrix and the compliance matrix must be symmetric in both the global and local coordinate system (i.e. $C_{ij} = C_{ji}$, $\overline{C}_{ij} = \overline{C}_{ji}$, $S_{ij} = S_{ji}$ and $\overline{S}_{ij} = \overline{S}_{ji}$, with: $i, j = 1, 2, ..., 6$). This results in a reduction of independent stiffness parameters for a general anisotropic material: 21 instead of 36 [10].

Compliance matrix of an orthotropic material

As mentioned before, FRP material shows orthotropic behaviour. An orthotropic material has three orthogonal local axes along which material properties are defined. Due to the orthogonality of local axes, 24 elements in the compliance matrix are equal to zero. The other 12 elements in the compliance matrix are determined by nine independent material parameters that are applicable to orthotropic material. For every principal direction, a different elastic modulus (E_1, E_2 or E_3), shear modulus (G_{12}, G_{13} or G_{23}) and Poisson's ratio (ν_{12}, ν_{13} or ν_{23}) is observed. The following relation is applicable to every orthotropic material:

$$\frac{\nu_{ij}}{E_i} = \frac{\nu_{ji}}{E_j} \qquad \text{with:} \quad i, j = 1,2,3 \tag{3.8}$$

Eventually, this results in the following compliance matrix for any orthotropic material:

$$\overline{\mathbf{S}} = \begin{bmatrix} \frac{1}{E_1} & -\frac{\nu_{12}}{E_1} & -\frac{\nu_{13}}{E_1} & 0 & 0 & 0 \\ -\frac{\nu_{12}}{E_1} & \frac{1}{E_2} & -\frac{\nu_{23}}{E_2} & 0 & 0 & 0 \\ -\frac{\nu_{13}}{E_1} & -\frac{\nu_{23}}{E_2} & \frac{1}{E_3} & 0 & 0 & 0 \\ 0 & 0 & 0 & \frac{1}{G_{23}} & 0 & 0 \\ 0 & 0 & 0 & 0 & \frac{1}{G_{13}} & 0 \\ 0 & 0 & 0 & 0 & 0 & \frac{1}{G_{12}} \end{bmatrix} \tag{3.9}$$

Compliance matrix of a transversely isotropic material

UD-plies show transversely isotropic behaviour. For UD-plies within an FRP material, it is common to distinguish the (1)-axis along the fibre direction (see also figure 2.1) and the (2)-axis perpendicular to the fibre direction, but in the plane of the ply. Finally the (3)-axis corresponds to the direction perpendicular to the plane of the ply. A transversely isotropic material has an extra plane of symmetry, leading to extra dependent parameters. From figure 2.2 it can be deduced that the properties for a UD-ply must be the same in both the (2)- and (3)-direction. Therefore, the elastic modulus is the same in all directions perpendicular to the fibre direction (i.e. $E_2 = E_3$). The same holds for the shear modulus ($G_{13} = G_{12}$) and the Poisson's ratio ($\nu_{13} = \nu_{12}$). Since a transversely isotropic material is isotropic in the (2,3)-plane, the following relation is valid for G_{23}:

$$G_{23} = \frac{E_2}{2\,(1+\nu_{23})} \tag{3.10}$$

In the end, five independent material constants can be distinguished for transversely isotropic materials: E_1, E_2, ν_{12}, ν_{23} and G_{12}. When the strain-stress relation is evaluated for transversely isotropic material, the following compliance matrix is obtained [10]:

$$\overline{\mathbf{S}} = \begin{bmatrix} \frac{1}{E_1} & -\frac{\nu_{12}}{E_1} & -\frac{\nu_{12}}{E_1} & 0 & 0 & 0 \\ -\frac{\nu_{12}}{E_1} & \frac{1}{E_2} & -\frac{\nu_{23}}{E_2} & 0 & 0 & 0 \\ -\frac{\nu_{12}}{E_1} & -\frac{\nu_{23}}{E_2} & \frac{1}{E_2} & 0 & 0 & 0 \\ 0 & 0 & 0 & \frac{2(1+\nu_{23})}{E_2} & 0 & 0 \\ 0 & 0 & 0 & 0 & \frac{1}{G_{12}} & 0 \\ 0 & 0 & 0 & 0 & 0 & \frac{1}{G_{12}} \end{bmatrix} \tag{3.11}$$

3.1.1. Plane stress condition

In the derivation of the CLT, plane stress conditions are assumed to be applicable to each individual ply. When a UD-ply is considered, the fibres are all parallel to the (1)-axis in the local coordinate system. It should be noted that the plane stress conditions are an approximation that are only applicable in a thin FRP plate when all the fibres are assumed to be parallel to the plane of the laminate [10]. The plies within a laminate are predominantly loaded in their plane, making out-of-plane stresses irrelevant. This means the out-of-plane stresses σ_{33}, σ_{23} and σ_{13} are assumed to be equal to zero. For a transversely isotropic material, the strain-stress relation presented in equation 3.7 can be evaluated when plane stress conditions are applicable:

$$\begin{bmatrix} \varepsilon_{11} \\ \varepsilon_{22} \\ \varepsilon_{33} \\ \gamma_{23} \\ \gamma_{13} \\ \gamma_{12} \end{bmatrix} = \begin{bmatrix} \frac{1}{E_1} & -\frac{\nu_{12}}{E_1} & -\frac{\nu_{12}}{E_1} & 0 & 0 & 0 \\ -\frac{\nu_{12}}{E_1} & \frac{1}{E_2} & -\frac{\nu_{23}}{E_2} & 0 & 0 & 0 \\ -\frac{\nu_{12}}{E_1} & -\frac{\nu_{23}}{E_2} & \frac{1}{E_2} & 0 & 0 & 0 \\ 0 & 0 & 0 & \frac{2(1+\nu_{23})}{E_2} & 0 & 0 \\ 0 & 0 & 0 & 0 & \frac{1}{G_{12}} & 0 \\ 0 & 0 & 0 & 0 & 0 & \frac{1}{G_{12}} \end{bmatrix} \begin{bmatrix} \sigma_{11} \\ \sigma_{22} \\ 0 \\ 0 \\ 0 \\ \sigma_{12} \end{bmatrix} = \begin{bmatrix} \varepsilon_{11} \\ \varepsilon_{22} \\ \varepsilon_{33} \\ 0 \\ 0 \\ \gamma_{12} \end{bmatrix} \tag{3.12}$$

It follows that the the out-of-plane shear strains γ_{23} and γ_{13} are equal to zero, but the out-of-plane axial strain ε_{33} is not necessarily equal to zero. Since the plane stress conditions are only applicable to thin laminates, it can be stated that the out-of-plane axial strain ε_{33} is not relevant thus is not taken into account in the derivation of the CLT. The plane stress conditions affect the elastic behaviour of a ply, thus the compliance matrix that is needed as input in the CLT is also affected. Due to the three stress components that are equal to zero and the corresponding strain components that are equal to zero or can be neglected, the compliance matrix can be reduced from a 6×6-matrix to a 3×3-matrix. This reduced stiffness matrix is indicated with a $\overline{\mathbf{Q}}$ in the local coordinate system:

$$\overline{\boldsymbol{\sigma}} = \overline{\mathbf{Q}}\overline{\boldsymbol{\varepsilon}} \tag{3.13}$$

$$\overline{\mathbf{Q}} = \begin{bmatrix} \overline{Q}_{11} & \overline{Q}_{12} & 0 \\ \overline{Q}_{12} & \overline{Q}_{22} & 0 \\ 0 & 0 & \overline{Q}_{66} \end{bmatrix} = \begin{bmatrix} \frac{1}{E_1} & -\frac{\nu_{12}}{E_1} & 0 \\ -\frac{\nu_{12}}{E_1} & \frac{1}{E_2} & 0 \\ 0 & 0 & \frac{1}{G_{12}} \end{bmatrix}^{-1} = \begin{bmatrix} \frac{E_1^2}{-\nu_{12}^2 E_2 + E_1} & -\frac{\nu_{12} E_1 E_2}{-\nu_{12}^2 E_2 + E_1} & 0 \\ -\frac{\nu_{12} E_1 E_2}{-\nu_{12}^2 E_2 + E_1} & \frac{E_1 E_2}{-\nu_{12}^2 E_2 + E_1} & 0 \\ 0 & 0 & G_{12} \end{bmatrix} \tag{3.14}$$

3.2. Transformation equations

When the elastic properties of a laminate are evaluated, one encounters the problem of different fibre orientations of plies within a laminate. To account for the orientation differences between individual plies in a laminate, transformation equations are needed. These relations translate the properties in a local coordinate system of a ply to properties in a global coordinate system of the complete laminate. In general, it is possible that all the axes show a different rotation, meaning the transformation equations will depend on these three independent rotations. The rotations are indicated with a Θ in figure 3.2a. These rotations Θ can be translated to rotations α, β and θ about the x-, y- and z-axis respectively(figure 3.2b).

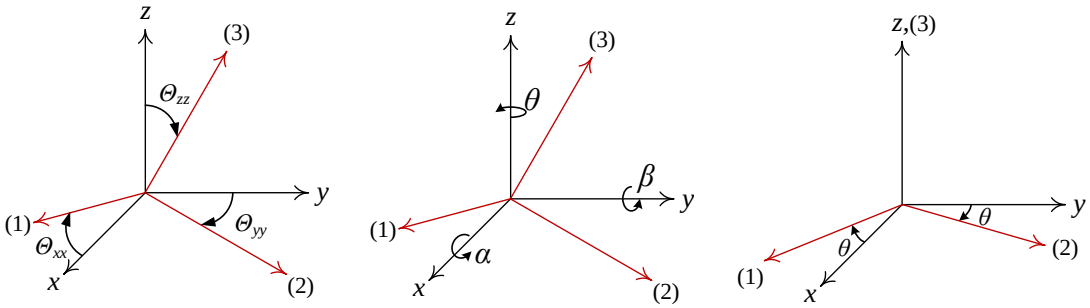

(a) Three different rotations of axes. (b) Three rotations about every axis. (c) Only rotation about the z-axis.

Figure 3.2: Transformation of axes.

For laminated composites, it is chosen that the (1)-axis coincides with the fibre direction of a ply. The (2)-axis is perpendicular to the fibre direction, but in the plane of the ply. The (3)-axis is both perpendicular to the fibre direction and perpendicular to the plane of the ply. When plies are stacked to create a laminate, it can be stated that the (3)-axis of all the plies are parallel. It is therefore not necessary to rotate the z-axis itself, only rotation about the z-axis is necessary. This results in only one rotation variable (θ), as can be seen in figure 3.2c. To express the local coordinate system in terms of the global coordinate system, the xy-plane is considered. An arbitrary point in space is taken, and its coordinates are derived in both coordinate systems. Figure 3.3 shows the assumed transformation from a global- to a local coordinate system.

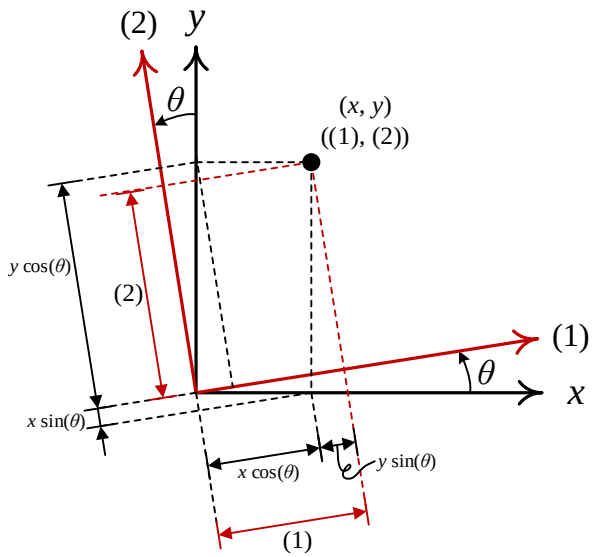

Figure 3.3: Transformation due to a rotation about the z-axis.

If the coordinates in the local coordinate system are expressed in terms of x, y and θ, the following relations are obtained:

$$\begin{cases} (1) = x\cos\theta + y\sin\theta \\ (2) = y\cos\theta - x\sin\theta \end{cases} \tag{3.15}$$

The equations above can be rewritten in matrix shape. The transformation from the z-axis to the (3)-axis, which is simply a factor 1, is also included for completeness:

$$\begin{bmatrix} (1) \\ (2) \\ (3) \end{bmatrix} = \begin{bmatrix} \cos\theta & \sin\theta & 0 \\ -\sin\theta & \cos\theta & 0 \\ 0 & 0 & 1 \end{bmatrix} \begin{bmatrix} x \\ y \\ z \end{bmatrix} = \mathbf{L}_z \begin{bmatrix} x \\ y \\ z \end{bmatrix} \tag{3.16}$$

Here, the subscript z indicates that the rotation matrix $\mathbf{L}_z$ is valid for a rotation about the z-axis. Similar relations can be derived for rotations about the x- and y-axis. If it is assumed α indicates a positive rotation about the x-axis and β indicates a positive rotation about the y-axis, the following rotation matrices will be valid:

$$\begin{bmatrix} (1) \\ (2) \\ (3) \end{bmatrix} = \begin{bmatrix} 1 & 0 & 0 \\ 0 & \cos\alpha & \sin\alpha \\ 0 & -\sin\alpha & \cos\alpha \end{bmatrix} \begin{bmatrix} x \\ y \\ z \end{bmatrix} = \mathbf{L}_x \begin{bmatrix} x \\ y \\ z \end{bmatrix} \tag{3.17}$$

$$\begin{bmatrix} (1) \\ (2) \\ (3) \end{bmatrix} = \begin{bmatrix} \cos\beta & 0 & \sin\beta \\ 0 & 1 & 0 \\ -\sin\beta & 0 & \cos\beta \end{bmatrix} \begin{bmatrix} x \\ y \\ z \end{bmatrix} = \mathbf{L}_y \begin{bmatrix} x \\ y \\ z \end{bmatrix} \tag{3.18}$$

Finally, the total rotation matrix $\mathbf{L}$ can be determined by multiplying the three rotation matrices, according to the definition of Euler angles [7]. In this case, a x-convention is chosen, which is common for engineering applications. It means the total rotation matrix can be determined by multiplication of the three rotation matrices in the following specific order:

$$\mathbf{L} = \mathbf{L}_z\mathbf{L}_y\mathbf{L}_x \tag{3.19}$$

For the CLT, it is assumed that the plies are in the xy-plane. This means the fibre orientation of the plies is defined as a rotation about the z-axis, thus only depends on θ. Therefore, both α and β are equal to zero. This results in identity matrices for $\mathbf{L}_x$ and $\mathbf{L}_y$, which means the total rotation matrix $\mathbf{L}$ is equal to $\mathbf{L}_z$:

$$\begin{bmatrix} (1) \\ (2) \\ (3) \end{bmatrix} = \mathbf{L} \begin{bmatrix} x \\ y \\ z \end{bmatrix} = \begin{bmatrix} \cos\theta & \sin\theta & 0 \\ -\sin\theta & \cos\theta & 0 \\ 0 & 0 & 1 \end{bmatrix} \begin{bmatrix} 1 & 0 & 0 \\ 0 & 1 & 0 \\ 0 & 0 & 1 \end{bmatrix} \begin{bmatrix} 1 & 0 & 0 \\ 0 & 1 & 0 \\ 0 & 0 & 1 \end{bmatrix} \begin{bmatrix} x \\ y \\ z \end{bmatrix} = \mathbf{L}_z \begin{bmatrix} x \\ y \\ z \end{bmatrix} \tag{3.20}$$

To transfer from a local to a global coordinate system, the rotation matrix $\mathbf{L}$ can be inverted. For the CLT, where θ is the only non-zero rotation, this inversion is as follows:

$$\begin{bmatrix} x \\ y \\ z \end{bmatrix} = \begin{bmatrix} \cos\theta & -\sin\theta & 0 \\ \sin\theta & \cos\theta & 0 \\ 0 & 0 & 1 \end{bmatrix} \begin{bmatrix} (1) \\ (2) \\ (3) \end{bmatrix} = \mathbf{L}^{-1} \begin{bmatrix} (1) \\ (2) \\ (3) \end{bmatrix} = \mathbf{L}^{T} \begin{bmatrix} (1) \\ (2) \\ (3) \end{bmatrix} \tag{3.21}$$

Note that the inverse of the rotation matrix is the same as the transpose of that matrix, so $\mathbf{L}$ is an orthogonal matrix. The transformation relations also apply to unit vectors in the two coordinate systems: $\overline{\boldsymbol{e}} = \mathbf{L}\boldsymbol{e}$, where $\overline{\boldsymbol{e}}$ indicates the unit vector in the local coordinate system and $\boldsymbol{e}$ indicates the unit vector in the global coordinate system [16]. The transformation of the coordinate system can be used to transfer stresses, strains and material properties from a local to a global coordinate system, as will be done in the following paragraphs with the assumption that both α and β are equal to zero, which is the case in the CLT.

Stress transformation

Since stress is a tensor, its transformation between coordinate systems can be performed in a similar manner as the transformation of the unit vector. However, due to the fact that stress is a second-order tensor, two transformations are needed. The following relations are valid for stress tensor transformation [16]:

$$\overline{\sigma}_{ij} = \mathbf{L}\sigma_{ij}\mathbf{L}^{T} \qquad \text{or:} \qquad \sigma_{ij} = \mathbf{L}^{T}\overline{\sigma}_{ij}\mathbf{L} \tag{3.22}$$

With:

$$\sigma_{ij} = \begin{bmatrix} \sigma_{xx} & \tau_{xy} & \tau_{xz} \\ \tau_{xy} & \sigma_{yy} & \tau_{yz} \\ \tau_{xz} & \tau_{yz} & \sigma_{zz} \end{bmatrix} \qquad \text{and} \qquad \overline{\sigma}_{ij} = \begin{bmatrix} \sigma_{11} & \sigma_{12} & \sigma_{13} \\ \sigma_{12} & \sigma_{22} & \sigma_{23} \\ \sigma_{13} & \sigma_{23} & \sigma_{33} \end{bmatrix} \tag{3.23}$$

Due to equilibrium, the stress tensor is a symmetric 3×3-matrix, which means six independent stress components can be identified. This holds for both the global and the local coordinate system. When the multiplications of matrices from equation 3.22 are performed, the total transformation matrix can be obtained. By rearranging the second order stress tensors (σ_{ij} and $\overline{\sigma}_{ij}$) to vectors with six components ($\boldsymbol{\sigma}$ and $\overline{\boldsymbol{\sigma}}$), a 6×6 transformation matrix can be obtained. When only the rotation θ about the z-axis is evaluated, the following 6×6 transformation matrix can be obtained:

$$\boldsymbol{\sigma} = \mathbf{T}\overline{\boldsymbol{\sigma}} \tag{3.24}$$

$$\begin{bmatrix} \sigma_{xx} \\ \sigma_{yy} \\ \sigma_{zz} \\ \tau_{yz} \\ \tau_{xz} \\ \tau_{xy} \end{bmatrix} = \begin{bmatrix} \cos^2\theta & \sin^2\theta & 0 & 0 & 0 & -2\cos\theta\sin\theta \\ \sin^2\theta & \cos^2\theta & 0 & 0 & 0 & 2\cos\theta\sin\theta \\ 0 & 0 & 1 & 0 & 0 & 0 \\ 0 & 0 & 0 & \cos\theta & \sin\theta & 0 \\ 0 & 0 & 0 & -\sin\theta & \cos\theta & 0 \\ \cos\theta\sin\theta & -\cos\theta\sin\theta & 0 & 0 & 0 & \cos^2\theta - \sin^2\theta \end{bmatrix} \begin{bmatrix} \sigma_{11} \\ \sigma_{22} \\ \sigma_{33} \\ \sigma_{23} \\ \sigma_{13} \\ \sigma_{12} \end{bmatrix} \tag{3.25}$$

To transfer stresses from a global to a local coordinate system, the transformation matrix can be inverted:

$$\overline{\boldsymbol{\sigma}} = \mathbf{T}^{-1}\boldsymbol{\sigma} \tag{3.26}$$

$$\begin{bmatrix} \sigma_{11} \\ \sigma_{22} \\ \sigma_{33} \\ \sigma_{23} \\ \sigma_{13} \\ \sigma_{12} \end{bmatrix} = \begin{bmatrix} \cos^2\theta & \sin^2\theta & 0 & 0 & 0 & 2\cos\theta\sin\theta \\ \sin^2\theta & \cos^2\theta & 0 & 0 & 0 & -2\cos\theta\sin\theta \\ 0 & 0 & 1 & 0 & 0 & 0 \\ 0 & 0 & 0 & \cos\theta & -\sin\theta & 0 \\ 0 & 0 & 0 & \sin\theta & \cos\theta & 0 \\ -\cos\theta\sin\theta & \cos\theta\sin\theta & 0 & 0 & 0 & \cos^2\theta - \sin^2\theta \end{bmatrix} \begin{bmatrix} \sigma_{xx} \\ \sigma_{yy} \\ \sigma_{zz} \\ \tau_{yz} \\ \tau_{xz} \\ \tau_{xy} \end{bmatrix} \tag{3.27}$$

Strain transformation

When the 2D-displacement field of an infinitesimal element is considered (figure 3.4), distinction must be made between the engineering shear strain (γ_{xy}) and the tensorial shear strain (ε_{xy} or ε_{yx}). The engineering shear strain is the total shear strain of an element. For the 2D-displacement, the engineering shear strain consists of the two tensorial shear strain components.

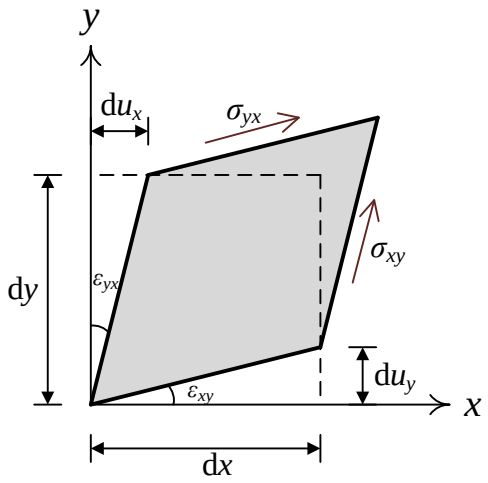

Figure 3.4: Shear strain on an infinitesimal element.

The tensorial shear strains ε_{xy} and ε_{yx} are displayed in figure 3.4. When strain is written as a vector, the engineering shear strain is usually used. The engineering shear strain is defined as the total change in angle between the two edges parallel to the x- and y-axis. This total change is composed of two tensorial shear components, as indicated in figure 3.4:

$$\begin{aligned}\gamma_{xy} &= \frac{\mathrm{d}u_y}{\mathrm{d}x} + \frac{\mathrm{d}u_x}{\mathrm{d}y} \\ &= \varepsilon_{xy} + \varepsilon_{yx} \\ &= 2\varepsilon_{xy}\end{aligned} \tag{3.28}$$

When the 2D-displacement of the other relevant shear strains are considered, the same relations are obtained: $\gamma_{yz} = 2\varepsilon_{yz}$ and $\gamma_{xz} = 2\varepsilon_{xz}$. The former also holds when a local coordinate system is considered instead of a global coordinate system, i.e. $\gamma_{23} = 2\varepsilon_{23}$, $\gamma_{13} = 2\varepsilon_{13}$ and $\gamma_{12} = 2\varepsilon_{12}$.

The strain transformation equations can be obtained from the stress transformation equations. The normal stress components can be replaced by the normal strain components [18]. The shear stress is related to the tensorial shear strain, since a single shear stress is not related to shear strains in two directions.

$$\begin{aligned}
&\sigma_{xx} \to \varepsilon_{xx} && \text{and} && \sigma_{11} \to \varepsilon_{11} \\
&\sigma_{yy} \to \varepsilon_{yy} && \text{and} && \sigma_{22} \to \varepsilon_{22} \\
&\sigma_{zz} \to \varepsilon_{zz} && \text{and} && \sigma_{33} \to \varepsilon_{33} \\
&\sigma_{yz} \to \frac{1}{2}\gamma_{yz} && \text{and} && \sigma_{23} \to \frac{1}{2}\gamma_{23} \\
&\sigma_{xz} \to \frac{1}{2}\gamma_{xz} && \text{and} && \sigma_{13} \to \frac{1}{2}\gamma_{13} \\
&\sigma_{xy} \to \frac{1}{2}\gamma_{xy} && \text{and} && \sigma_{12} \to \frac{1}{2}\gamma_{12}
\end{aligned} \tag{3.29}$$

The relations above can be inserted in equation 3.27. When that equation is rewritten, the following strain transformation is obtained:

$$\begin{bmatrix} \varepsilon_{11} \\ \varepsilon_{22} \\ \varepsilon_{33} \\ \gamma_{23} \\ \gamma_{13} \\ \gamma_{12} \end{bmatrix} = \begin{bmatrix} \cos^2\theta & \sin^2\theta & 0 & 0 & 0 & \cos\theta\sin\theta \\ \sin^2\theta & \cos^2\theta & 0 & 0 & 0 & -\cos\theta\sin\theta \\ 0 & 0 & 1 & 0 & 0 & 0 \\ 0 & 0 & 0 & \cos\theta & -\sin\theta & 0 \\ 0 & 0 & 0 & \sin\theta & \cos\theta & 0 \\ -2\cos\theta\sin\theta & 2\cos\theta\sin\theta & 0 & 0 & 0 & \cos^2\theta - \sin^2\theta \end{bmatrix} \begin{bmatrix} \varepsilon_{xx} \\ \varepsilon_{yy} \\ \varepsilon_{zz} \\ \gamma_{yz} \\ \gamma_{xz} \\ \gamma_{xy} \end{bmatrix} \tag{3.30}$$

It follows that the strain transformation matrix is the transpose of the stress transformation matrix:

$$\overline{\boldsymbol{\varepsilon}} = \mathbf{T}^T \boldsymbol{\varepsilon} \tag{3.31}$$

Inverting equation 3.30 results in a transformation from a local to a global coordinate system:

$$\boldsymbol{\varepsilon} = \mathbf{T}^{-T} \overline{\boldsymbol{\varepsilon}} \tag{3.32}$$

$$\begin{bmatrix} \varepsilon_{xx} \\ \varepsilon_{yy} \\ \varepsilon_{zz} \\ \gamma_{yz} \\ \gamma_{xz} \\ \gamma_{xy} \end{bmatrix} = \begin{bmatrix} \cos^2\theta & \sin^2\theta & 0 & 0 & 0 & -\cos\theta\sin\theta \\ \sin^2\theta & \cos^2\theta & 0 & 0 & 0 & \cos\theta\sin\theta \\ 0 & 0 & 1 & 0 & 0 & 0 \\ 0 & 0 & 0 & \cos\theta & \sin\theta & 0 \\ 0 & 0 & 0 & -\sin\theta & \cos\theta & 0 \\ 2\cos\theta\sin\theta & -2\cos\theta\sin\theta & 0 & 0 & 0 & \cos^2\theta - \sin^2\theta \end{bmatrix} \begin{bmatrix} \varepsilon_{11} \\ \varepsilon_{22} \\ \varepsilon_{33} \\ \gamma_{23} \\ \gamma_{13} \\ \gamma_{12} \end{bmatrix} \tag{3.33}$$

Stiffness transformation

The transformation matrix can also be used to transfer the stiffness matrix from a local to a global coordinate system. This will be useful when multiple plies with different fibre directions in a laminate need to be considered. When the equations 3.3 and 3.24 are combined, the following relation is obtained:

$$\boldsymbol{\sigma} = \mathbf{T}\overline{\mathbf{C}}\overline{\boldsymbol{\varepsilon}} \tag{3.34}$$

Equation 3.31 gives an expression for $\overline{\boldsymbol{\varepsilon}}$, which can be inserted in equation 3.34. This leads to a relation to transform the stiffness matrix from a local to a global coordinate system:

$$\boldsymbol{\sigma} = \mathbf{T}\overline{\mathbf{C}}\mathbf{T}^T\boldsymbol{\varepsilon} \tag{3.35}$$

Or:

$$\boldsymbol{\sigma} = \mathbf{C}\boldsymbol{\varepsilon} \qquad \text{with:} \qquad \mathbf{C} = \mathbf{T}\overline{\mathbf{C}}\mathbf{T}^T \tag{3.36}$$

Where $\mathbf{C}$ indicates the stiffness matrix in the global coordinate system. Due to the matrix multiplications, $\mathbf{C}$ does not contain zero entries any more. However, $\mathbf{C}$ is still a symmetric matrix.

3.2.1. Plane stress condition

When plane stress conditions are applicable, it is assumed that the stresses with a direction perpendicular to the ply (σ_{33}, σ_{23} and σ_{13}) are equal to zero. When the stress transformation from equation 3.25 is evaluated for plane stress conditions, the corresponding stresses σ_{zz}, τ_{yz} and τ_{xz} in the global coordinate system are also equal to zero. Therefore, the third, fourth and fifth row and column of the transformation matrix $\mathbf{T}$ can be deleted. This reduced transformation matrix $\mathbf{T}_\mathrm{r}$ can be used to transfer the reduced stiffness matrix $\mathbf{Q}$ from a local to a global coordinate system:

$$\boldsymbol{\sigma} = \mathbf{Q}\boldsymbol{\varepsilon} \qquad \text{with:} \qquad \mathbf{Q} = \mathbf{T}_\mathrm{r}\overline{\mathbf{Q}}\mathbf{T}_\mathrm{r}^T \tag{3.37}$$

$$\mathbf{T}_\mathrm{r} = \begin{bmatrix} \cos^2\theta & \sin^2\theta & -2\cos\theta\sin\theta \\ \sin^2\theta & \cos^2\theta & 2\cos\theta\sin\theta \\ \cos\theta\sin\theta & -\cos\theta\sin\theta & \cos^2\theta - \sin^2\theta \end{bmatrix} \tag{3.38}$$

3.3. Laminate constitutive equations

An FRP laminate consists of several plies with different fibre orientation, thus a different reduced stiffness matrix in the global coordinate system is applicable for each ply. To obtain a stress-strain relation of a complete laminate, the properties of the individual plies must be combined in order to obtain stiffness properties that are applicable to the whole laminate. It is assumed that a perfect bond between the plies is achieved, and that each ply has a uniform thickness. Furthermore, the thickness of the laminate is considered to be much smaller compared to the width and length of a laminate plate. This means the 3D problem can be translated into a problem to be solved with plate theory. Kirchhoff plate theory is used [16], in which the following three assumptions are made:

- Straight lines perpendicular to the mid-surface of the plate remain straight after deformation of the plate.
- Straight lines perpendicular to the mid-surface remain perpendicular to the mid-surface after deformation of the plate.
- The thickness of the plate remains unchanged during deformation of the plate.

Due to the last assumption, it can be stated that the axial strain perpendicular to the plane of the ply ε_{zz} is equal to zero. Furthermore, out-of-plane shear strains are not possible if straight lines perpendicular to the mid-surface must remain perpendicular to the mid-surface. This means the shear strain components γ_{yz} and γ_{xz} must be equal to zero. The mid-surface is taken as a reference surface to determine the strains of the laminate. Strains in a thin plate can be evaluated using the strain of the mid-surface (ε^0) and the curvature of the plate (κ):

$$\varepsilon\left(x, y, z\right) = \varepsilon^0\left(x, y\right) + z\kappa\left(x, y\right) \tag{3.39}$$

Locally, equation 3.39 simplifies to:

$$\varepsilon\left(z\right) = \varepsilon^0 + z\kappa \tag{3.40}$$

Or in matrix notation for the three relevant strains:

$$\boldsymbol{\varepsilon} = \boldsymbol{\varepsilon}^0 + z\boldsymbol{\kappa} \tag{3.41}$$

$$\begin{bmatrix} \varepsilon_{xx} \\ \varepsilon_{yy} \\ \gamma_{xy} \end{bmatrix} = \begin{bmatrix} \varepsilon^0_{xx} \\ \varepsilon^0_{yy} \\ \gamma^0_{xy} \end{bmatrix} + z \begin{bmatrix} \kappa_{xx} \\ \kappa_{yy} \\ \kappa_{xy} \end{bmatrix} \tag{3.42}$$

This definition for the strain can be implemented in equation 3.37, leading to the following stress-strain relation for a single ply in the global coordinate system:

$$\boldsymbol{\sigma} = \mathbf{Q}\boldsymbol{\varepsilon} \tag{3.43}$$

$$\begin{bmatrix} \sigma_{xx} \\ \sigma_{yy} \\ \tau_{xy} \end{bmatrix} = \mathbf{Q}\left(\begin{bmatrix} \varepsilon^0_{xx} \\ \varepsilon^0_{yy} \\ \gamma^0_{xy} \end{bmatrix} + z \begin{bmatrix} \kappa_{xx} \\ \kappa_{yy} \\ \kappa_{xy} \end{bmatrix} \right) \tag{3.44}$$

The next step is to combine all the plies. Therefore, the total force and moment in a cross section must be related to the stress resultants. The stress resultants can be determined by assuming a constant strain over the cross section. The six relevant deformation components (ε^0_{xx}, ε^0_{yy}, γ^0_{xy}, κ_{xx}, κ_{yy} and κ_{xy}) need to be considered individually. Figure 3.5 shows the cross section of a single ply, where the individual fibres are not shown. When a single axial strain component is applied (ε^0_{xx} or ε^0_{yy}), the corresponding stress (σ_{xx} or σ_{yy}) will also be constant. This constant stress can be multiplied with the ply thickness to obtain the normal force (N_{xx} or N_{yy}) that acts on the ply due to the applied strain. When a constant curvature (κ_{xx} or κ_{yy}) is applied, a linear stress distribution (σ_{xx} or σ_{yy}) can be observed. This results in a bending moment (M_{xx} or M_{yy}) acting on the ply.

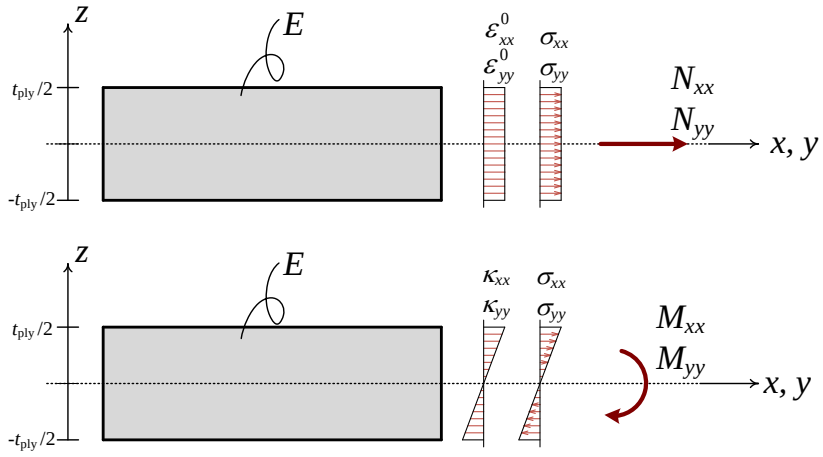

Figure 3.5: Resultant force and moment in a single ply of a laminate.

The shear component and the torsional component can be derived similarly. Figure 3.6 shows a three-dimensional representation of a single ply, where a constant shear strain γ^0_{xy} is applied on the plane with the x-axis as the outward normal. The plane with the y-axis as outward normal shows the torsional curvature κ_{xy} and the corresponding shear stress.

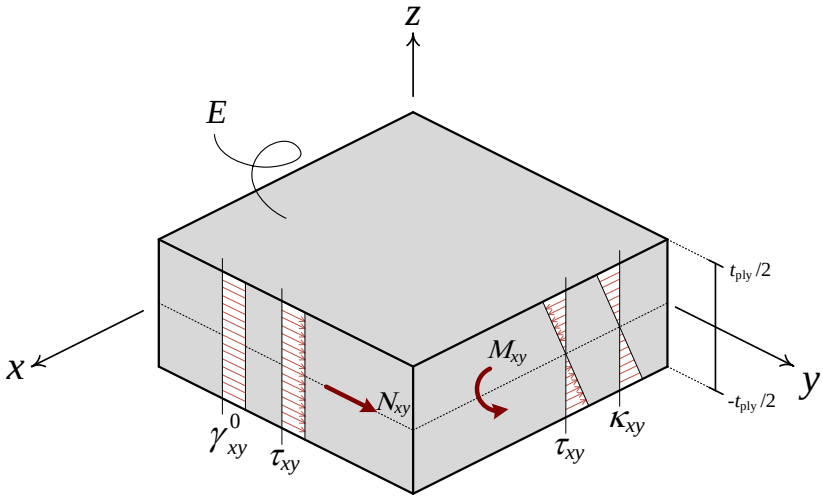

Figure 3.6: Resultant force and moment in a single ply of a laminate.

By definition, the resultant normal force and moment are given by the following integrals [14]:

$$\begin{aligned} N_{xx} &= \int_{-\frac{1}{2}t_{ply}}^{\frac{1}{2}t_{ply}} \sigma_{xx} dz & N_{yy} &= \int_{-\frac{1}{2}t_{ply}}^{\frac{1}{2}t_{ply}} \sigma_{yy} dz & N_{xy} &= \int_{-\frac{1}{2}t_{ply}}^{\frac{1}{2}t_{ply}} \tau_{xy} dz \\ M_{xx} &= \int_{-\frac{1}{2}t_{ply}}^{\frac{1}{2}t_{ply}} \sigma_{xx} z dz & M_{yy} &= \int_{-\frac{1}{2}t_{ply}}^{\frac{1}{2}t_{ply}} \sigma_{yy} z dz & M_{xy} &= \int_{-\frac{1}{2}t_{ply}}^{\frac{1}{2}t_{ply}} \tau_{xy} z dz \end{aligned} \tag{3.45}$$

Note that these forces and moments are still per unit width, so N has a unit of kN/m and M has a unit of kNm/m. If multiple plies are considered in a laminate, the strain distribution will remain linear over the height. However, the stresses will redistribute, since every ply can have a different elastic modulus in the considered direction. This means when a uniform strain is applied, the stress distribution will consist of different constant stresses for each ply. Besides a resultant normal force, this may lead to a resultant moment. When a linear strain distribution due to curvature of a ply is assumed, it is possible that a resultant normal force appears, besides the resultant moment. These two facts are the origin of the coupling effects in a laminate, which cause, for example, out-of-plane deformations when an in-plane normal force is applied. Figure 3.7 shows an example of what the stress

distributions could look like in a laminate for the in-plane force and moment resultants (N_{xx}, N_{yy}, M_{xx} and M_{yy}).

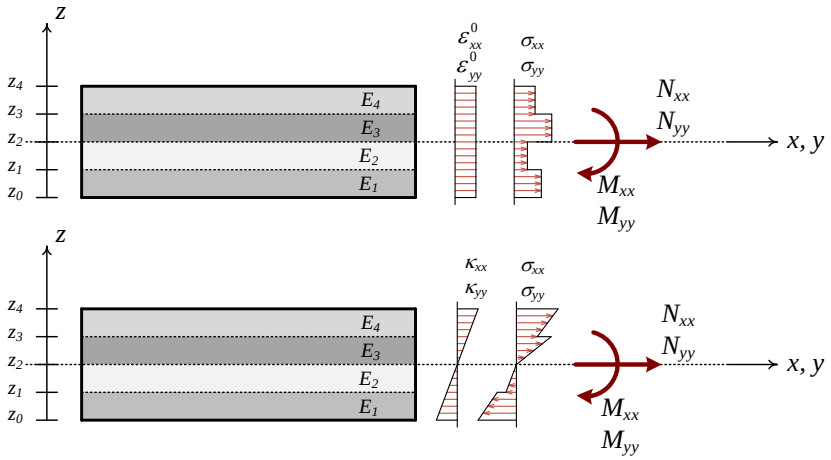

Figure 3.7: Resultant forces and moments a laminate. It is assumed that $E_3 > E_1 > E_4 > E_2$.

The shear force component N_{xy} and the torsional moment M_{xy} can be determined in a similar way. Figure 3.8 represents the derivation of the shear stress τ_{xy} due to a constant applied shear strain γ^0_{xy} on the plane with the x-axis as outward normal. The shear stress due to torsional curvature κ_{xy} is shown on the plane with the y-axis as outward normal in figure 3.8.

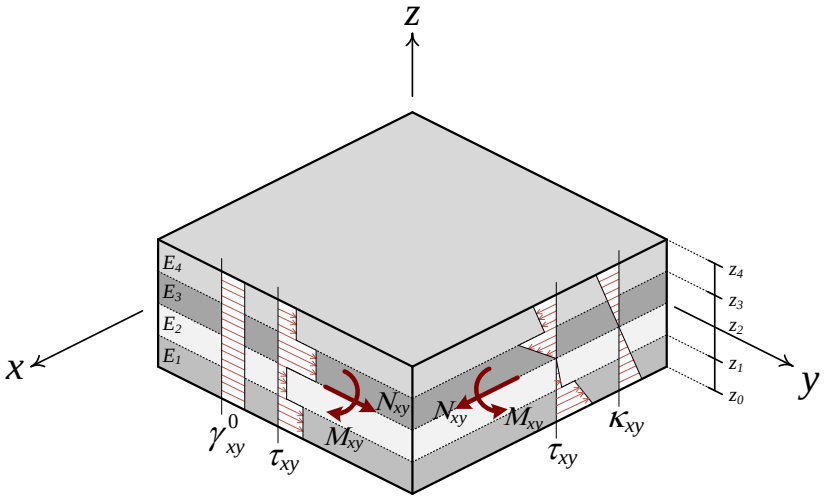

Figure 3.8: Resultant forces and moments a laminate due to shear strain and torsional curvature.

To evaluate the total forces and moments in a laminate, the components of each ply can be summed. Furthermore, the integrals in equation 3.45 could be written in matrix shape. The following relations are obtained:

$$\boldsymbol{N} = \begin{bmatrix} N_{xx} \\ N_{yy} \\ N_{xy} \end{bmatrix} = \sum_{i=1}^{n} \int_{z_{i-1}}^{z_i} \begin{bmatrix} \sigma_{xx} \\ \sigma_{yy} \\ \tau_{xy} \end{bmatrix} dz \tag{3.46}$$

$$\boldsymbol{M} = \begin{bmatrix} M_{xx} \\ M_{yy} \\ M_{xy} \end{bmatrix} = \sum_{i=1}^{n} \int_{z_{i-1}}^{z_i} z \begin{bmatrix} \sigma_{xx} \\ \sigma_{yy} \\ \tau_{xy} \end{bmatrix} dz \tag{3.47}$$

Here, i indicates the ply number, and n represents the total number of plies in a laminate. Note that in figure 3.7 and 3.8, the line of $z = 0$ coincides with the mid-surface of the laminate. This means z_0 and z_1 have a

negative value. When equation 3.44 is implemented in the relations above, the normal forces and moments can be expressed in terms of strain and curvature. The deformations ε^0 and κ are independent of the height of the ply, as well as the stiffness matrix $\mathbf{Q}$, so these can be taken out of the integrals.

$$\begin{bmatrix} N_{xx} \\ N_{yy} \\ N_{xy} \end{bmatrix} = \sum_{i=1}^{n} \left(\mathbf{Q}_i \begin{bmatrix} \varepsilon^0_{xx} \\ \varepsilon^0_{yy} \\ \gamma^0_{xy} \end{bmatrix} \int_{z_{i-1}}^{z_i} dz + \mathbf{Q}_i \begin{bmatrix} \kappa_{xx} \\ \kappa_{yy} \\ \kappa_{xy} \end{bmatrix} \int_{z_{i-1}}^{z_i} z dz \right) \tag{3.48}$$

$$\begin{bmatrix} M_{xx} \\ M_{yy} \\ M_{xy} \end{bmatrix} = \sum_{i=1}^{n} \left(\mathbf{Q}_i \begin{bmatrix} \varepsilon^0_{xx} \\ \varepsilon^0_{yy} \\ \gamma^0_{xy} \end{bmatrix} \int_{z_{i-1}}^{z_i} z dz + \mathbf{Q}_i \begin{bmatrix} \kappa_{xx} \\ \kappa_{yy} \\ \kappa_{xy} \end{bmatrix} \int_{z_{i-1}}^{z_i} z^2 dz \right) \tag{3.49}$$

Evaluating the integrals results in:

$$\begin{bmatrix} N_{xx} \\ N_{yy} \\ N_{xy} \end{bmatrix} = \sum_{i=1}^{n} \left(\mathbf{Q}_i \begin{bmatrix} \varepsilon^0_{xx} \\ \varepsilon^0_{yy} \\ \gamma^0_{xy} \end{bmatrix} (z_i - z_{i-1}) + \mathbf{Q}_i \begin{bmatrix} \kappa_{xx} \\ \kappa_{yy} \\ \kappa_{xy} \end{bmatrix} \frac{1}{2} \left(z_i^2 - z_{i-1}^2 \right) \right) \tag{3.50}$$

$$\begin{bmatrix} M_{xx} \\ M_{yy} \\ M_{xy} \end{bmatrix} = \sum_{i=1}^{n} \left(\mathbf{Q}_i \begin{bmatrix} \varepsilon^0_{xx} \\ \varepsilon^0_{yy} \\ \gamma^0_{xy} \end{bmatrix} \frac{1}{2} \left(z_i^2 - z_{i-1}^2 \right) + \mathbf{Q}_i \begin{bmatrix} \kappa_{xx} \\ \kappa_{yy} \\ \kappa_{xy} \end{bmatrix} \frac{1}{3} \left(z_i^3 - z_{i-1}^3 \right) \right) \tag{3.51}$$

The equations above can be written together in matrix shape with an ABD-matrix:

$$\begin{bmatrix} \boldsymbol{N} \\ \boldsymbol{M} \end{bmatrix} = \begin{bmatrix} \mathbf{A} & \mathbf{B} \\ \mathbf{B} & \mathbf{D} \end{bmatrix} \begin{bmatrix} \boldsymbol{\varepsilon^0} \\ \boldsymbol{\kappa} \end{bmatrix} \tag{3.52}$$

With:

$$\begin{aligned} \mathbf{A} &= \sum_{i=1}^{n} (z_i - z_{i-1}) \mathbf{Q}_i \\ \mathbf{B} &= \sum_{i=1}^{n} \frac{1}{2} \left(z_i^2 - z_{i-1}^2 \right) \mathbf{Q}_i \\ \mathbf{D} &= \sum_{i=1}^{n} \frac{1}{3} \left(z_i^3 - z_{i-1}^3 \right) \mathbf{Q}_i \end{aligned} \tag{3.53}$$

All the elements in $\mathbf{Q}$ have a unit kN/m^2. It follows that the elements from $\mathbf{A}$, $\mathbf{B}$ and $\mathbf{D}$ have a unit of kN/m, kN and kNm respectively. $\mathbf{A}$ is called the extensional stiffness matrix [17], which relates the mid-surface strains to in-plane normal forces. $\mathbf{D}$ is the bending stiffness matrix, relating the curvature to the moments. The coupling stiffness matrix $\mathbf{B}$ relates the curvature to the in-plane normal forces and the mid-surface strains to the moments. The ABD-matrix is a symmetric 6×6-matrix, where all the entries depend on the lay-up of the laminate and the material properties of the plies:

$$\left[\begin{array}{c} N_{xx} \\ N_{yy} \\ N_{xy} \\ M_{xx} \\ M_{yy} \\ M_{xy} \end{array}\right] = \left[\begin{array}{ccc:ccc} A_{11} & A_{12} & A_{16} & B_{11} & B_{12} & B_{16} \\ A_{12} & A_{22} & A_{26} & B_{12} & B_{22} & B_{26} \\ A_{16} & A_{26} & A_{66} & B_{16} & B_{26} & B_{66} \\ \hdashline B_{11} & B_{12} & B_{16} & D_{11} & D_{12} & D_{16} \\ B_{12} & B_{22} & B_{26} & D_{12} & D_{22} & D_{26} \\ B_{16} & B_{26} & B_{66} & D_{16} & D_{26} & D_{66} \end{array}\right] \left[\begin{array}{c} \varepsilon^0_{xx} \\ \varepsilon^0_{yy} \\ \gamma^0_{xy} \\ \kappa_{xx} \\ \kappa_{yy} \\ \kappa_{xy} \end{array}\right] \tag{3.54}$$

3.4. Engineering constants

In a Finite Element (FE) analysis, it is often not possible or desirable to implement composite materials in a model. Using individual plies in a finite element model is labour-intensive, thus not preferable in a preliminary design phase. Equivalent engineering constants can be derived, which will relate the laminate ABD-matrix to transversely isotropic properties of a homogeneous material in the global coordinate system (E_x, E_y, G_{xy} and ν_{xy}). These properties could be used as input for the (orthotropic) material properties in an FE analysis. It should be noted that distinction must be made between in-plane engineering constants and flexural engineering constants, which follows from the difference in dependence on the laminate height $t_{\text{tot},0}$. In-plane stiffnesses are related to the order $\sim t_{\text{tot},0}$, where flexural stiffnesses are related to the order $\sim t_{\text{tot},0}^3$. This can be derived using the equations for axial- and bending stress:

$$\text{Axial:} \qquad \sigma = \frac{N}{A} = \frac{N}{b t_{\text{tot},0}} \tag{3.55}$$

$$\text{Bending:} \qquad \sigma = \frac{Mz}{I_{zz}} = \frac{Mz}{\frac{1}{12} b t_{\text{tot},0}^3} \tag{3.56}$$

Next, it is assumed that the problem is considered per unit width, so $b = 1$. The goal is to find an expression for the elastic modulus E. Therefore, the constitutive equation can be used to replace σ by $E\left(\varepsilon^0 + z\kappa\right)$. When the in-plane stiffness is sought, it must be assumed that the curvature κ is equal to zero. For the flexural stiffness, the strain of the mid-surface ε^0 must be zero:

$$\text{Axial:} \qquad E\varepsilon^0 = \frac{N}{t_{\text{tot},0}} \qquad \rightarrow \qquad E = \frac{N / t_{\text{tot},0}}{\varepsilon_0} \tag{3.57}$$

$$\text{Bending:} \qquad Ez\kappa = \frac{Mz}{\frac{1}{12} t_{\text{tot},0}^3} \qquad \rightarrow \qquad E = \frac{12M / t_{\text{tot},0}^3}{\kappa} \tag{3.58}$$

Great care should be taken when engineering constants are used, since the coupling effects are neglected. For example, the in-plane engineering constants are derived under the assumption that no curvatures are observed when the laminate is loaded in its plane. Therefore, the in-plane engineering constants will only be applicable when a laminate is predominantly loaded in its plane. Also, for the flexural engineering constants, no strain of the mid-surface of the laminate is assumed. Thus the flexural engineering constants are only applicable if bending is the dominant type of load on a laminate.

In-plane engineering constants

As an example, the in-plane elastic modulus in the x-direction is derived. The other engineering constants can be found in a similar manner. The laminate constitutive equations (equation 3.52) are the starting point for the derivation of the engineering constants. When an elastic modulus in the x-direction ($E_{x,\text{ip}}$) is sought for the in-plane engineering constants, only a load F_x needs to be applied [14]:

$$\begin{bmatrix} F_x \\ 0 \\ 0 \\ 0 \\ 0 \\ 0 \end{bmatrix} = \left[\begin{array}{ccc:ccc} A_{11} & A_{12} & A_{16} & B_{11} & B_{12} & B_{16} \\ A_{12} & A_{22} & A_{26} & B_{12} & B_{22} & B_{26} \\ A_{16} & A_{26} & A_{66} & B_{16} & B_{26} & B_{66} \\ \hdashline \overline{B}_{11} & \overline{B}_{12} & \overline{B}_{16} & \overline{D}_{11} & \overline{D}_{12} & \overline{D}_{16} \\ B_{12} & B_{22} & B_{26} & D_{12} & D_{22} & D_{26} \\ B_{16} & B_{26} & B_{66} & D_{16} & D_{26} & D_{66} \end{array}\right] \begin{bmatrix} \varepsilon_{xx}^0 \\ \varepsilon_{yy}^0 \\ \gamma_{xy}^0 \\ \kappa_{xx} \\ \kappa_{yy} \\ \kappa_{xy} \end{bmatrix} \tag{3.59}$$

Equation 3.59 needs to be solved for ε^0_{xx}. Cramer's rule can be used:

$$\varepsilon^0_{xx} = \frac{\left|\begin{array}{cccc|ccc} F_x & A_{12} & A_{16} & B_{11} & B_{12} & B_{16} \\ 0 & A_{22} & A_{26} & B_{12} & B_{22} & B_{26} \\ 0 & A_{26} & A_{66} & B_{16} & B_{26} & B_{66} \\ \hline 0 & B_{12} & B_{16} & D_{11} & D_{12} & D_{16} \\ 0 & B_{22} & B_{26} & D_{12} & D_{22} & D_{26} \\ 0 & B_{26} & B_{66} & D_{16} & D_{26} & D_{66} \end{array}\right|}{\left|\begin{array}{cccc|ccc} A_{11} & A_{12} & A_{16} & B_{11} & B_{12} & B_{16} \\ A_{12} & A_{22} & A_{26} & B_{12} & B_{22} & B_{26} \\ A_{16} & A_{26} & A_{66} & B_{16} & B_{26} & B_{66} \\ \hline B_{11} & B_{12} & B_{16} & D_{11} & D_{12} & D_{16} \\ B_{12} & B_{22} & B_{26} & D_{12} & D_{22} & D_{26} \\ B_{16} & B_{26} & B_{66} & D_{16} & D_{26} & D_{66} \end{array}\right|} = F_x \frac{\left|\begin{array}{cccc|ccc} A_{22} & A_{26} & B_{12} & B_{22} & B_{26} \\ A_{26} & A_{66} & B_{16} & B_{26} & B_{66} \\ \hline B_{12} & B_{16} & D_{11} & D_{12} & D_{16} \\ B_{22} & B_{26} & D_{12} & D_{22} & D_{26} \\ B_{26} & B_{66} & D_{16} & D_{26} & D_{66} \end{array}\right|}{\left|\begin{array}{cccc|ccc} A_{11} & A_{12} & A_{16} & B_{11} & B_{12} & B_{16} \\ A_{12} & A_{22} & A_{26} & B_{12} & B_{22} & B_{26} \\ A_{16} & A_{26} & A_{66} & B_{16} & B_{26} & B_{66} \\ \hline B_{11} & B_{12} & B_{16} & D_{11} & D_{12} & D_{16} \\ B_{12} & B_{22} & B_{26} & D_{12} & D_{22} & D_{26} \\ B_{16} & B_{26} & B_{66} & D_{16} & D_{26} & D_{66} \end{array}\right|} = \frac{F_x \mathrm{M}_{1,1}}{\det[ABD]} \tag{3.60}$$

Here, $\mathrm{M}_{1,1}$ is called the minor of the (1,1) element (in this case F_x) and is defined by the determinant of the ABD-matrix when the first row and the first column are deleted. From Hooke's law, it follows that the elastic modulus in x-direction ($E_{x,\mathrm{ip}}$) will be the following:

$$E_{x,\mathrm{ip}} = \frac{\sigma_x}{\varepsilon_x} = \frac{F_x / t_{\mathrm{tot},0}}{\varepsilon^0_{xx}} = \frac{F_x / t_{\mathrm{tot},0}}{\frac{F_x \mathrm{M}_{1,1}}{\det[ABD]}} = \frac{\det[ABD]}{\mathrm{M}_{1,1}\, t_{\mathrm{tot},0}} \tag{3.61}$$

Here, $t_{\mathrm{tot},0}$ indicates the total height of the panel. The other in-plane engineering constants can be derived in a similar way, and will be the following:

$$\begin{aligned} E_{y,\mathrm{ip}} &= \frac{\det[ABD]}{\mathrm{M}_{2,2}\, t_{\mathrm{tot},0}} \\ G_{xy,\mathrm{ip}} &= \frac{\det[ABD]}{\mathrm{M}_{3,3}\, t_{\mathrm{tot},0}} \\ \nu_{xy,\mathrm{ip}} &= \frac{\mathrm{M}_{1,2}}{\mathrm{M}_{1,1}} \end{aligned} \tag{3.62}$$

The Poisson's ratio shows a minor of a non-diagonal element, since the Poisson's ratio $\nu_{xy,\mathrm{ip}}$ relates the deformation in y-direction to the load in x-direction (F_x).

When a symmetric and balanced lay-up of a laminate is considered, the ABD-matrix contains many zero entries since, for example, no coupling effects are present. This means the in-plane engineering constants simplify to the following relations:

$$\begin{aligned} E_{x,\mathrm{ip}} &= \frac{A_{11} A_{22} - A_{12}^2}{A_{22}\, t_{\mathrm{tot},0}} \\ E_{y,\mathrm{ip}} &= \frac{A_{11} A_{22} - A_{12}^2}{A_{11}\, t_{\mathrm{tot},0}} \\ G_{xy,\mathrm{ip}} &= \frac{A_{66}}{t_{\mathrm{tot},0}} \\ \nu_{xy,\mathrm{ip}} &= \frac{A_{12}}{A_{22}} \end{aligned} \tag{3.63}$$

Flexural engineering constants

For the flexural engineering constants, the same approach can be applied as for the in-plane engineering constants. However, for the flexural engineering constants, moments are applied and curvatures are evaluated, instead of axial loads and strains respectively. The engineering elastic modulus in x-direction $E_{x,\mathrm{f}}$ will be taken as an example again. Therefore, a moment T_x is applied in order to determine the curvature κ_{xx}:

$$\begin{bmatrix} 0 \\ 0 \\ 0 \\ T_x \\ 0 \\ 0 \end{bmatrix} = \left[\begin{array}{ccc:ccc} A_{11} & A_{12} & A_{16} & B_{11} & B_{12} & B_{16} \\ A_{12} & A_{22} & A_{26} & B_{12} & B_{22} & B_{26} \\ A_{16} & A_{26} & A_{66} & B_{16} & B_{26} & B_{66} \\ \hdashline B_{11} & B_{12} & B_{16} & D_{11} & D_{12} & D_{16} \\ B_{12} & B_{22} & B_{26} & D_{12} & D_{22} & D_{26} \\ B_{16} & B_{26} & B_{66} & D_{16} & D_{26} & D_{66} \end{array}\right] \begin{bmatrix} \varepsilon^0_{xx} \\ \varepsilon^0_{yy} \\ \gamma^0_{xy} \\ \kappa_{xx} \\ \kappa_{yy} \\ \kappa_{xy} \end{bmatrix} \tag{3.64}$$

Using Cramer's rule gives the solution for κ_{xx}:

$$\kappa_{xx} = \frac{\left|\begin{array}{ccc:ccc} A_{11} & A_{12} & A_{16} & 0 & B_{12} & B_{16} \\ A_{12} & A_{22} & A_{26} & 0 & B_{22} & B_{26} \\ A_{16} & A_{26} & A_{66} & 0 & B_{26} & B_{66} \\ \hdashline B_{11} & B_{12} & B_{16} & T_x & D_{12} & D_{16} \\ B_{12} & B_{22} & B_{26} & 0 & D_{22} & D_{26} \\ B_{16} & B_{26} & B_{66} & 0 & D_{26} & D_{66} \end{array}\right|}{\left|\begin{array}{ccc:ccc} A_{11} & A_{12} & A_{16} & B_{11} & B_{12} & B_{16} \\ A_{12} & A_{22} & A_{26} & B_{12} & B_{22} & B_{26} \\ A_{16} & A_{26} & A_{66} & B_{16} & B_{26} & B_{66} \\ \hdashline B_{11} & B_{12} & B_{16} & D_{11} & D_{12} & D_{16} \\ B_{12} & B_{22} & B_{26} & D_{12} & D_{22} & D_{26} \\ B_{16} & B_{26} & B_{66} & D_{16} & D_{26} & D_{66} \end{array}\right|} = \frac{T_x \left|\begin{array}{ccc:ccc} A_{11} & A_{12} & A_{16} & B_{12} & B_{16} \\ A_{12} & A_{22} & A_{26} & B_{22} & B_{26} \\ A_{16} & A_{26} & A_{66} & B_{26} & B_{66} \\ \hdashline B_{12} & B_{22} & B_{26} & D_{22} & D_{26} \\ B_{16} & B_{26} & B_{66} & D_{26} & D_{66} \end{array}\right|}{\left|\begin{array}{ccc:ccc} A_{11} & A_{12} & A_{16} & B_{11} & B_{12} & B_{16} \\ A_{12} & A_{22} & A_{26} & B_{12} & B_{22} & B_{26} \\ A_{16} & A_{26} & A_{66} & B_{16} & B_{26} & B_{66} \\ \hdashline B_{11} & B_{12} & B_{16} & D_{11} & D_{12} & D_{16} \\ B_{12} & B_{22} & B_{26} & D_{12} & D_{22} & D_{26} \\ B_{16} & B_{26} & B_{66} & D_{16} & D_{26} & D_{66} \end{array}\right|} = \frac{T_x \mathrm{M}_{4,4}}{\det[ABD]} \tag{3.65}$$

The flexural engineering elastic modulus in x-direction can be derived using Hooke's law:

$$E_{x,\mathrm{f}} = \frac{\sigma_x}{\varepsilon_x} = \frac{12 M_x / t^3_{\mathrm{tot},0}}{\kappa_{xx}} = \frac{12 T_x / t^3_{\mathrm{tot},0}}{\frac{T_x \mathrm{M}_{4,4}}{\det[ABD]}} = \frac{12 \det[ABD]}{\mathrm{M}_{4,4} t^3_{\mathrm{tot},0}} \tag{3.66}$$

The other flexural engineering constants can be derived similarly and are shown below:

$$\begin{aligned} E_{y,\mathrm{f}} &= \frac{12 \det[ABD]}{\mathrm{M}_{5,5} t^3_{\mathrm{tot},0}} \\ G_{xy,\mathrm{f}} &= \frac{12 \det[ABD]}{\mathrm{M}_{6,6} t^3_{\mathrm{tot},0}} \\ \nu_{xy,\mathrm{f}} &= \frac{\mathrm{M}_{4,5}}{\mathrm{M}_{4,4}} \end{aligned} \tag{3.67}$$

For a balanced and symmetric laminate, these engineering constants simplify to the following:

$$\begin{aligned} E_{x,\mathrm{f}} &= \frac{12\left(D_{11} D_{22} - D_{12}^2\right)}{D_{22} t^3_{\mathrm{tot},0}} \\ E_{y,\mathrm{f}} &= \frac{12\left(D_{11} D_{22} - D_{12}^2\right)}{D_{11} t^3_{\mathrm{tot},0}} \\ G_{xy,\mathrm{f}} &= \frac{12 D_{66}}{t^3_{\mathrm{tot},0}} \\ \nu_{xy,\mathrm{f}} &= \frac{D_{12}}{D_{22}} \end{aligned} \tag{3.68}$$

4

Implementation inclination in the CLT

In this chapter, a modified Classical Laminate Theory will be derived, which accounts for an extra rotation that is present in a laminate with inclined plies. The same procedure as described in chapter 3 will be used. The goal is to find a new ABD-matrix which takes the extra rotation into account.

4.1. Elastic behaviour

The CLT makes use of plane stress assumptions in order to simplify the problem. For laminates without inclined plies, these are valid assumptions, since in every ply the fibres are parallel to the plane of the laminate. This means the dominant stresses are transferred in the plane of the laminate and the out-of-plane stresses (σ_{33}, σ_{23} and σ_{13}) can be neglected. When a rotation about the x-axis is present in the plies within a laminate, it is possible that out-of-plane stresses occur in those plies. In figure 4.1, a 90°-ply with an inclination α is shown. The resulting fibre direction is indicated with the dashed lines and coincides with the (1)-axis in the local coordinate system. When a normal force N_{yy} is applied to this single ply, it is expected that a normal stress perpendicular to the fibres could occur, which will be the normal stress σ_{33} in the local coordinate system of the ply. Furthermore, due to the difference in stiffness along the (1)- and (3)-axis, it is expected that out-of-plane shear deformations could occur. The stiffness along the fibre direction is significantly higher compared to the stiffness perpendicular to the fibre direction. This will lead to a smaller elongation along the fibre direction compared to the elongation perpendicular to the fibre direction. For the case in figure 4.1, the out-of-plane shear deformation γ^0_{yz} will have a direction as shown with the dotted deformed shape in that figure. Correspondingly, the out-of-plane shear deformation γ^0_{xz} could also occur when for example an inclination is added to a 45°-ply.

The original CLT derived in section 3.3 is no longer applicable. However, the same approach can be used to derive the modified CLT. It is now assumed that σ_{33}, σ_{23} and σ_{13} can be present, so plane stress conditions are not assumed to be applicable in the local coordinate system of each ply.

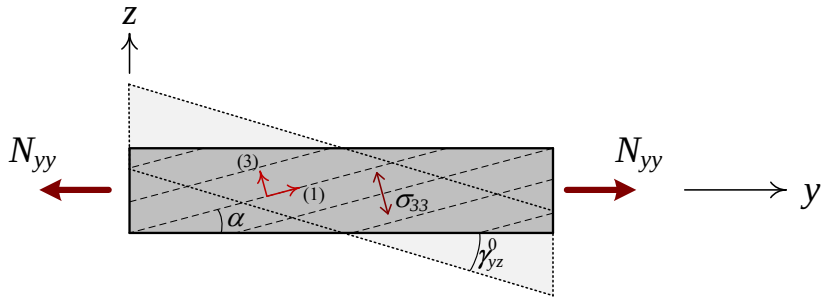

Figure 4.1: Possible stresses on a ply within a laminate with inclined plies.

For the individual plies, the constitutive relation in the local coordinate system from equation 3.6 is still the starting point. The 6×6 compliance matrix ($\overline{\mathbf{S}}$) for transversely isotropic materials has already been given in equation 3.11. For the regular CLT, this compliance matrix was reduced to meet the plane stress requirements. Since all

six stress components need to be taken into account for the modified CLT, no reduction of the compliance matrix is possible. The laminate constitutive equations require the stiffness matrix of a laminate as input, which can be obtained by taking the inverse of the compliance matrix (equation 3.5).

4.2. Transformation equations

The inclination that could be present in plies will affect the elastic behaviour of a laminate. To account for the inclination, a rotation about the x-axis is assumed in the derivation of the modified CLT. Figure 4.2 shows that α indicates a positive rotation from y to z. In this figure, the fibres in the 0°-plies are parallel to the x-axis[1]. The fibres in the 90°-plies are not oriented parallel to the y-axis due to the inclination α.

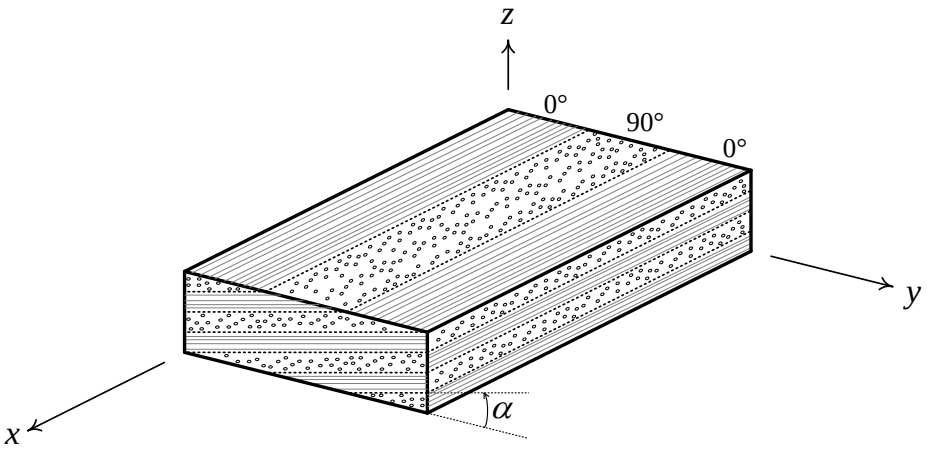

Figure 4.2: 3D representation of the inclined plies for 0°- and 90°-plies.

Section 3.2 contains an explanation of the transformation equations used in the CLT. Here, it was introduced that α, β and θ indicate a rotation about the x-, y- and z-axis respectively. For a laminate with inclined plies, it is assumed that θ still indicates the fibre orientation of the plies before an inclination is added. Furthermore, α relates to the additional rotation present in a laminate with inclined plies. Finally, the rotation β about the y-axis is still assumed to be zero, meaning $\mathbf{L}_y$ is equal to the identity matrix. Using the x-convention of the Euler angles, the total rotation matrix can be obtained by multiplication of the individual rotation matrices in the following specific order:

$$\mathbf{L} = \mathbf{L}_z\mathbf{L}_y\mathbf{L}_x = \begin{bmatrix} \cos\theta & \sin\theta & 0 \\ -\sin\theta & \cos\theta & 0 \\ 0 & 0 & 1 \end{bmatrix} \begin{bmatrix} 1 & 0 & 0 \\ 0 & 1 & 0 \\ 0 & 0 & 1 \end{bmatrix} \begin{bmatrix} 1 & 0 & 0 \\ 0 & \cos\alpha & \sin\alpha \\ 0 & -\sin\alpha & \cos\alpha \end{bmatrix} = \begin{bmatrix} \cos\theta & \cos\alpha\sin\theta & \sin\alpha\sin\theta \\ -\sin\theta & \cos\alpha\cos\theta & \sin\alpha\cos\theta \\ 0 & -\sin\alpha & \cos\alpha \end{bmatrix} \tag{4.1}$$

Section 3.2 also contains the derivation that relates the rotation matrix to the total transformation matrix using stress transformation from a local to a global coordinate system (equation 3.22). The resulting 3×3 stress tensor $\boldsymbol{\sigma}$ can be rearranged to a 6×1 stress vector using the matrix multiplication $\mathbf{L}^T\overline{\boldsymbol{\sigma}}\mathbf{L}$, which leads to the total transformation matrix:

$$\boldsymbol{\sigma} = \mathbf{T}_{\theta\alpha}\overline{\boldsymbol{\sigma}} \tag{4.2}$$

With:

$$\mathbf{T}_{\theta\alpha} = \begin{bmatrix} \cos\theta^2 & \sin\theta^2 & 0 & 0 & 0 & -2\cos\theta\sin\theta \\ \cos\alpha^2\sin\theta^2 & \cos\theta^2\cos\alpha^2 & \sin\alpha^2 & -2\cos\theta\sin\alpha\cos\alpha & -2\cos\alpha\sin\theta\sin\alpha & 2\cos\alpha^2\sin\theta\cos\theta \\ \sin\theta^2\sin\alpha^2 & \cos\theta^2\sin\alpha^2 & \cos\alpha^2 & 2\cos\theta\sin\alpha\cos\alpha & 2\cos\alpha\sin\theta\sin\alpha & 2\sin\theta\sin\alpha^2\cos\theta \\ \sin\theta^2\sin\alpha\cos\alpha & \cos\theta^2\sin\alpha\cos\alpha & -\cos\alpha\sin\alpha & \cos\alpha^2\cos\theta - \sin\alpha^2\cos\theta & \cos\alpha^2\sin\theta - \sin\alpha^2\sin\theta & 2\cos\alpha\sin\theta\sin\alpha\cos\theta \\ \cos\theta\sin\alpha\sin\theta & -\cos\theta\sin\alpha\sin\theta & 0 & -\cos\alpha\sin\theta & \cos\alpha\cos\theta & \cos\theta^2\sin\alpha - \sin\theta^2\sin\alpha \\ \cos\theta\cos\alpha\sin\theta & -\cos\theta\cos\alpha\sin\theta & 0 & \sin\alpha\sin\theta & -\sin\alpha\cos\theta & \cos\theta^2\cos\alpha - \sin\theta^2\cos\alpha \end{bmatrix} \tag{4.3}$$

[1]The x-axis corresponds to the main span direction of InfraCore panels.

Here, $\mathbf{T}_{\theta\alpha}$ represents the total transformation matrix after the two rotations θ and α. This matrix can be used to transfer the stiffness matrix in the local coordinate system to a stiffness matrix in the global coordinate system for every ply, which is needed as input for the laminate constitutive equations in the CLT:

$$\mathbf{C} = \mathbf{T}_{\theta\alpha}\overline{\mathbf{C}}\mathbf{T}_{\theta\alpha}^{T} \tag{4.4}$$

4.3. Laminate constitutive equations

For the laminate constitutive equations in the regular CLT, Kirchhoff assumptions were made for the plies and the laminate. For a laminate with inclined plies, it can still be assumed that straight lines perpendicular to the mid-surface remain straight after deformation of the laminate due to the fact that the laminate is still assumed to be a thin plate. However, the other two Kirchhoff assumptions are no longer valid in the derivation of the modified CLT. Since out-of-plane shear deformations could occur, it can no longer be stated that straight lines perpendicular to the mid-surface remain perpendicular to the mid-surface after deformation of the laminate. This means both γ_{xz}^{0} and γ_{yx}^{0} should be taken into account. Furthermore, it can no longer be assumed that the strain perpendicular to the plane of the ply (ε_{33}^{0}) is negligible, since the stress component σ_{33} must be taken into account, as described in section 4.1. As a result, the axial strain in the global z-direction will also be observed when the modified CLT is derived. All six strain components need to be taken into account. All six deformation components depend on the strain of the mid-surface of a ply and the curvature of the ply. Equation 3.42 can be expanded:

$$\begin{bmatrix} \varepsilon_{xx} \\ \varepsilon_{yy} \\ \varepsilon_{zz} \\ \gamma_{yz} \\ \gamma_{xz} \\ \gamma_{xy} \end{bmatrix} = \begin{bmatrix} \varepsilon_{xx}^{0} \\ \varepsilon_{yy}^{0} \\ \varepsilon_{zz}^{0} \\ \gamma_{yz}^{0} \\ \gamma_{xz}^{0} \\ \gamma_{xy}^{0} \end{bmatrix} + z \begin{bmatrix} \kappa_{xx} \\ \kappa_{yy} \\ \kappa_{zz} \\ \kappa_{yz} \\ \kappa_{xz} \\ \kappa_{xy} \end{bmatrix} \tag{4.5}$$

The definition for strain shown above could be implemented in the constitutive equation 3.1. This will relate the six stress components to the six strain components using the stiffness matrix $\mathbf{C}$ in the global coordinate system:

$$\boldsymbol{\sigma} = \mathbf{C}\boldsymbol{\varepsilon} \tag{4.6}$$

$$\begin{bmatrix} \sigma_{xx} \\ \sigma_{yy} \\ \sigma_{zz} \\ \tau_{yz} \\ \tau_{xz} \\ \tau_{xy} \end{bmatrix} = \mathbf{C}\left(\begin{bmatrix} \varepsilon_{xx}^{0} \\ \varepsilon_{yy}^{0} \\ \varepsilon_{zz}^{0} \\ \gamma_{yz}^{0} \\ \gamma_{xz}^{0} \\ \gamma_{xy}^{0} \end{bmatrix} + z \begin{bmatrix} \kappa_{xx} \\ \kappa_{yy} \\ \kappa_{zz} \\ \kappa_{yz} \\ \kappa_{xz} \\ \kappa_{xy} \end{bmatrix} \right) \tag{4.7}$$

Next, the resultant normal forces and moments need to be derived. Equation 3.45 gives the relevant integrals for the components that are needed in the derivation of the regular CLT. The normal force vector has six elements in total, three of which were also found in the regular CLT. The same holds for the moment vector. In total, twelve integrals need to be evaluated to determine the laminate stiffness matrix when plane stress conditions are not applicable. The following six integrals complete the result:

$$\begin{aligned} N_{zz} &= \int_{-\frac{1}{2}t_{\text{ply}}}^{\frac{1}{2}t_{\text{ply}}} \sigma_{zz}\,dz & N_{yz} &= \int_{-\frac{1}{2}t_{\text{ply}}}^{\frac{1}{2}t_{\text{ply}}} \tau_{yz}\,dz & N_{xz} &= \int_{-\frac{1}{2}t_{\text{ply}}}^{\frac{1}{2}t_{\text{ply}}} \tau_{xz}\,dz \\ M_{zz} &= \int_{-\frac{1}{2}t_{\text{ply}}}^{\frac{1}{2}t_{\text{ply}}} \sigma_{zz}z\,dz & M_{yz} &= \int_{-\frac{1}{2}t_{\text{ply}}}^{\frac{1}{2}t_{\text{ply}}} \tau_{yz}z\,dz & M_{xz} &= \int_{-\frac{1}{2}t_{\text{ply}}}^{\frac{1}{2}t_{\text{ply}}} \tau_{xz}z\,dz \end{aligned} \tag{4.8}$$

To derive the total forces and moments in a laminate, the individual plies must be combined. For a laminate analysed with the regular CLT, this was done by assuming a uniform strain over the height of the laminate. This would mean no jumps or kinks are observed in the strain diagram. However, due to the difference in effective

elastic modulus in the considered global direction, there are jumps and kinks observed in the stress diagram. This is also indicated in figure 3.7 and 3.8. The six force components can be written in vector shape, as well as the six moment components. To stack all the plies, the stiffness properties per ply can be added to each other to obtain the result for the complete laminate:

$$\boldsymbol{N} = \begin{bmatrix} N_{xx} \\ N_{yy} \\ N_{zz} \\ N_{yz} \\ N_{xz} \\ N_{xy} \end{bmatrix} = \sum_{i=1}^{n} \int_{z_{i-1}}^{z_i} \begin{bmatrix} \sigma_{xx} \\ \sigma_{yy} \\ \sigma_{zz} \\ \tau_{yz} \\ \tau_{xz} \\ \tau_{xy} \end{bmatrix} dz = \sum_{i=1}^{n} \left(\mathbf{C}_i \begin{bmatrix} \varepsilon^0_{xx} \\ \varepsilon^0_{yy} \\ \varepsilon^0_{zz} \\ \gamma^0_{yz} \\ \gamma^0_{xz} \\ \gamma^0_{xy} \end{bmatrix} \int_{z_{i-1}}^{z_i} dz + \mathbf{C}_i \begin{bmatrix} \kappa_{xx} \\ \kappa_{yy} \\ \kappa_{zz} \\ \kappa_{yz} \\ \kappa_{xz} \\ \kappa_{xy} \end{bmatrix} \int_{z_{i-1}}^{z_i} z dz \right) \tag{4.9}$$

$$\boldsymbol{M} = \begin{bmatrix} M_{xx} \\ M_{yy} \\ M_{zz} \\ M_{yz} \\ M_{xz} \\ M_{xy} \end{bmatrix} = \sum_{i=1}^{n} \int_{z_{i-1}}^{z_i} z \begin{bmatrix} \sigma_{xx} \\ \sigma_{yy} \\ \sigma_{zz} \\ \tau_{yz} \\ \tau_{xz} \\ \tau_{xy} \end{bmatrix} dz = \sum_{i=1}^{n} \left(\mathbf{C}_i \begin{bmatrix} \varepsilon^0_{xx} \\ \varepsilon^0_{yy} \\ \varepsilon^0_{zz} \\ \gamma^0_{yz} \\ \gamma^0_{xz} \\ \gamma^0_{xy} \end{bmatrix} \int_{z_{i-1}}^{z_i} z dz + \mathbf{C}_i \begin{bmatrix} \kappa_{xx} \\ \kappa_{yy} \\ \kappa_{zz} \\ \kappa_{yz} \\ \kappa_{xz} \\ \kappa_{xy} \end{bmatrix} \int_{z_{i-1}}^{z_i} z^2 dz \right) \tag{4.10}$$

Next, the integrals can be evaluated. It is assumed that both $\boldsymbol{\varepsilon^0}$ and $\boldsymbol{\kappa}$ are independent of z, so they can be taken out of the integrals. In the end, the following relation is obtained:

$$\begin{bmatrix} \boldsymbol{N} \\ \boldsymbol{M} \end{bmatrix} = \begin{bmatrix} \mathbf{A} & \mathbf{B} \\ \mathbf{B} & \mathbf{D} \end{bmatrix} \begin{bmatrix} \boldsymbol{\varepsilon^0} \\ \boldsymbol{\kappa} \end{bmatrix} \tag{4.11}$$

With:

$$\begin{aligned} \mathbf{A} &= \sum_{i=1}^{n} (z_i - z_{i-1}) \mathbf{C}_i \\ \mathbf{B} &= \sum_{i=1}^{n} \frac{1}{2} \left(z_i^2 - z_{i-1}^2 \right) \mathbf{C}_i \\ \mathbf{D} &= \sum_{i=1}^{n} \frac{1}{3} \left(z_i^3 - z_{i-1}^3 \right) \mathbf{C}_i \end{aligned} \tag{4.12}$$

Note that the ABD-matrix is no longer a 6×6-matrix, which was the case when plane stress conditions were applicable. Due to the three extra force components and the three extra moment components, the ABD-matrix will become a 12×12-matrix, which is shown in equation 4.14. Here, all the black elements are also present when plane stress conditions are assumed and a 6×6 ABD-matrix is obtained. However, the values are not the same compared to the entries in the 6×6 ABD-matrix:

$$\mathrm{ABD}_{ij}^{6\times6} \neq \mathrm{ABD}_{ij}^{12\times12} \tag{4.13}$$

For the 12×12 ABD-matrix, other multiplications have been performed compared to the ABD-matrix from the regular CLT, since both the transformation matrix and the stiffness matrix in the local coordinate system are larger. Furthermore, all the entries in the 12×12 matrix are now a function of α, which is completely absent in the regular CLT. The blue elements relate to the additional obtained stiffness parameters when the plane stress conditions are rejected.

$$\begin{bmatrix} N_{xx} \\ N_{yy} \\ N_{zz} \\ N_{yz} \\ N_{xz} \\ N_{xy} \\ \hdashline M_{xx} \\ M_{yy} \\ M_{zz} \\ M_{yz} \\ M_{xz} \\ M_{xy} \end{bmatrix} = \left[\begin{array}{cccccc:cccccc} A_{11} & A_{12} & A_{13} & A_{14} & A_{15} & A_{16} & B_{11} & B_{12} & B_{13} & B_{14} & B_{15} & B_{16} \\ A_{12} & A_{22} & A_{23} & A_{24} & A_{25} & A_{26} & B_{12} & B_{22} & B_{23} & B_{24} & B_{25} & B_{26} \\ A_{13} & A_{23} & A_{33} & A_{34} & A_{35} & A_{36} & B_{13} & B_{23} & B_{33} & B_{34} & B_{35} & B_{36} \\ A_{14} & A_{24} & A_{34} & A_{44} & A_{45} & A_{46} & B_{14} & B_{24} & B_{34} & B_{44} & B_{45} & B_{46} \\ A_{15} & A_{25} & A_{35} & A_{45} & A_{55} & A_{56} & B_{15} & B_{25} & B_{35} & B_{45} & B_{55} & B_{56} \\ A_{16} & A_{26} & A_{36} & A_{46} & A_{56} & A_{66} & B_{16} & B_{26} & B_{36} & B_{46} & B_{56} & B_{66} \\ \hdashline B_{11} & B_{12} & B_{13} & B_{14} & B_{15} & B_{16} & D_{11} & D_{12} & D_{13} & D_{14} & D_{15} & D_{16} \\ B_{12} & B_{22} & B_{23} & B_{24} & B_{25} & B_{26} & D_{12} & D_{22} & D_{23} & D_{24} & D_{25} & D_{26} \\ B_{13} & B_{23} & B_{33} & B_{34} & B_{35} & B_{36} & D_{13} & D_{23} & D_{33} & D_{34} & D_{35} & D_{36} \\ B_{14} & B_{24} & B_{34} & B_{44} & B_{45} & B_{46} & D_{14} & D_{24} & D_{34} & D_{44} & D_{45} & D_{46} \\ B_{15} & B_{25} & B_{35} & B_{45} & B_{55} & B_{56} & D_{15} & D_{25} & D_{35} & D_{45} & D_{55} & D_{56} \\ B_{16} & B_{26} & B_{36} & B_{46} & B_{56} & B_{66} & D_{16} & D_{26} & D_{36} & D_{46} & D_{56} & D_{66} \end{array}\right] \begin{bmatrix} \varepsilon^0_{xx} \\ \varepsilon^0_{yy} \\ \varepsilon^0_{zz} \\ \gamma^0_{yz} \\ \gamma^0_{xz} \\ \gamma^0_{xy} \\ \hdashline \kappa_{xx} \\ \kappa_{yy} \\ \kappa_{zz} \\ \kappa_{yz} \\ \kappa_{xz} \\ \kappa_{xy} \end{bmatrix} \tag{4.14}$$

The 12×12 ABD-matrix can be evaluated for a laminate without inclined plies (α=0). The result will be comparable with the regular CLT, with the difference that plane stress conditions are not assumed. The result is shown in equation 4.15, where it can be seen that many zero entries appear for α=0. These follow from the matrix multiplications done to obtain the global stiffness matrix (equation 4.4). Since the transformation matrix $\mathbf{T}_{\theta\alpha}$ reduces to the transformation matrix $\mathbf{T}$ used in the regular CLT (equation 3.25), it contains many zero entries for α=0. The stiffness matrix in the local coordinate system $\overline{\mathbf{C}}$ also contains many zeros for a transversely isotropic material. Due to all these zeros present in the transformation matrix and the stiffness matrix, the resulting 12×12 ABD-matrix also contains many zero's:

$$\begin{bmatrix} N_{xx} \\ N_{yy} \\ N_{zz} \\ N_{yz} \\ N_{xz} \\ N_{xy} \\ \hdashline M_{xx} \\ M_{yy} \\ M_{zz} \\ M_{yz} \\ M_{xz} \\ M_{xy} \end{bmatrix} = \left[\begin{array}{cccccc:cccccc} A_{11} & A_{12} & A_{13} & 0 & 0 & A_{16} & B_{11} & B_{12} & B_{13} & 0 & 0 & B_{16} \\ A_{12} & A_{22} & A_{23} & 0 & 0 & A_{26} & B_{12} & B_{22} & B_{23} & 0 & 0 & B_{26} \\ A_{13} & A_{23} & A_{33} & 0 & 0 & A_{36} & B_{13} & B_{23} & \boxed{0} & 0 & 0 & B_{36} \\ 0 & 0 & 0 & A_{44} & A_{45} & 0 & 0 & 0 & 0 & B_{44} & B_{45} & 0 \\ 0 & 0 & 0 & A_{45} & A_{55} & 0 & 0 & 0 & 0 & B_{45} & B_{55} & 0 \\ A_{16} & A_{26} & A_{36} & 0 & 0 & A_{66} & B_{16} & B_{26} & B_{36} & 0 & 0 & B_{66} \\ \hdashline B_{11} & B_{12} & B_{13} & 0 & 0 & B_{16} & D_{11} & D_{12} & D_{13} & 0 & 0 & D_{16} \\ B_{12} & B_{22} & B_{23} & 0 & 0 & B_{26} & D_{12} & D_{22} & D_{23} & 0 & 0 & D_{26} \\ B_{13} & B_{23} & \boxed{0} & 0 & 0 & B_{36} & D_{13} & D_{23} & D_{33} & 0 & 0 & D_{36} \\ 0 & 0 & 0 & B_{44} & B_{45} & 0 & 0 & 0 & 0 & D_{44} & D_{45} & 0 \\ 0 & 0 & 0 & B_{45} & B_{55} & 0 & 0 & 0 & 0 & D_{45} & D_{55} & 0 \\ B_{16} & B_{26} & B_{36} & 0 & 0 & B_{66} & D_{16} & D_{26} & D_{36} & 0 & 0 & D_{66} \end{array}\right] \begin{bmatrix} \varepsilon^0_{xx} \\ \varepsilon^0_{yy} \\ \varepsilon^0_{zz} \\ \gamma^0_{yz} \\ \gamma^0_{xz} \\ \gamma^0_{xy} \\ \hdashline \kappa_{xx} \\ \kappa_{yy} \\ \kappa_{zz} \\ \kappa_{yz} \\ \kappa_{xz} \\ \kappa_{xy} \end{bmatrix} \tag{4.15}$$

It can be seen that the out-of-plane shear forces N_{yz} and N_{xz} are only related to the out-of-plane shear strains and curvatures. This confirms that no out-of-plane shear deformations are possible for an axially loaded laminate without inclined plies, thus the Kirchhoff assumption that straight lines perpendicular to the mid-surface remain perpendicular to the mid-surface after deformation is valid for a laminate without inclined plies. Furthermore, since the stress σ_{33} was neglected for the regular CLT, the strain in z-direction was not taken into account. All the terms with a 3 in the subscript relate to the lateral contraction due to Poisson's ratio in the z-direction, which is now taken into account.

It should be noted that no coupling effect is present between N_{zz} and κ_{zz}. Correspondingly, there is also no coupling between M_{zz} and ε^0_{zz}, since both coupling effects are determined by the B_{33} element in the ABD-matrix, which is equal to zero as indicated with the boxes in equation 4.14. When a normal force in z-direction is applied to a laminate without inclination (α=0) and the lateral contraction is neglected (i.e. ν_{12} and ν_{23} are equal to zero), ε^0_{zz} is the only possible strain that could occur. This is indicated in figure 4.3, where the dashed lines indicate the deformation of the complete laminate due to N_{zz}. This kind of loading cannot lead to a curvature κ_{zz}, which leads to a value of zero for B_{33} for every laminate without inclined plies.

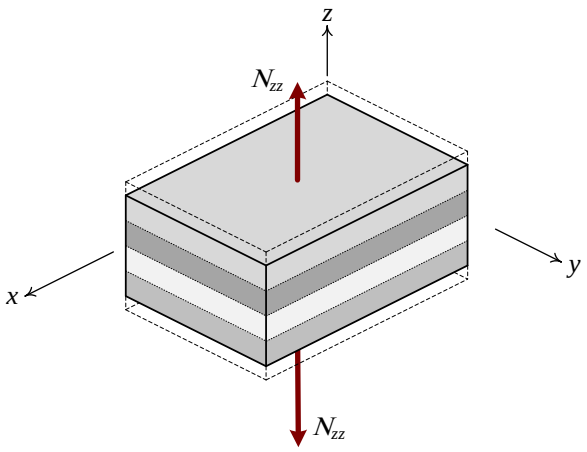

Figure 4.3: Normal force N_{zz} applied to a laminate without extra inclination.

4.3.1. Reduction of the ABD-matrix of the modified CLT

The ABD-matrix obtained with the modified CLT can be used to determine the elastic behaviour of laminated plates. The thickness is often very small compared to other plate dimensions. This means certain forces and moments can be neglected. First of all, the normal force in z-direction, as shown in figure 4.3, is usually not present, meaning N_{zz} can be assumed to be equal to zero. Furthermore, the additional moments that appear in the modified CLT (M_{zz}, M_{xz} and M_{yz}) are also not relevant and can therefore assumed to be equal to zero. When these conditions are applied to the inverse of equation 4.14, the corresponding rows and columns of the inverse of the ABD-matrix can be deleted. This will result in an 8×8-matrix. When that matrix is inverted back again, the following relation can be obtained:

$$\begin{bmatrix} N_{xx} \\ N_{yy} \\ N_{yz} \\ N_{xz} \\ N_{xy} \\ M_{xx} \\ M_{yy} \\ M_{xy} \end{bmatrix} = \left[\begin{array}{ccccc:ccc} A_{11} & A_{12} & A_{14} & A_{15} & A_{16} & B_{11} & B_{12} & B_{16} \\ A_{12} & A_{22} & A_{24} & A_{25} & A_{26} & B_{12} & B_{22} & B_{26} \\ A_{14} & A_{24} & A_{44} & A_{45} & A_{46} & B_{14} & B_{24} & B_{46} \\ A_{15} & A_{25} & A_{45} & A_{55} & A_{56} & B_{15} & B_{25} & B_{56} \\ A_{16} & A_{26} & A_{46} & A_{56} & A_{66} & B_{16} & B_{26} & B_{66} \\ \hdashline B_{11} & B_{12} & B_{14} & B_{15} & B_{16} & D_{11} & D_{12} & D_{16} \\ B_{12} & B_{22} & B_{24} & B_{25} & B_{26} & D_{12} & D_{22} & D_{26} \\ B_{16} & B_{26} & B_{46} & B_{56} & B_{66} & D_{16} & D_{26} & D_{66} \end{array}\right] \begin{bmatrix} \varepsilon^0_{xx} \\ \varepsilon^0_{yy} \\ \gamma^0_{yz} \\ \gamma^0_{xz} \\ \gamma^0_{xy} \\ \kappa_{xx} \\ \kappa_{yy} \\ \kappa_{xy} \end{bmatrix} \tag{4.16}$$

It should be stressed that the entries in the ABD-matrix in equation 4.16 are not equal to the corresponding entries in the ABD-matrix in equation 4.14:

$$\mathrm{ABD}_{ij}^{8\times 8} \neq \mathrm{ABD}_{ij}^{12\times 12} \tag{4.17}$$

In the determination of the engineering constants of the regular CLT described in section 3.4, only one type of loading is applied in order to determine an engineering constant. The other forces or moments are equal to zero. For the modified CLT, the same method can be used to determine the engineering constants. The additional forces and moments (N_{zz}, M_{zz}, M_{xz} and M_{yz}) are also equal to zero in the determination of the engineering constants of the modified CLT, meaning the engineering constants obtained with the 12×12 ABD-matrix will be equal to the engineering constants obtained with the reduced 8×8 ABD-matrix.

In conclusion, the reduced 8×8 ABD-matrix is a more compact form of the modified CLT. It is more practical in use since the irrelevant forces, moments, strains and curvatures are not taken into account.

4.4. Assumptions and limitations

The derivation of the modified CLT presented in this chapter has been done by making some assumptions. These assumptions lead to some limitations which should be mentioned before further results are produced.

4.4.1. Location of the ABD-matrix result

When an extra rotation about the x-axis is added to the plies within a laminate, the z-coordinate of a ply varies along the y-axis. In figure 4.4, a four-ply laminate is presented, including the extra inclination α. It can be seen that every ply runs from the bottom to the top within a laminate. This creates differences in lay-up of a laminate along its y-axis. This will eventually lead to an ABD-matrix that can only be assigned to one location of a laminate. So the ABD-matrix of an inclined laminate differs along the y-axis and, correspondingly, the equivalent stiffnesses differ along the y-axis.

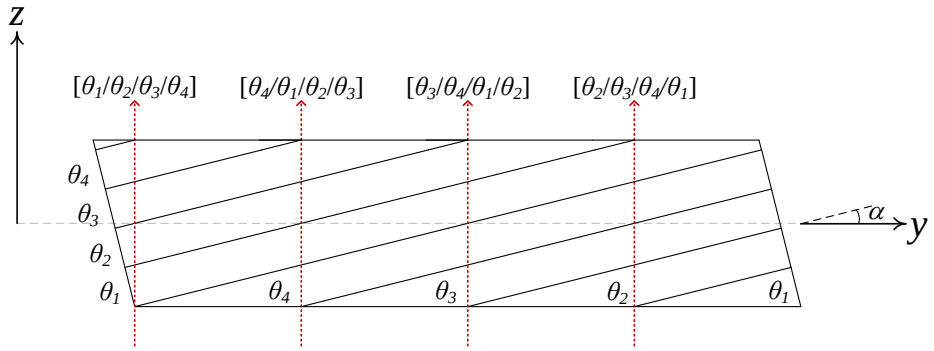

Figure 4.4: Location of the lay-up of an inclined laminate.

4.4.2. Thickness of the plies

In the original CLT, the thickness of the plies is required as input for the **A**, **B** and **D** matrices. The thickness is used to obtain the z-coordinate of the top and the bottom of a single ply within a laminate. It is assumed that the thickness measured perpendicular to the plane of the ply (t_{ply}) is constant. As the angle α increases, the thickness of the ply measured perpendicular to the plane of the laminate (t_α) will increase, since the cosine for α smaller than 90° is always smaller than 1.

$$\cos\alpha = \frac{t_{\text{ply}}}{t_\alpha} \qquad \Longrightarrow \qquad t_\alpha = \frac{t_{\text{ply}}}{\cos\alpha} \tag{4.18}$$

The total thickness of a laminate depends on the number of plies, and the thickness of each ply. If the laminate is inclined, the total thickness measured perpendicular to the plane of the laminate also depends on the inclination angle α.

$$t_{\text{tot},\alpha} = n\,t_\alpha = n\frac{t_{\text{ply}}}{\cos\alpha} \tag{4.19}$$

$$t_{\text{tot},0} = n\,t_{\text{ply}} \tag{4.20}$$

In figure 4.5, laminates with and without inclination α are shown. The total thickness is measured along the blue dashed line (perpendicular to the laminate). The red part located on the top of the inclined laminate is the extra thickness, and is the difference between the total thickness of a laminate with and without an extra inclination α, which will be referred to as Δt_{tot}:

$$\begin{aligned}\Delta t_{\text{tot}} &= t_{\text{tot},\alpha} - t_{\text{tot},0} \\ &= n\,t\left(\frac{1}{\cos\alpha} - 1\right)\end{aligned} \tag{4.21}$$

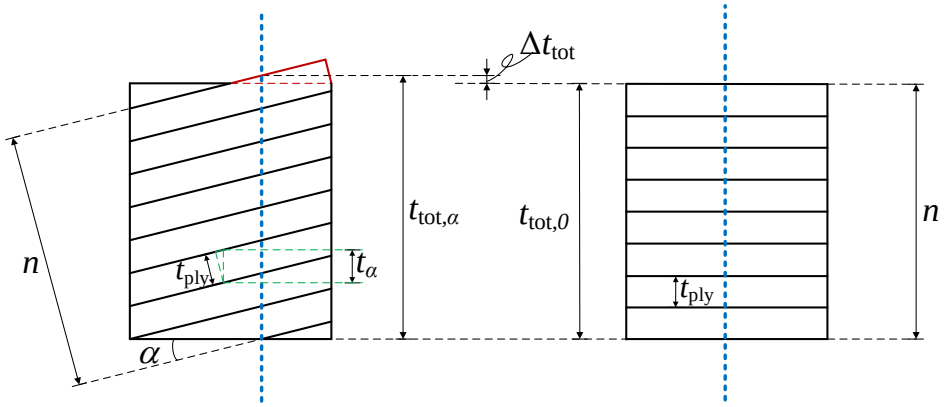

Figure 4.5: Assumed dimensions of an inclined laminate, where n indicates the number of plies.

Equation 4.21 has been divided by nt_{ply} on both sides in order to obtain the relative increase of the total thickness difference as a function of α. The result can be seen in figure 4.6, and confirms that the total thickness increases when α increases. For $\alpha = 90°$, the cosine will be equal to 0, which means the thickness of an inclined ply t_α will go to infinity. Therefore, it must be mentioned that α must be smaller than 90° for the derivation of the modified CLT presented in the previous sections to have a practical meaning. For the moment, it is assumed that the results for $\alpha < 20°$ will provide sufficient insight in the increase of thickness.

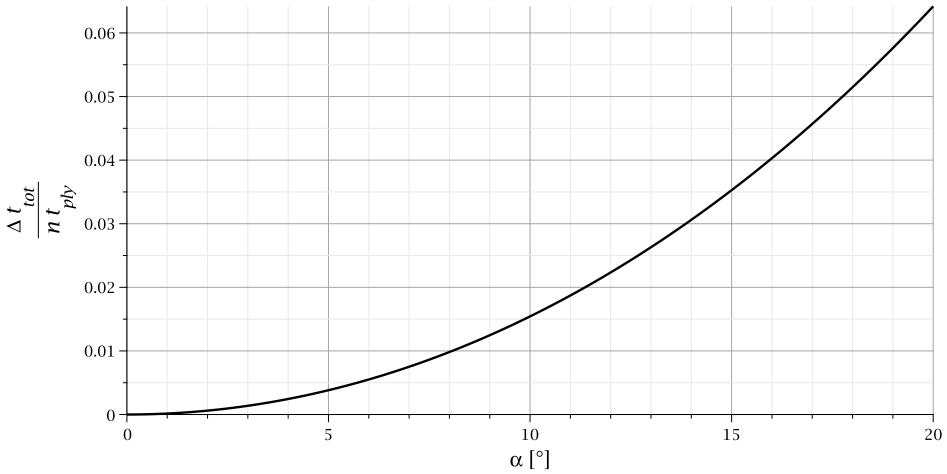

Figure 4.6: Increase of the total thickness difference, with respect to the total thickness nt_{ply} for a laminate without inclination.

As mentioned before in section 4.4.1, the result of the modified CLT will only be applicable to one location in the cross section. This means that the difference in thickness of the plies when the angle α increases does not cause a problem for the modified CLT. Since only one location is considered in the modified CLT, the thickness of the plies, which serves as input for the modified CLT, can simply be altered to the desired thickness.

4.4.3. Modified ABD-matrix with respect to InfraCore

The skin of an InfraCore panel consists of plies that continue through the web and to the other skin. The presented modified CLT is only applicable to the skins of the InfraCore panel. Figure 4.7 shows a close up of the top skin, where the orange lines are added to indicate the extra inclination that is present. It can also clearly be seen that the plies from the webs enter the skin, causing differences in lay-up.

Figure 4.7: Close up of an InfraCore skin.

The plies that enter the skin from the web are usually the ±45°-layers. In the skin, these plies are complemented with extra plies in the 0°-direction. The InfraCore panel is finished with a horizontal top ply, which will not be taken into account in the modified CLT. In figure 4.8a, the InfraCore skin has been simplified to uniform plies that run from the bottom to the top within a laminate. In this figure, it is assumed that five webs are present, namely on every location where the plies start at the bottom, so where the dashed lines are shown. As mentioned before, the plies end at the top of the laminate, causing a sawtooth-shaped laminate. However, this shape cannot be expressed in a plate theory like the CLT. Therefore, the sawtooth-shaped skin has been simplified to a plate with inclined plies. This can be seen in figure 4.8b, where the blue lines correspond to the sawtooth shaped skin of InfraCore.

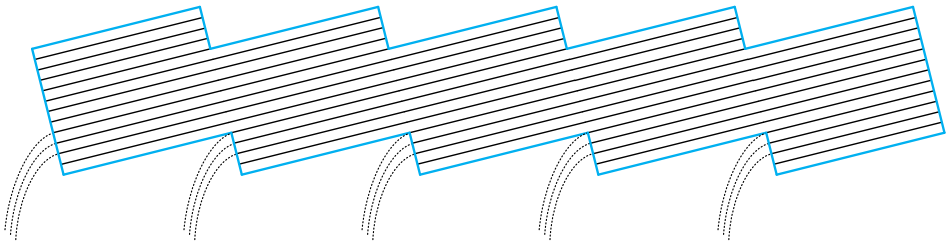

(a) Simplification of an InfraCore skin with the sawtooth shape. The dashed lines indicate the ±45° plies that continue in the web of an InfraCore panel.

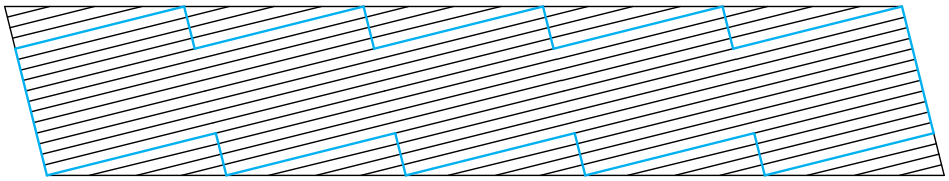

(b) InfraCore skin simplification for the modified CLT.

Figure 4.8: Simplifications of an InfraCore skin.

It should be noted that since the result of the modified CLT is only applicable to a single location in the laminate (as described in section 4.4.1), the differences between the simplifications shown in the figures 4.8a and 4.8b will only affect the lay-up input of the modified CLT.

4.4.4. Input modified CLT

In the modified CLT, individual plies can be inserted. Every ply is rotated with angle α individually, creating a complete inclined laminate. It is however also possible to use the original CLT to obtain engineering constants for the laminates that represent the InfraCore skins. These engineering constants could be used as input for the orthotropic material properties of one equivalent ply representing the complete InfraCore skin. This equivalent ply could then be rotated with angle α using the modified CLT. It should be checked whether differences occur between the two methods and, if this is the case, what these differences comprise.

5

Numerical verification of the modified CLT

The derived modified CLT must be verified before it can be used properly to obtain relevant results. A finite element (FE) analysis has been used to check the validity of the modified CLT.

5.1. Finite element model

The regular CLT results in a 6×6 ABD-matrix, which relates the strains and curvatures to the normal forces and moments. Here, both the normal forces and the moments are defined per unit width, since an integration over the thickness of the laminate is applied in the derivation of the regular CLT. For the verification of the regular CLT, a plate with unit length along both edges has been chosen: $l_x = l_y = 1$ m, as can be seen in figure 5.1. The thickness t of the plate depends on the type of laminate that is compared and will be specified later.

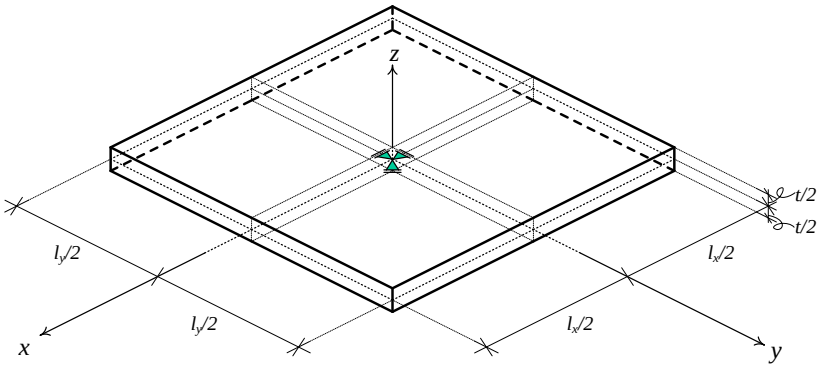

Figure 5.1: FE model of a plate simply supported at its center.

The plate is simply supported in all three directions at its center. Since the plate can still rotate in three directions around its center, there are still three extra boundary conditions needed to make the three-dimensional problem kinematically determinate. When a total of six boundary conditions is used, the structure will be statically determinate and all deformations will still be possible to occur. These extra boundary conditions depend on the type of loading, as they may not hinder the possible deformations due to a certain type of loading. Laminates are often predominantly loaded in their plane, which makes the normal force components N_{xx} and N_{yy} the most relevant loading types to be checked. These loads will be applied to certain laminates and the corresponding strains and curvatures according to the regular CLT will show which kind of deformations of the plate are possible. This will lead to the relevant extra boundary conditions that need to be applied to each case. To determine the analytic result, it is necessary to invert the ABD-matrix:

$$\begin{bmatrix} \boldsymbol{\varepsilon^0} \\ \boldsymbol{\kappa} \end{bmatrix} = \begin{bmatrix} \mathbf{A} & \mathbf{B} \\ \mathbf{B} & \mathbf{D} \end{bmatrix}^{-1} \begin{bmatrix} \boldsymbol{N} \\ \boldsymbol{M} \end{bmatrix} \tag{5.1}$$

The procedure described above is necessary to check whether the regular CLT results can be compared to FE analyses. It is therefore assumed that the analytic results of the regular CLT are correct. If the FE analysis

gives the same results for all the strains and curvatures, it can be assumed that the method used to extract the results from the FE model is correct. The next step is to check whether the analytic result from the modified CLT matches with the result from an FE analysis. In that case, the ABD-matrix in equation 5.1 will be a 12×12 matrix and three extra strain components and three extra curvature components appear. The full 12×12 ABD-matrix will be used for the verification, since it is a more complete result of the modified CLT. The reduced 8×8 ABD-matrix will give the same results, so the verification of the 12×12 ABD-matrix will also suffice for the reduced 8×8 ABD-matrix. The next section will discuss the method to obtain the strains and curvatures from the FE results.

5.2. Processing finite element results

In the FE analysis, the plate is loaded by edge forces. These are all in equilibrium, for example the same load N_{xx} is applied in negative direction on the negative x-face as the load N_{xx} in positive direction on the positive x-face. This ensures all the support reactions are equal to zero, making the boundary conditions only necessary for making the problem kinematically determinate. The results that need to be obtained are displacements and rotations of nodes. Every node has an x-, y- and z-coordinate, so the displacement and rotation results will be written as a function of those coordinates:

$$\begin{aligned}
\text{Displacment in } x\text{-direction} &\rightarrow U_x(x,y,z)\\
\text{Displacment in } y\text{-direction} &\rightarrow U_y(x,y,z)\\
\text{Displacment in } z\text{-direction} &\rightarrow U_z(x,y,z)\\
\text{Rotation about the } x\text{-axis} &\rightarrow \Phi_x(x,y,z)\\
\text{Rotation about the } y\text{-axis} &\rightarrow \Phi_y(x,y,z)\\
\text{Rotation about the } z\text{-axis} &\rightarrow \Phi_z(x,y,z)
\end{aligned} \tag{5.2}$$

For the FE model, only nodal values can be evaluated. For a laminate, there is often more than one strain or curvature present. If the displacements and rotations are evaluated along the mid-lines of the plate, the different strains and curvatures do not impede with each other. For example, the displacement of the positive x-face can correctly be determined by evaluating the displacement at the node with the coordinates $\left(\frac{l_x}{2},0,0\right)$, where l_x is defined in figure 5.1.

To obtain the right strains and curvatures from an FE analysis, all those deformation variables must be defined properly for the (laminated) plate depicted in figure 5.1. The modified CLT contains six strain components and six curvature components. For the regular CLT, this reduces to three strain components and three curvature components, but these are defined the same as the corresponding components in the modified CLT.

5.2.1. Strains

Distinction can be made between axial strains (ε^0_{xx}, ε^0_{yy} and ε^0_{zz}) and shear strains (γ^0_{yz}, γ^0_{xz} and γ^0_{xy}). These are all strains of the mid-surface, hence the 0 in the superscript.

Axial strains

The axial strains can appear in all three global directions. For both the regular and modified CLT, the strains in x- and y-direction are present. The axial strain in z-direction only appears in the non-reduced modified CLT. Figure 5.2 shows the three types of axial strains.

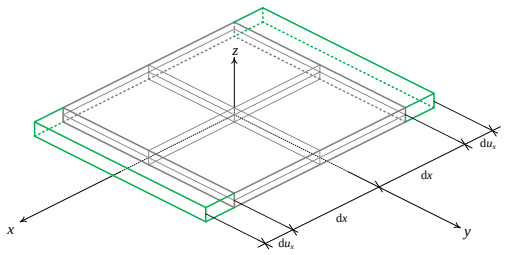

(a) Axial strain in x-direction (ε^0_{xx}).

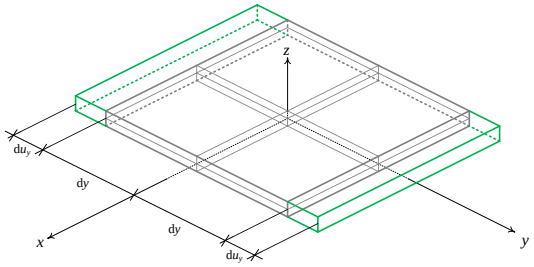

(b) Axial strain in y-direction (ε^0_{yy}).

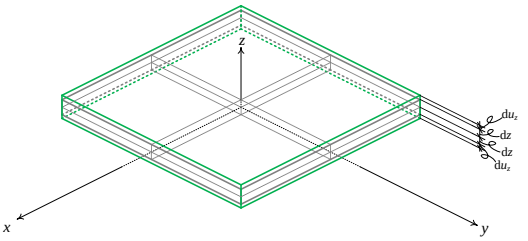

(c) Axial strain in z-direction (ε^0_{zz}).

Figure 5.2: Axial strains. The green lines indicate the deformed shape of the plate.

An axial strain is defined as the ratio between the elongation and the length in the global direction of a plate [3]. The values for l_x and l_y are equal to 1 for the current case, but t is kept variable, since it depends on the type of laminate that is evaluated. It should also be noted that the average is taken between the nodal displacements at both ends. Due to the negative direction of the assumed displacement u_i at the negative face i, this value must be subtracted from the corresponding displacement u_i at the positive face i (with $i = x, y, z$). This results in the following equations for the axial strains:

$$\varepsilon^0_{xx} = \frac{\partial u_x}{\partial x} = \frac{U_x\left(\frac{l_x}{2},0,0\right) - U_x\left(-\frac{l_x}{2},0,0\right)}{l_x} = U_x\left(\tfrac{1}{2},0,0\right) - U_x\left(-\tfrac{1}{2},0,0\right) \tag{5.3}$$

$$\varepsilon^0_{yy} = \frac{\partial u_y}{\partial y} = \frac{U_y\left(0,\frac{l_y}{2},0\right) - U_y\left(0,-\frac{l_y}{2},0\right)}{l_y} = U_y\left(0,\tfrac{1}{2},0\right) - U_y\left(0,-\tfrac{1}{2},0\right) \tag{5.4}$$

$$\varepsilon^0_{zz} = \frac{\partial u_z}{\partial z} = \frac{U_z\left(0,0,\frac{t}{2}\right) - U_z\left(0,0,-\frac{t}{2}\right)}{t} \tag{5.5}$$

Shear strains

There are two types of shear strains that could occur for a plate. The in-plane shear strain γ^0_{xy} appears in both the regular and modified CLT. Out-of-plane shear strains (γ^0_{yz} and γ^0_{xz}) could also occur in the modified CLT. These are shear strains that cause out-of-plane deformations, thus these do not appear in the regular CLT where Kirchhoff assumptions were applicable. The positive definitions for the shear strains are given in figure 5.3.

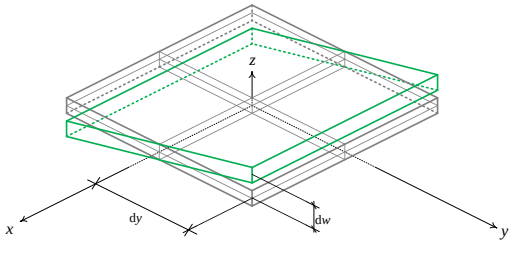

(a) Out-of-plane shear strain γ^0_{yz}.

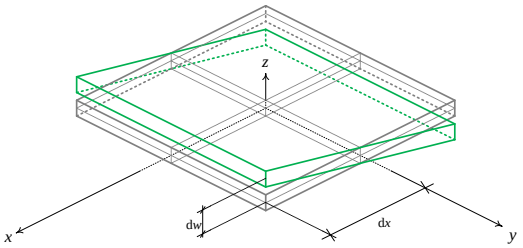

(b) Out-of-plane shear strain γ^0_{xz}.

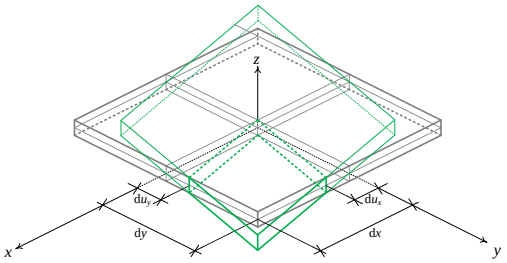

(c) In-plane shear strain γ^0_{xy}.

Figure 5.3: Shear strains. The green lines indicate the deformed shape of the plate.

The out-of-plane shear strains can be determined by evaluating the ratio between the deflection w and the distance to the origin of that deflection [3]. The average of both faces has been taken for the out-of-plane shear strains. It should be noted that a positive shear strain γ^0_{yz} is defined as a positive displacement in z-direction at the positive y-edge. For the shear strain γ^0_{xz}, the positive definition is given as a positive displacement in z-direction of the positive x-face. The in-plane shear strain γ^0_{xy} corresponds to the engineering shear strain, and depends on the deformation in both x- and y-direction, as well as on the dimensions in x- and y-direction [3].

$$\gamma^0_{yz} = \frac{\partial w}{\partial y} = \frac{U_z\left(0, \frac{l_y}{2}, 0\right) - U_z\left(0, -\frac{l_y}{2}, 0\right)}{l_y} = U_z\left(0, \tfrac{1}{2}, 0\right) - U_z\left(0, -\tfrac{1}{2}, 0\right) \tag{5.6}$$

$$\gamma^0_{xz} = \frac{\partial w}{\partial x} = \frac{-U_z\left(\frac{l_x}{2}, 0, 0\right) + U_z\left(-\frac{l_x}{2}, 0, 0\right)}{l_x} = U_z\left(\tfrac{1}{2}, 0, 0\right) - U_z\left(-\tfrac{1}{2}, 0, 0\right) \tag{5.7}$$

$$\gamma^0_{xy} = \frac{\partial u_x}{\partial y} + \frac{\partial u_y}{\partial x} = \frac{U_x\left(0, \frac{l_y}{2}, 0\right)}{\frac{l_y}{2}} + \frac{U_y\left(\frac{l_x}{2}, 0, 0\right)}{\frac{l_x}{2}} = 2\left(U_x\left(0, \tfrac{1}{2}, 0\right) + U_y\left(\tfrac{1}{2}, 0, 0\right)\right) \tag{5.8}$$

5.2.2. Curvatures

Distinction can be made between bending curvatures (κ_{xx}, κ_{yy} and κ_{zz}) and torsional curvatures (κ_{yz}, κ_{xz} and κ_{xy}).

Bending curvatures

The out-of-plane bending curvatures κ_{xx} and κ_{yy} are included in both the regular and modified CLT. The in-plane bending curvature κ_{zz} only appears in the non-reduced modified CLT, but is deleted when the reduced modified CLT is obtained. It is defined as the variation in axial strain ε^0_{xx} in z-direction. This cannot be visualised for a single layer and is therefore not taken into account in the verification. The positive definitions of the other two bending curvatures are shown in figure 5.4.

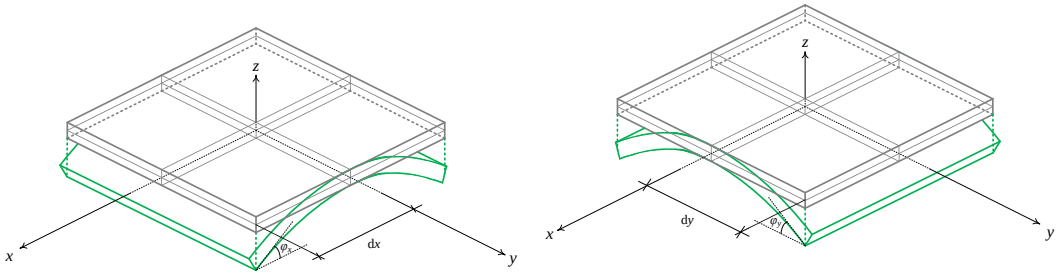

(a) Out-of-plane bending curvature κ_{xx}.

(b) Out-of-plane bending curvature κ_{yy}.

Figure 5.4: Bending curvatures. The green lines indicate the deformed shape of the plate.

The out-of-plane bending curvatures κ_{xx} and κ_{yy} are defined using the rotations at the end of the plate [3]. The positive rotation in x-direction (φ_x) is defined by the deformed shape due to a positive bending moment M_{xx}. It corresponds to the positive rotation of the plate about the y-axis. This means the rotation Φ_y is needed to evaluate the out-of-plane bending curvatures κ_{xx}. The same holds for the positive rotation in y-direction (φ_y), which is defined by the deformed shape due to a positive bending moment M_{yy}. It corresponds to the negative rotation of the plate about the x-axis from the FE results. Note the extra minus sign due to the fact that a positive deformed shape results in a negative rotation at the end of the plate.

$$\kappa_{xx} = \frac{\partial \varphi_x}{\partial x} = \frac{\Phi_y\left(\frac{l_x}{2},0,0\right) - \Phi_y\left(-\frac{l_x}{2},0,0\right)}{l_x} = \Phi_y\left(\tfrac{1}{2},0,0\right) - \Phi_y\left(-\tfrac{1}{2},0,0\right) \tag{5.9}$$

$$\kappa_{yy} = \frac{\partial \varphi_y}{\partial y} = \frac{-\Phi_x\left(0,\frac{l_y}{2},0\right) + \Phi_x\left(0,-\frac{l_y}{2},0\right)}{l_y} = -\Phi_x\left(0,\tfrac{1}{2},0\right) + \Phi_x\left(0,-\tfrac{1}{2},0\right) \tag{5.10}$$

Torsional curvatures

Two types of in-plane torsional curvatures arise in the non-reduced modified CLT: κ_{yz} and κ_{xz}. The out-of-plane torsional curvature κ_{xy} appears in both the regular and modified CLT. Figure 5.5 shows the deformed shapes for the three torsional curvatures.

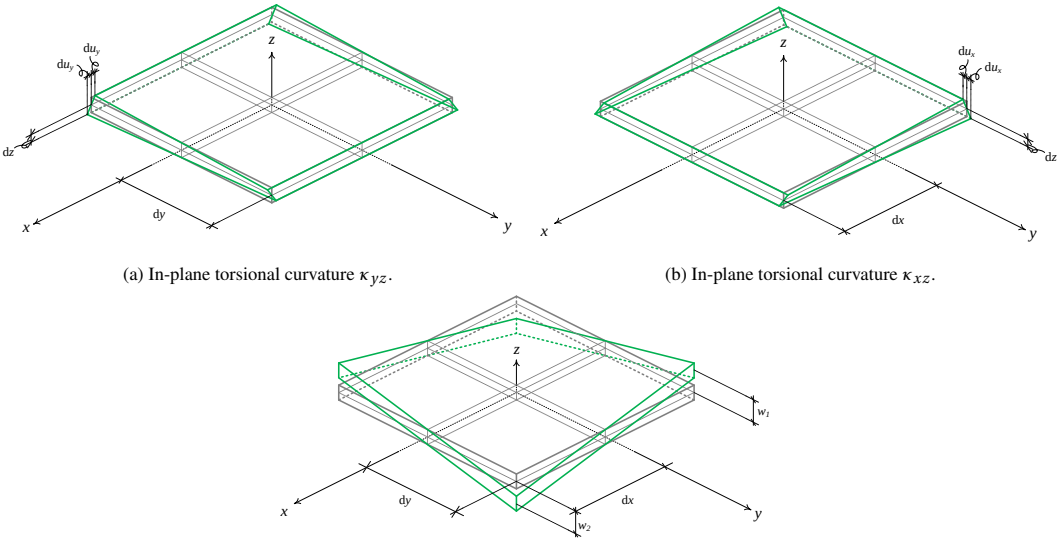

(a) In-plane torsional curvature κ_{yz}.

(b) In-plane torsional curvature κ_{xz}.

(c) Out-of-plane torsional curvature κ_{xy}.

Figure 5.5: Torsional curvatures. The green lines indicate the deformed shape of the plate.

Since it is assumed that the thickness is small compared to the plate dimensions, it can be assumed that the in-plane torsional curvatures are not relevant and thus do not have to be evaluated from the FE results. The in-plane torsional curvatures are also deleted in the derivation of the reduced modified CLT.

The definition of the out-of-plane torsional curvature is given by the second partial derivative of the deflection w with respect to x and y [3]. The corner deflections are needed from the FE results in order to obtain the right value for κ_{xy}. All four corners are used to evaluate the average out-of-plane torsional curvature.

$$\begin{aligned}\kappa_{xy} = -2\frac{\partial^2 w}{\partial x \partial y} = -2\frac{w_1 - w_2}{2\frac{l_x}{2}\frac{l_y}{2}} &= 2\frac{\frac{U_z\left(\frac{l_x}{2},-\frac{l_y}{2},0\right)+U_z\left(-\frac{l_x}{2},\frac{l_y}{2},0\right)}{2} - \frac{U_z\left(\frac{l_x}{2},\frac{l_y}{2},0\right)+U_z\left(-\frac{l_x}{2},-\frac{l_y}{2},0\right)}{2}}{\frac{1}{2}l_x l_y} \\ &= 2\left(U_z\left(\tfrac{1}{2},-\tfrac{1}{2},0\right) + U_z\left(-\tfrac{1}{2},\tfrac{1}{2},0\right) - U_z\left(\tfrac{1}{2},\tfrac{1}{2},0\right) - U_z\left(-\tfrac{1}{2},-\tfrac{1}{2},0\right)\right)\end{aligned} \tag{5.11}$$

5.3. Regular CLT comparison

To compare the regular CLT results with the result from an FE analysis, a four-ply laminate has been chosen. It has a lay-up of $[0/-45/0/90]$, making it non-symmetric and non-balanced. This means the ABD-matrix will only contain non-zero entries, so for every type of loading, all three strain components and all three curvature components from the regular CLT will appear. This means only one type of loading will suffice to check whether the method to evaluate the strains and curvatures from the FE analysis is correct. In this case, a normal force in x-direction N_{xx} will be applied. No extra boundary conditions are applied, in order to obtain rotational symmetric displacements with respect to the mid-point.

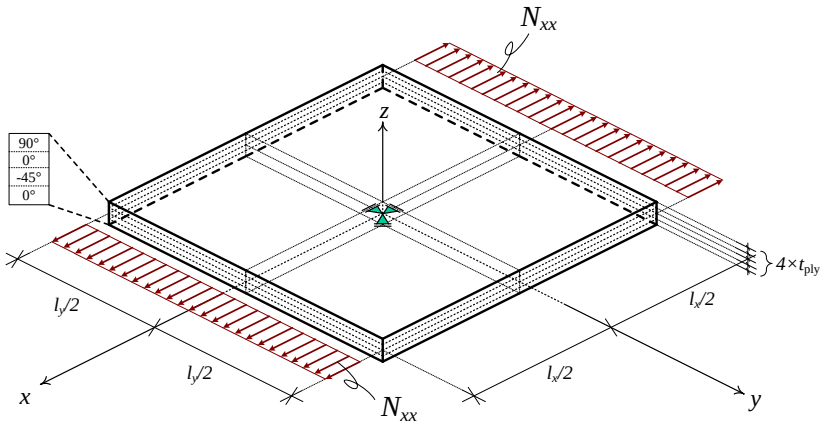

Figure 5.6: FE model of a four-ply laminate loaded by a normal force N_{xx}.

Figure 5.6 shows the model used to compare the values of the CLT with FE results. The mid-surface is shown to indicate where the boundary conditions in the center are applied. This mid-surface is located between the $-45°$ ply and the second $0°$ ply. The lay-up is shown on the left in the figure, where the first ply in the $[0/-45/0/90]$ lay-up is located at the bottom of the laminate. Both l_x and l_y are equal to 1 m and the ply thickness t_{ply} is equal to 0.0005 m, making the total laminate thickness equal to 0.002 m. All the input variables are included in table 5.1. The five independent transversely isotropic material parameters for a unidirectional E-glass/epoxy ply are given in table 2.3.

Table 5.1: Input variables for the four-ply laminate.

Property	Value
Lay-up	$[0/-45/0/90]$
l_x	1 m
l_y	1 m
t_{ply}	0.0005 m
N_{xx}	10000 N/m

Using the relation in equation 5.1, the strains and curvatures corresponding to a N_{xx} load can be determined and will be the following:

$$\begin{bmatrix} \varepsilon^0_{xx} \\ \varepsilon^0_{yy} \\ \gamma^0_{xy} \\ \kappa_{xx} \\ \kappa_{yy} \\ \kappa_{xy} \end{bmatrix} = \begin{bmatrix} 0.0002205 \\ -0.0000510 \\ 0.0000445 \\ 0.1078517 \\ 0.0311241 \\ -0.0281576 \end{bmatrix} \tag{5.12}$$

These values need to be compared to results from an FE analysis. For the regular CLT, there are two options which will both be discussed. First of all, many FE packages include the option to assign the values of an ABD-matrix to a sheet. This should give very similar results compared to the analytic solution, since the same assumptions are applicable to both a thin sheet structure in an FE analysis and a laminate in the regular CLT (plane stress conditions and Kirchhoff assumptions). The second possibility is to add every ply individually with solid elements. Every ply can have its own local coordinate system, making it possible to assign different material orientations to each ply. It should be noted that with use of solid elements, the FE results are not obtained under plane stress conditions or Kirchhoff assumptions. However, if a sufficiently thin plate is used, the solid elements approach the Kirchhoff assumptions for the complete structure. In this case, the length to width ratio is equal to 500 for the complete laminate, meaning the laminate can be assumed to be a very thin plate. Due to this high length to width ratio, it can be assumed that the FE result with solid elements should be comparable to the FE results of a sheet.

5.3.1. ABD-matrix input

Diana has been used to perform the FE analysis. The ABD-matrix entries of the regular CLT for the four-ply laminate have been used as input for a laminated composite material. Four sheets have been used, in order to be able to add the boundary conditions at the center of the plate, as can be seen in figure 5.7a. Furthermore, an outward normal distributed force of 10000 N/m is applied on both the positive and negative x-edges of the plate to represent the load N_{xx}. A Q20SF element has been used, which is a four-node quadrilateral flat shell element with five degrees of freedom per node. As element size 0.0025 m is used, resulting in a total of 1600 elements. The mesh is shown in figure 5.7b.

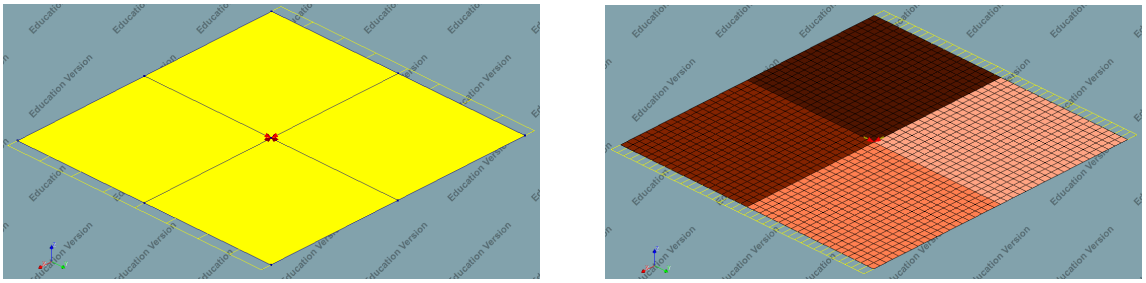

(a) Geometry overview.

(b) Mesh overview.

Figure 5.7: Diana model of a sheet with ABD-matrix properties.

A structural linear static analysis has been performed, since the CLT is also only applicable to linear elastic material behaviour and no dynamic loading is applied. Due to the non-zero **B**-matrix, out-of-plane deformations should occur as a result of coupling effects. Figure 5.8 shows the displacements in z-direction. These are exactly equal to zero at the center of the plate due to the applied boundary conditions. All the edges do show an out-of-plane deformation, confirming the presence the coupling effect.

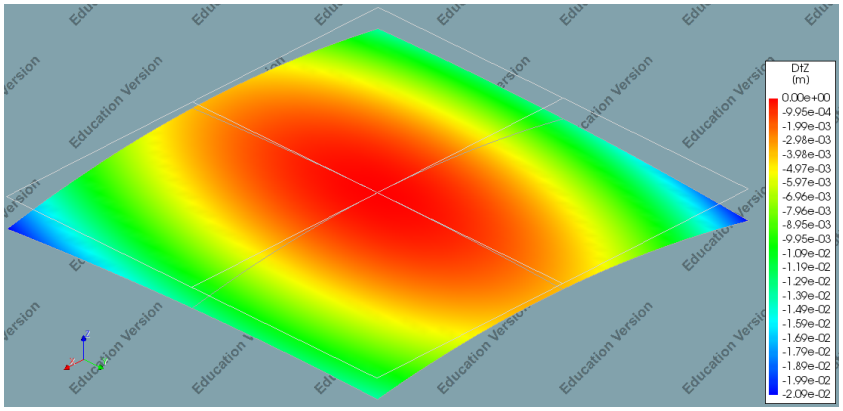

Figure 5.8: Displacements in z-direction for the four-ply laminate with ABD-matrix input.

The results for the six deformation variables are shown in table 5.2. Here, the first column contains the analytic results, which were also presented in equation 5.12. The second column indicates the FE results according to all the relations derived in section 5.2. The values in these first two columns have been rounded to nine decimal places for simplicity in the table. The last column shows the ratio between the former two columns, where the non-rounded values of the FE results have been divided by the non-rounded values of the analytic CLT results. It can be seen that all the ratios are very close to 1. On average, the ratios are only 1.6×10^{-6} off of 1 (or 0.00016%), meaning the results from the FE analysis are very close to the analytic results from the CLT. The small differences can be assigned to numerical errors in the FE analysis due to discretisation of the problem.

Table 5.2: Results of a four-ply laminate with a load N_{xx} with the ABD-matrix used as input in the FE analysis.

	CLT value	FE result	Ratio FE/CLT
ε^0_{xx}	0.000220499	0.000220499	1.00000033
ε^0_{yy}	−0.000050998	−0.000050998	0.99999946
γ^0_{xy}	0.000044530	0.000044530	0.99999876
κ_{xx}	0.107851705	0.107851805	1.00000092
κ_{yy}	0.031124138	0.031124043	0.99999694
κ_{xy}	−0.028157583	−0.028157679	1.00000341

5.3.2. Solid elements input

Another possibility to compare the CLT result to results from an FE analysis, is to use solid elements. Every ply will be put individually as a block element in the Diana model. For the four-ply laminate, this means a total of 16 block elements are needed, since there must be a node present at the center of the structure. Due to the high thickness to width ratio, the geometry looks like a sheet in figure 5.9a, but the close-up in figure 5.9c shows that indeed four individual layers of solid elements have been used to represent the plies.

In order to assign the transversely isotropic material properties to each ply, an orthotropic material is chosen. It has nine input parameters, of which five are independent for a transversely isotropic material. The other four dependent material properties can be derived using the relations given in section 3.1. Every ply has its own local coordinate system. In Diana, this requires input of the global coordinates of an arbitrary point on the local x- and y-axis. The corresponding local z-axis is then derived automatically for a right-handed coordinate system. For the four-ply laminate with lay-up $[0/-45/0/90]$, the global coordinates are shown in table 5.3.

Table 5.3: Global coordinates of an arbitrary point on the local x- and y-axis.

	Local x-axis			Local y-axis		
	x	y	z	x	y	z
0°	1	0	0	0	1	0
−45°	1	-1	0	1	1	0
0°	1	0	0	0	1	0
90°	0	1	0	1	0	0

The Diana model makes use of HX24L elements, which is an eight-node brick element with three translational degrees of freedom per node. There are no rotational degrees of freedom in the nodes, but to evaluate the curvatures κ_{xx} and κ_{yy} the rotation about the y- and x-axis are needed respectively (see also equations 5.9 and 5.10). The thin plate does have a rotation about the x- and y-axis, but due to the limitation of the solid finite element used, it cannot be read in the results. The solution is to add an extra sheet with four-node quadrilateral flat shell elements (Q20SF). These elements do have rotational degrees of freedom, which means the rotation about the x- and y-axis can be extracted from the FE results. The very thin sheet ($t = 10^{-5}$ m) is assigned with very low isotropic material properties ($E = 0.1$ N/m^2, $\nu = 0$) compared to the ply properties, so the extra sheet does not affect the FE results in a way that it could prevent the possibility of comparing the FE results with the analytic results from the CLT. It is only added to be able to read the rotation about the x- and y-axis.

The solid elements used require a minimal thickness, so they do behave as a solid element [6]. If the thickness is too small compared to the length and width of the element, it might not perform well since it would behave like a shell element. This means a small mesh size is required to meet the minimal thickness requirement of the solid elements. An element size of 0.02 m has been chosen, making a total of 2500 solid elements per ply and thus 10000 solid elements in total. An extra 2500 shell elements have been used to discretise the thin sheet.

To apply the load N_{xx} to the laminate, a distributed force q_x has been applied to the positive and negative x-face. This force is distributed over the surface of the faces, thus it has a unit of N/m^2. This means the load N_{xx} must be divided by the laminate thickness to obtain the correct distributed force:

$$q_x = \frac{N_{xx}}{4 \times t_{\text{ply}}} = \frac{10000}{4 \times 0.0005} = 5 \times 10^6 \text{ N/m}^2 \tag{5.13}$$

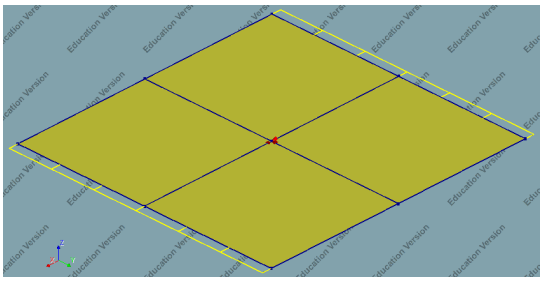

(a) Geometry overview.

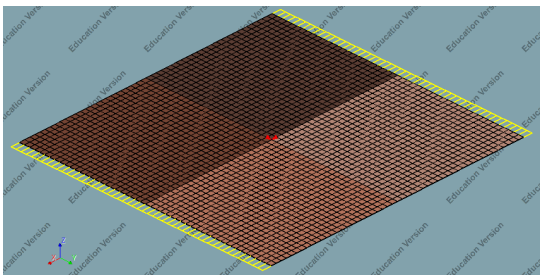

(b) Mesh overview.

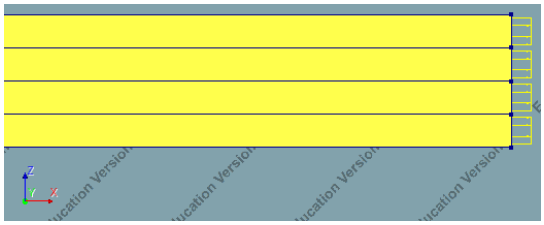

(c) Close-up of the geometry to confirm four individual layers of solid elements have been used to represent the plies. The distributed force q_x on the positive x-face can also be seen.

Figure 5.9: Diana model of a sheet with ABD-matrix properties.

Again, a structural linear static analysis is performed. Since the input is similar to the laminate with ABD-matrix input, the results of both analyses should also agree. Figure 5.10 shows the displacements in z-direction,

confirming again the out-of-plane deformations due to the coupling effect as a result from the non-zero **B**-matrix. This figure is very similar to figure 5.8.

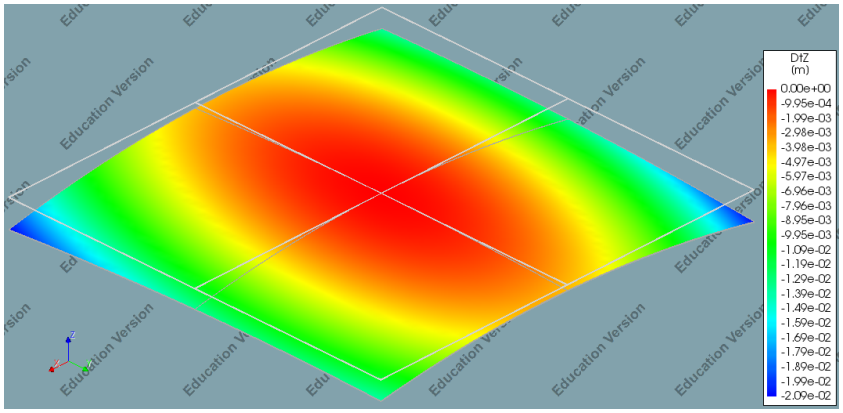

Figure 5.10: Displacements in z-direction for the four-ply laminate with solid elements.

Finally, the numerical values of all the deformation components need to be compared, which is shown in table 5.4. The ratio between the FE result with solid elements and the analytical values from the CLT are still very close to 1. On average, they are 7.1×10^{-4} off of 1 (or 0.071%), which is more than the difference from the ABD-matrix FE results. This increase in difference can be assigned to the fact that solid elements do not make use of Kirchhoff assumptions or plane stress conditions, where the regular CLT does. Since a very thin plate is discretised with solid elements, the plate does approximate the Kirchhoff assumptions. Therefore, the solid elements show behaviour that approximates behaviour of a flat shell element.

Table 5.4: Results of a four-ply laminate with a load N_{xx} with solid elements used in the FE analysis for the regular CLT.

	Regular CLT	FE analysis	Ratio FE/CLT
ε^0_{xx}	0.000220499	0.000220434	0.99970356
ε^0_{yy}	−0.000050998	−0.000051047	1.00095943
γ^0_{xy}	0.000044530	0.000044527	0.99994335
κ_{xx}	0.107851705	0.108054028	1.00187594
κ_{yy}	0.031124138	0.031093866	0.99902715
κ_{xy}	−0.028157583	−0.028160938	1.00011913

In conclusion, all the values from both FE analyses are very close to the analytic result from the regular CLT. It is therefore assumed that the method to represent a laminate and extract the deformation variables from Diana is correct and can be applied to verify the modified CLT. It should be noted that the three extra strain components (ε^0_{zz}, γ^0_{yz} and γ^0_{xz}) are not compared yet. However, since all the other deformation variables are in accordance with the regular CLT results, it is assumed that the extra three strain components are also correct, because they are derived in a similar manner, as described in section 5.2.

5.4. Modified CLT comparison

The modified CLT derived in chapter 4 is verified using several FE analyses. First of all, the four-ply laminate used in section 5.3.2 is evaluated with the modified CLT. In that case, no inclination is present yet. Next, individual plies with an inclination are checked, since the behaviour of an individual ply is much easier to predict and analyse because there are no coupling effects present. Finally, an inclination is added to the four-ply laminate.

5.4.1. Four-ply laminate without inclination

The analytic result of the four-ply laminate with lay-up $[0/-45/0/90]$ can be determined for both the regular CLT and the modified CLT. The corresponding entries in the 6×6 ABD-matrix of the regular CLT are not the

same for the 12×12 ABD-matrix of the modified CLT. The 12×12 ABD-matrix needs to be inverted in order to determine the strains and curvatures that correspond to a certain type of loading in the modified CLT. Again, a load $N_{xx} = 10000$ N/m has been applied on the laminate. The resulting strains and curvatures are given in table 5.5, where the in-plane curvatures κ_{zz}, κ_{yz} and κ_{xz} are not taken into account for the same reason as described in section 5.2.2.

The four-ply laminate with lay-up $[0/-45/0/90]$ has already been evaluated with an FE analysis in the previous section. The results of the FE analysis with solid elements will be used, since it better represents the same assumptions made in the modified CLT. In this case, the three extra out-of-plane strain components ε^0_{zz}, γ^0_{yz} and γ^0_{xz} will also be evaluated. Table 5.5 summarises the results of the modified CLT and the FE analysis with solid elements. The last column indicates the ratio between the modified CLT results and the FE results obtained with solid elements.

Table 5.5: Results of a four-ply laminate with a load N_{xx} with solid elements used in the FE analysis for the modified CLT.

	Modified CLT	FE analysis	Ratio FE/CLT
ε^0_{xx}	0.000220485	0.000220434	0.99976814
ε^0_{yy}	−0.00005098	−0.000051046	1.001180327
ε^0_{zz}	−0.00006939	−0.000069351	0.999385351
γ^0_{yz}	0	-1.4×10^{-8}	–
γ^0_{xz}	0	-2.0×10^{-8}	–
γ^0_{xy}	0.000044518	0.000044527	1.000181674
κ_{xx}	0.107832726	0.108054028	1.002052277
κ_{yy}	0.031131708	0.03109386	0.998784241
κ_{xy}	−0.028148312	−0.028160938	1.000448537

The FE results show very small out-of-plane shear deformations, which should be equal to zero according to the modified CLT. These values are much smaller compared to the other deformation variables from the FE analysis. It can therefore be assumed that they come from rounding errors and can be neglected.

The strain in z-direction due to lateral contraction of the laminate is the only extra occurring deformation variable in the modified CLT. Its value agrees with the value from the FE analysis. This confirms that the determination of the strain in z-direction with the modified CLT is correct.

The ratios between the two results are on average 0.08% off of 1, which is in the same order of magnitude compared to the ratios where the regular CLT was used. Because the differences are relatively small, it can be stated that for a laminate without extra inclination, the modified CLT is a good representation of that laminate when plane stress conditions are not applicable.

5.4.2. Individual plies with an inclination

The most important difference of the modified CLT compared to the regular CLT, is that the modified CLT allows plies to have an extra rotation α about the global x-axis. This inclination could result in out-of-plane shear deformations, which cannot be observed in a laminate evaluated with the regular CLT. To check whether the out-of-plane shear deformation is correct, four individual plies have been modelled. First, both a 0°-ply and a 90°-ply without lateral contraction ($\nu_{12} = \nu_{23} = 0$) are tested. The lateral contraction is neglected in order to make it easier to predict what will happen to a ply under a certain loading. Next, the lateral contraction is added to the 0°-ply and the 90°-ply to see how it affects the behaviour of a single ply. An overview of all the input parameters for all four cases is presented in table 5.6.

Table 5.6: Input variables for the modified CLT check with individual plies.

Property	0°-ply $\nu = 0$	90°-ply $\nu = 0$	0°-ply $\nu \neq 0$	90°-ply $\nu \neq 0$
Lay-up	[0]	[90]	[0]	[90]
α [°]	10	10	10	10
l_x [m]	1	1	1	1
l_y [m]	1	1	1	1
t_{ply} [m]	0.005	0.005	0.005	0.005
E_1 [GPa]	39	39	39	39
E_2 [GPa]	8.6	8.6	8.6	8.6
G_{12} [GPa]	3.8	3.8	3.8	3.8
ν_{12} [-]	0	0	0.28	0.28
ν_{23} [-]	0	0	0.4	0.4
N_{xx} [N/m]	1000000	1000000	1000000	1000000
N_{yy} [N/m]	1000000	1000000	1000000	1000000

The plies are loaded by a normal force in x-direction and y-direction separately. Since the extra inclination is added as a rotation about the x-axis, it is expected that γ^0_{yz} is the only extra out-of-plane shear deformation that could occur. This means the plate should be able to rotate about the x-axis to be able to evaluate the displacement in z-direction, which is needed for γ^0_{yz} according to equation 5.6. It should be noted that a true rotation of the ply would indicate kinematic indeterminacy. For this reason, a tying has been added on both the positive and negative y-face. This tying ensures the y-displacement of a y-face is the same for that complete y-face. This means the top line ($z = \frac{t_{\text{ply}}}{2}$) has the same y-displacement as the bottom line ($z = -\frac{t_{\text{ply}}}{2}$), which will indicate an out-of-plane shear deformation of the mid-surface γ^0_{yz}, as shown for example in figure 4.1.

Extra boundary conditions have been added at the coordinates $\left(\frac{l_x}{2}, 0, 0\right)$, which prevent displacement in both the y- and z-direction. The displacement in x-direction at $\left(0, \frac{l_y}{2}, 0\right)$ is also prevented as an extra boundary condition. A structural overview for both loading cases is shown in figure 5.11.

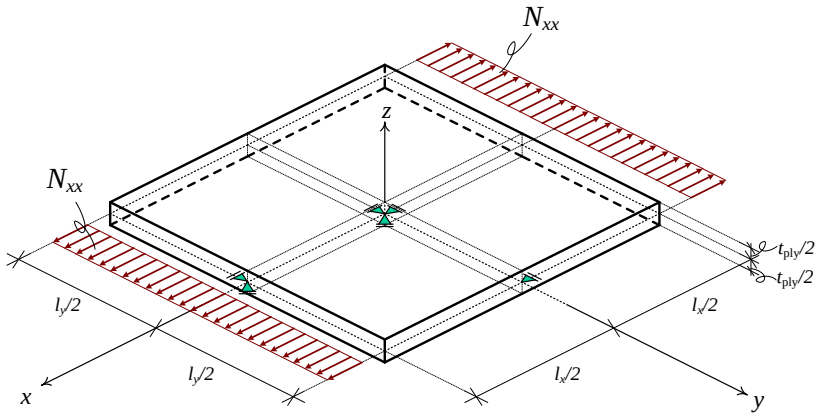

(a) Structural overview for load N_{xx}.

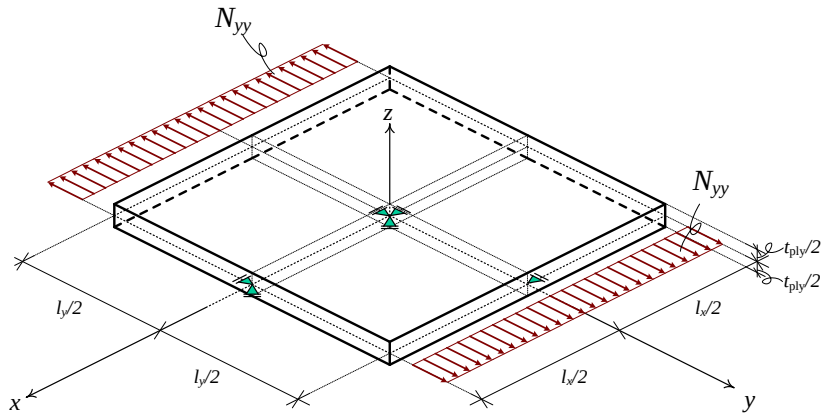

(b) Structural overview for load N_{yy}.

Figure 5.11: FE model of a ply loaded by normal forces. The mid-surface of the ply has also been indicated.

In the FE model, the individual plies also require a mid-surface to be able to add the boundary conditions at the right locations and insert the sheet needed to evaluate the rotations of the mid-surface. An element size of 0.01 m is used. In total 20000 solid elements (HX24L) are used for the ply. The sheet to represent the mid-surface is discretised using 10000 flat shell elements (Q20SF), and has the same isotropic material parameters and dimensions as mentioned in section 5.3.2. This very fine mesh is needed to meet the minimal thickness requirement of the solid elements.

Every ply requires its own local coordinate system. Since α is unequal to zero for the plies, the local x- and y-axis will include global z-coordinates unequal to zero. The values can be determined using trigonometry, where a unit length of the local axes is assumed. The values are given in table 5.7. It should be noted that this model of an inclined ply does not represent a real ply under an inclination. It is a plate with rotated material properties. However, since the modified CLT is only applicable to one location along the y-axis, this FE model still can be used to verify the modified CLT.

Table 5.7: Global coordinates of an arbitrary point on the local x- and y-axis for a single ply with inclination.

	Local x-axis			Local y-axis		
	x	y	z	x	y	z
0°	1	0	0	0	0.9848	0.1736
90°	0	0.9848	0.1736	-1	0	0

The Diana model for a ply with an inclination under a load N_{xx} is shown in figure 5.12. When a load N_{yy} is applied, the only thing that changes in the model is the type of loading. A distributed force per unit area q_x has been used to represent the N_{xx} load. Similarly, q_y corresponds to a load N_{yy}. The load provided in table 5.6

should be divided by the thickness of the ply to obtain the right distributed forces:

$$q_x = \frac{N_{xx}}{t_{\text{ply}}} = \frac{1000000}{0.0005} = 2 \times 10^8 \text{ N/m}^2 \qquad \text{and} \qquad q_y = \frac{N_{yy}}{t_{\text{ply}}} = \frac{1000000}{0.0005} = 2 \times 10^8 \text{ N/m}^2 \tag{5.14}$$

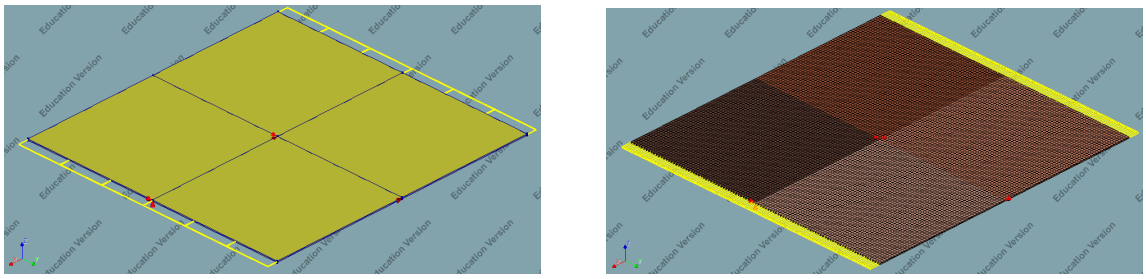

(a) Geometry overview.

(b) Mesh overview.

Figure 5.12: Diana model of a single ply.

The four cases presented in table 5.6 will be dealt with individually. Every case will include a prediction of the possible deformation variables that could occur and a verification of the results.

0°-ply without lateral contraction

The simplest case to be checked is a single 0°-ply where the lateral contraction is neglected. Figure 5.13 shows a cross section of such a ply. If an inclination is present, the material properties do not differ in the global coordinate system compared to the local coordinate system.

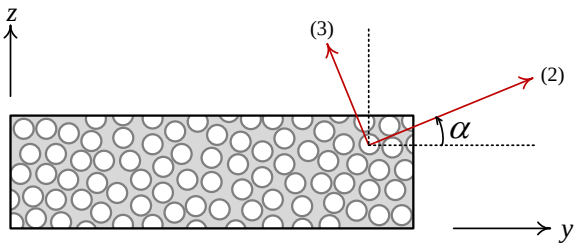

Figure 5.13: Local coordinate system of a 0°-ply with inclination.

A single ply cannot cause coupling effects, so the **B**-matrix must be equal to zero. Furthermore, the Poisson's ratios are equal to zero, which means lateral contraction will not occur. Therefore, the 12×12 ABD-matrix reduces for this case to a diagonal matrix, which means if an axial load is applied, the only deformation that should occur is the axial strain corresponding to the same direction as the loading. Table 5.8 summarises the results for both loading types. The FE results show the same values for the relevant strains. Other (very small) deformations are also observed in the FE results, but these can be assigned to rounding errors in the numerical solution of the FE analysis. It can be concluded that the modified CLT is correct for the 0°-ply with an inclination and no lateral contraction.

Table 5.8: Results of a 0°-ply with an inclination of 10° and no lateral contraction.

	$N_{xx} = 10^6$ N/m			$N_{yy} = 10^6$ N/m		
	Modified CLT	FE analysis	Ratio FE/CLT	Modified CLT	FE analysis	Ratio FE/CLT
ε^0_{xx}	0.00512821	0.00512821	1.00000000	0	1.01×10^{-16}	–
ε^0_{yy}	0	2.54×10^{-17}	–	0.02325581	0.02325581	1.00000000
ε^0_{zz}	0	3.28×10^{-18}	–	0	3.45×10^{-18}	–
γ^0_{yz}	0	-1.97×10^{-13}	–	0	-1.04×10^{-12}	–
γ^0_{xz}	0	-8.75×10^{-13}	–	0	2.09×10^{-12}	–
γ^0_{xy}	0	-2.45×10^{-15}	–	0	5.86×10^{-15}	–
κ_{xx}	0	-2.41×10^{-13}	–	0	-5.31×10^{-13}	–
κ_{yy}	0	-4.00×10^{-13}	–	0	-2.69×10^{-12}	–
κ_{xy}	0	-1.85×10^{-12}	–	0	9.21×10^{-12}	–

90°-ply without lateral contraction

In a 90°-ply with an inclination, the fibre direction is rotated about the x-axis. It is expected that this will lead to an out-of-plane shear deformation γ^0_{yz} when a load in y-direction is applied, as indicated in figure 5.14. The stiffness of the (3)-direction is lower compared to the stiffness of the (1)-direction. This means the (1)-direction will elongate less than the (3)-direction under this type of loading, causing an out-of-plane shear deformation.

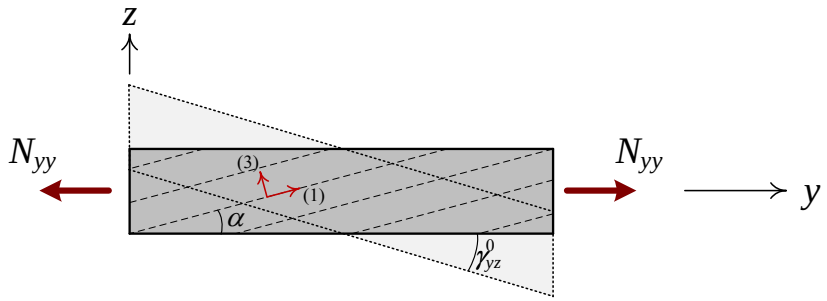

Figure 5.14: Out-of-plane shear deformation for a 90°-ply without lateral contraction.

Since the Poisson's ratios are still equal to zero, lateral contraction will not occur, so axial strains will only occur in the loading direction. Only one ply is considered, so the **B**-matrix will be zero and no coupling effect can be observed. In the complete ABD-matrix, off-diagonal terms appear in both the **A**- and **D**-matrix, which means more than one type of deformation could occur under certain type of loading. For example, a load in y-direction will cause the expected axial strain ε^0_{yy} and out-of-plane shear deformation γ^0_{yz}. However, due to the inclined plies, an extra strain in z-direction ε^0_{zz} is also observed, which is caused by the difference in stiffness of the (1)- and (3)-direction. Table 5.9 shows all the results for a 90°-ply with an inclination of 10° and no lateral contraction under a loading of N_{xx} and N_{yy}.

Table 5.9: Results of a 90°-ply with an inclination of 10° and no lateral contraction.

	$N_{xx} = 10^6$ N/m			$N_{yy} = 10^6$ N/m		
	Modified CLT	FE analysis	Ratio FE/CLT	Modified CLT	FE analysis	Ratio FE/CLT
ε^0_{xx}	0.02325581	0.02325581	1.00000000	0	-2.88×10^{-18}	–
ε^0_{yy}	0	4.15×10^{-18}	–	0.00638393	0.00638392	0.99999952
ε^0_{zz}	0	-2.87×10^{-18}	–	−0.00070911	−0.00070911	0.99999761
γ^0_{yz}	0	-1.60×10^{-13}	–	−0.00699651	−0.00699650	0.99999888
γ^0_{xz}	0	1.83×10^{-12}	–	0	1.42×10^{-10}	–
γ^0_{xy}	0	0	–	0	0	–
κ_{xx}	0	4.82×10^{-12}	–	0	4.25×10^{-10}	–
κ_{yy}	0	-1.92×10^{-14}	–	0	-1.80×10^{-12}	–
κ_{xy}	0	8.14×10^{-13}	–	0	2.60×10^{-11}	–

The most important deformation component of the modified CLT that should match with the results of an FE analysis, is the out-of-plane shear strain γ^0_{yz}, because the modified CLT distinguishes from the regular CLT in out-of-plane deformations that can occur. The table above shows that the values for γ^0_{yz} match perfectly. Figure 5.15a represents the displacements in z-direction, where it can be seen that out-of-plane deformations occur. A close-up of the displacements in z-direction of the positive y-face is shown in figure 5.15b, where the nodes are also indicated with black dots. Due to the tyings that are applied, the nodes at a certain y-coordinate will have the same displacement in y-direction. This means the out-of-plane deformations fully come from shear deformations and not from a rotation of the plate. In conclusion, the modified CLT results in a correct out-of-plane shear deformation for a 90°-ply with inclination and without lateral contraction.

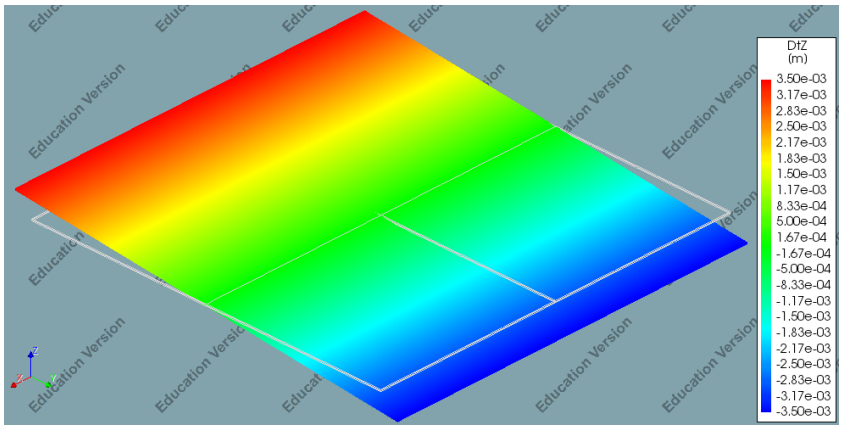

(a) Overview.

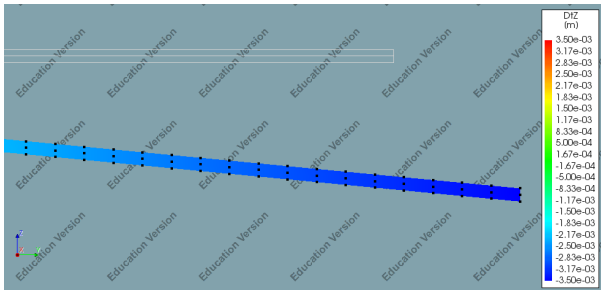

(b) Close-up of the positive y-face.

Figure 5.15: Displacement in z-direction of a 90°-ply with a load N_{yy}.

The next step is to add a Poisson's ratio to the plies, in order to take the lateral contraction into account.

0°-ply with lateral contraction

A 0°-ply with an inclination and Poisson's ratios that are unequal to zero is axially loaded. As mentioned before, the inclination does not affect the material properties of a ply, because it can be modelled with transversely isotropic material properties. The ply is rotated around its local (1)-axis. Since the material properties are the same in the (2)- and (3)-direction of a transversely isotropic material, this extra rotation does not affect the behaviour of the ply. It is therefore expected that the only occurring deformation variables will be the three axial strains (ε^0_{xx}, ε^0_{yy} and ε^0_{zz}). For a load in x-direction, which corresponds to the (1)-direction for 0°-ply with an inclination, the lateral contraction in y- and z-direction will be the same, since the corresponding Poisson's ratios are the same for a transversely isotropic material ($\nu_{12} = \nu_{13}$). For a load in y-direction, the lateral contraction will occur in the x- and z-direction, making the Poisson's ratios ν_{12} and ν_{23} relevant. These are not the same for a transversely isotropic material, thus the strain in x- and z-direction will not be the same. Table 5.10 gives all the results for a load N_{xx} and a load N_{yy}.

Table 5.10: Results of a 0°-ply with an inclination of 10° and lateral contraction.

	$N_{xx} = 10^6$ N/m			$N_{yy} = 10^6$ N/m		
	Modified CLT	FE analysis	Ratio FE/CLT	Modified CLT	FE analysis	Ratio FE/CLT
ε^0_{xx}	0.00512821	0.00512821	1.00000000	−0.00143590	−0.00143590	1.00000000
ε^0_{yy}	−0.00143590	−0.00143590	1.00000000	0.02325581	0.02325581	1.00000000
ε^0_{zz}	−0.00143590	−0.00143590	1.00000000	−0.00930233	−0.00930233	1.00000000
γ^0_{yz}	0	-9.87×10^{-13}	–	0	9.16×10^{-12}	–
γ^0_{xz}	0	9.52×10^{-12}	–	0	-1.40×10^{-12}	–
γ^0_{xy}	0	8.15×10^{-16}	–	0	6.31×10^{-16}	–
κ_{xx}	0	5.02×10^{-13}	–	0	6.05×10^{-14}	–
κ_{yy}	0	-4.47×10^{-12}	–	0	2.86×10^{-11}	–
κ_{xy}	0	1.87×10^{-11}	–	0	1.12×10^{-11}	–

The values for all the axial strains perfectly match for the modified CLT and the results from an FE analysis. It can be stated that the lateral contraction due to the addition of Poisson's ratios is correctly taken into account in the modified CLT.

90°-ply with lateral contraction

For a 90°-ply with Poisson's ratios unequal to zero and with an inclination, it is expected that all three axial strains will occur for both loading cases N_{xx} and N_{yy}. The out-of-plane shear strain γ^0_{yz} will also be present for a load in y-direction.

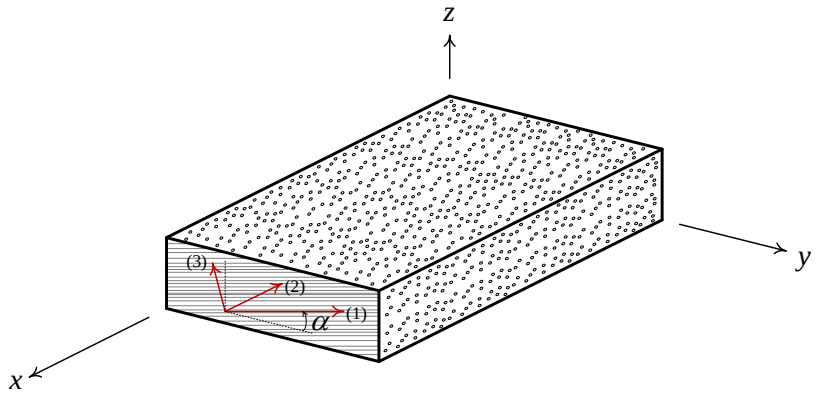

Figure 5.16: Local coordinate system of a 90°-ply.

Figure 5.16 shows the local coordinate system in red for a 90°-ply with an inclination α. Since the Poisson's

ratios ν_{12} and ν_{23} have different values, the lateral contraction due to a load in x-direction will not be the same in the (1)- and (3)-direction. Thus the axial strains in y- and z-direction will also not be the same. Due to the inclination, the strains along the local axes will differ from the strains along the global axes. This will cause an out-of-plane shear deformation γ^0_{yz} for a load N_{xx} when the Poisson's ratios are taken into account.

Table 5.11: Results of a 90°-ply with an inclination of 10° and lateral contraction.

	$N_{xx} = 10^6$ N/m			$N_{yy} = 10^6$ N/m		
	Modified CLT	FE analysis	Ratio FE/CLT	Modified CLT	FE analysis	Ratio FE/CLT
ε^0_{xx}	0.02325581	0.02325581	1.00000000	−0.001673099	−0.001673099	0.99999965
ε^0_{yy}	−0.00167310	−0.00167310	0.99999965	0.006299942	0.006299939	0.99999955
ε^0_{zz}	−0.00906512	−0.00906512	1.000000065	−0.00206102	−0.002061018	0.99999927
γ^0_{yz}	0.00269048	0.00269047	0.999998799	−0.006535023	−0.006535016	0.99999888
γ^0_{xz}	0	4.23×10^{-11}	–	0	-7.15×10^{-11}	–
γ^0_{xy}	0	0	–	0	0	–
κ_{xx}	0	1.35×10^{-10}	–	0	-2.24×10^{-10}	–
κ_{yy}	0	-3.00×10^{-13}	–	0	6.00×10^{-13}	–
κ_{xy}	0	-4.00×10^{-12}	–	0	3.18×10^{-11}	–

Table 5.11 summarises all the results for a 90°-ply with Poisson's ratio included. Again, all the occurring deformation variables perfectly match for both loading cases, meaning the modified CLT does also take the lateral contraction correctly into account for the 90°-ply with an inclination.

5.4.3. Four-ply laminate with inclination

The final step in the verification of the modified CLT is to check whether the FE results of the four-ply laminate with inclined plies correspond to the results from the modified CLT. Again, a laminate with a lay-up of $[0/-45/0/90]$ with a load in x-direction has been used, as depicted in figure 5.6. The same dimensions, material parameters and loading is used, as given in the tables 2.3 and 5.1. An extra rotation of $\alpha = 10°$ has been added to the plies in the laminate. Since the laminate is non-symmetric, non-balanced and has a ply inclination, the 12×12 ABD-matrix will not contain any zero entries. This means for every type of loading, all six strain components and all six curvature components will occur. The in-plane curvatures κ_{yz}, κ_{xz} and κ_{zz} are again not taken into account, because these are not relevant for a thin plate. The strains and curvatures that occur for $N_{xx} = 10000$ N/m are given in table 5.13.

To determine the FE results of the four-ply laminate with inclined plies, the same type of elements, mesh size and distributed force q_x have been used as described in section 5.3.2. The only difference with the analysis performed in that section, is that the local axes of each ply now also contain a global z-coordinate. Table 5.12 gives the input for the local coordinate system of each ply.

Table 5.12: Global coordinates of an arbitrary point on the local x- and y-axis for the four-ply laminate with inclination.

	Local x-axis			Local y-axis		
	x	y	z	x	y	z
0°	1	0	0	0	0.9848	0.1736
−45°	0.7071	-0.6963	-0.1228	0.7071	0.6963	0.1228
0°	1	0	0	0	0.9848	0.1736
90°	0	0.9848	0.1736	-1	0	0

A structural linear static analysis is performed. All nine relevant deformation components should be observed from the FE analysis, since the modified CLT result from table 5.13 shows no zero strain or zero curvature. Figure 5.17 shows the displacements in z-direction, which are very similar to the displacements in z-direction of a laminate without inclined plies. The differences are very small due to the fact that a 10°-angle as inclination is not very large, which is confirmed by the fact that the results from the modified CLT for a laminate without

inclined plies in table 5.5 are very similar to the results presented for the modified CLT for a laminate with inclined plies in table 5.13.

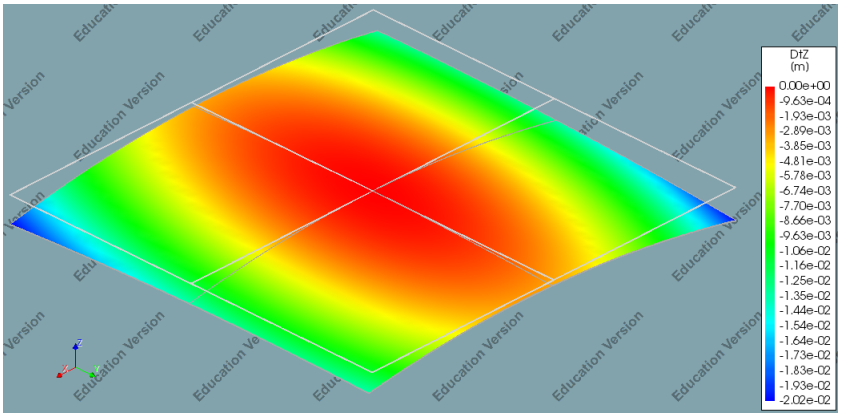

Figure 5.17: Displacements in z-direction for the four-ply laminate with inclination.

Finally, the results from the FE analysis need to be compared with the modified CLT results, which is done in table 5.13. On average, the ratios between the FE results and the modified CLT results are 2% off of 1. The deformation variable with the largest difference is the curvature κ_{yy} with a ratio of 0.94 (or 6%). It can be concluded that this deformation variable has the same order of magnitude for both the FE result and the modified CLT result. The difference is assigned to fact that no tyings or extra boundary conditions are applied to the laminate in the FE analysis for a laminate with inclined plies. Extra constraints in any direction could hinder possible deformations. All deformation variables must be able to occur for the load N_{xx}, so the extra constraints (tyings or boundary conditions) are not applied.

It is observed that the out-of-plane shear deformations are unequal to zero for the laminate with inclined plies. These out-of-plane shear strains are the most important differences between the laminate with or without inclination in the plies. It is therefore assumed that the differences in the values of the modified CLT are small enough compared to the FE results, so the modified CLT is also valid for the four-ply laminate with inclined plies.

Table 5.13: Results of a four-ply laminate with a load N_{xx} with solid elements used in the FE analysis for the modified CLT.

	Modified CLT	FE analysis	Ratio FE/CLT
ε^0_{xx}	0.00022049	0.00022081	1.00145856
ε^0_{yy}	−0.00005154	−0.00005182	1.00538069
ε^0_{zz}	−0.00006884	−0.00006884	0.99994446
γ^0_{yz}	0.00000630	0.00000620	0.98437270
γ^0_{xz}	0.00000773	0.00000757	0.97903866
γ^0_{xy}	0.00004384	0.00004188	0.95522471
κ_{xx}	0.10783273	0.10833944	1.00469910
κ_{yy}	0.02837461	0.02665153	0.93927400
κ_{xy}	−0.02772068	−0.02687440	0.96947126

Due to the inclination in the plies, the strains and curvatures differ from the strains and curvatures from the same laminate without inclination. The modified CLT values from table 5.5, where no inclination was present, can be compared with the table results shown above. This has been done by taking the ratio between the modified CLT results of the laminate without inclination and the modified CLT results of the laminate with inclination. The results are shown in table 5.14, where it can be seen that ε^0_{xx} and κ_{xx} are not affected by the inclination since a ratio of 1 is found. The out-of-plane shear strains are zero when no inclination is present, meaning they cannot be compared with the laminate with inclination. Furthermore, an increase of ε^0_{yy} is observed when an inclination is added. The four other relevant deformation components ε^0_{zz}, γ^0_{xy}, κ_{yy} and κ_{xy} show a decrease due

to the inclination, where the curvature κ_{yy} depends the most on the inclination with a decrease of 8.9%. These values strongly depend on the material properties of the plies, the laminate lay-up and the inclination angle. For a non-balanced, non-symmetric laminate it is difficult to predict and explain the strains and curvatures due to coupling effects. Therefore, the differences between the strains of a laminate without inclination and the strains of a laminate with inclination will not be further discussed.

Table 5.14: Comparison between the modified CLT results for the laminate without inclined plies and the laminate with inclined plies.

	Ratio inclination/ no inclination
ε^0_{xx}	1.00000000
ε^0_{yy}	1.01088634
ε^0_{zz}	0.99200139
γ^0_{yz}	–
γ^0_{xz}	–
γ^0_{xy}	0.98480775
κ_{xx}	1.00000000
κ_{yy}	0.91143752
κ_{xy}	0.98480775

5.5. Conclusion

Four different verifications have been performed. First of all, the results from the regular CLT were compared with two types of FE analyses, one with an ABD-matrix as input and one with solid elements as input. The results of the analysis with ABD-matrix match perfectly with the regular CLT results and the very small differences could be assigned to rounding errors. The analysis with solid elements showed errors within the same order of magnitude. All six deformation variables should be able to occur, so no extra boundary conditions or tyings could be applied. So not all the Kirchhoff assumptions could be applied to the laminate modelled with solid elements, causing the small difference. It is concluded that the method to extract the strains and curvatures from the FE results was correct.

Secondly, the modified CLT was evaluated for a four-ply laminate without inclined laminates. The only extra deformation variable that could occur, was the axial strain in z-direction ε^0_{zz}. Its value matched with the modified CLT result, meaning the modified CLT is correct for a laminate without inclined plies.

Thirdly, four individual plies with an inclination were evaluated. Since not all nine deformation variables of the modified CLT could occur, extra boundary conditions and tyings were applied to the plies. This means the Kirchhoff assumption that straight lines perpendicular to the mid-surface remain straight after deformation could be met. Furthermore, extra boundary conditions could ensure the plate was kinematically determinate, thus preventing unwanted rotations of the plate. It was shown that the modified CLT results perfectly matched with the FE results, including the extra out-of-plane shear strain which distinguishes the modified CLT from the regular CLT.

Finally, a four-ply laminate with inclined plies was checked. The values of the modified CLT and the FE analysis were quite close, but still differed 2% on average. These differences come from the fact that no extra boundary conditions or tyings could be applied, since they would hinder some relevant deformation components that should be able to occur.

All in all, it can be stated that the modified CLT results match with results from FE analyses. It is therefore assumed that ply inclination has correctly been implemented and that the presented modified CLT can be used to obtain further results in this report.

6

Influence of the ply inclination

The modified CLT can be used to determine the influence of the inclination in the plies of a laminate. The verification of the modified CLT in chapter 5 already showed that a laminate with inclined plies shows extra deformation components compared to a laminate without inclined plies. Furthermore, some deformation variables that were present for a laminate without inclined plies changed when the inclination was added. The results might not be constant for any inclination, thus the relations between the inclination angle α and the results must be checked.

First, the influence of α on the strains for in-plane axial loading N_{xx} and N_{yy} on a laminate will be evaluated. Next, the equivalent stiffnesses can be determined as a function of α. The behaviour of an individual ply is simpler to explain compared to a complete laminate, for example due to the absence of coupling effects in a single ply, thus the strains will only be evaluated for individual plies with different fibre orientation. For the equivalent stiffnesses, distinction will be made between individual plies, balanced and symmetric laminates, and a four-ply non-balanced and non-symmetric laminate.

The modified CLT requires input to develop all the results. Besides the five independent transversely isotropic material parameters, the thickness and fibre orientation of the plies is needed. The fibre orientation will differ per ply or per laminate and will be specified later. The extra rotation α is variable, so it is not yet required as input for the modified CLT. For all the results presented in this chapter, the material parameters shown in table 2.3 have been chosen and the ply thickness is assumed to be equal to 0.0005 m.

6.1. Strains

In this section, a 0°-ply and a 90°-ply will be evaluated. The plies will be loaded by an axial load in x- and y-direction. For both N_{xx} and N_{yy}, a load of 10000 N/m is used to obtain all the strains of the individual plies, which will be plotted as a function of the inclination angle α. A single ply is considered, which means no coupling effects are present, thus no curvatures will occur when an axial load is applied.

For every type of loading, the relative axial strains will be plotted. These relative strains are defined as the ratio between the axial strain as a function of α and the corresponding constant strain for $\alpha = 0°$. Since lateral contraction is taken into account, all three axial strains are unequal to zero for any type of loading. It is not possible to plot the relative shear strains, since for $\alpha = 0°$ the out-of-plane shear strains are always equal to zero for the loads N_{xx} and N_{yy}. The shear strains are plotted as absolute shear strains, representing the actual value that is obtained by the applied load. All plots are given for α from 0° to 90°.

6.1.1. 0°-ply

The 0°-ply with $\alpha > 0°$ will have the same material properties in the global x-, y- and z-direction as the local (1)-, (2)- and (3)-direction respectively, despite the different orientation of the (2)- and (3)-axes in comparison to a 0°-ply with $\alpha = 0°$. From figure 5.13, it can be seen that when the angle α is altered, the fibres will still be oriented in the exact same direction. Therefore the material properties do not differ for any α and thus the 12×12 ABD-matrix will be independent of α. For any type of loading, all the strains (or curvatures) should therefore be independent of α.

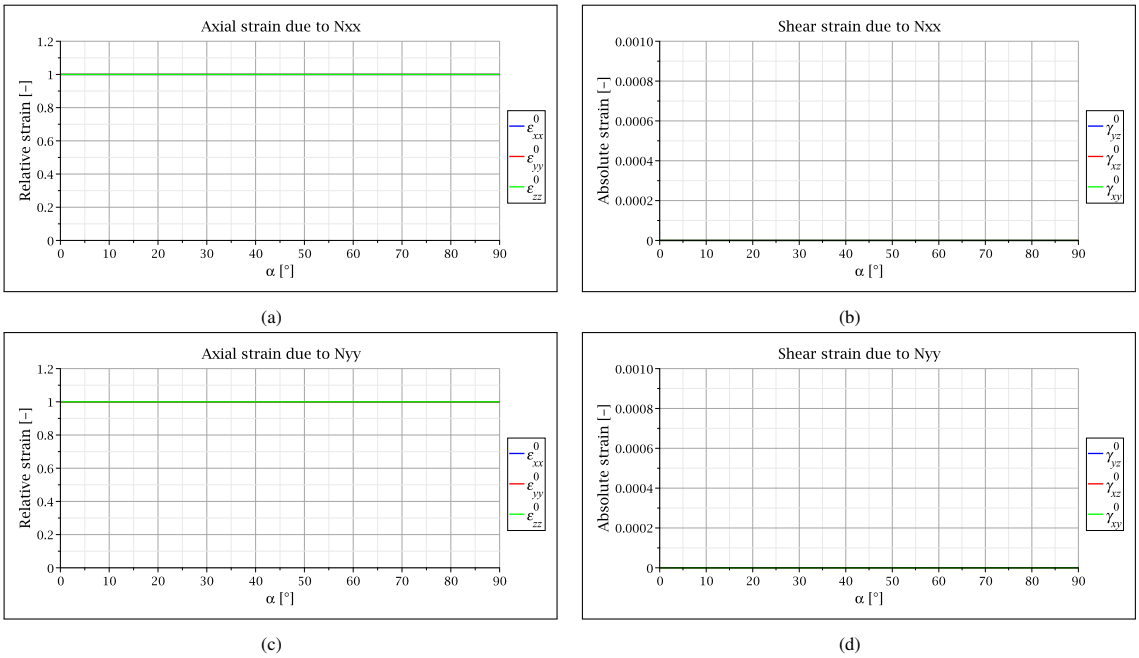

Figure 6.1: Strains due to an axial load N_{xx} and N_{yy} for a 0°-ply.

Figure 6.1 gives all the strains as function of α. It can be seen that for both loading types, all the relative axial strains are constant and equal to 1. Therefore, the axial strains do not depend on α. The absolute shear strains in the figures 6.1b and 6.1d are all equal to zero, as was expected since the inclination does not affect the properties of a 0°-ply.

6.1.2. 90°-ply

In contrast to the 0°-ply, the results of a 90°-ply will depend on α. For example, when the 90°-ply is axially loaded in y-direction, the influence of transverse stiffness in the (3)-direction on the global strain in y-direction will increase as α increases. Since the elastic modulus in the (3)-direction is much lower than the elastic modulus in the (1)-direction of a ply, it can be stated that the axial strain in the global y-direction will increase as α increases. Figure 6.2 shows a cross section of a 90°-ply along the x-axis.

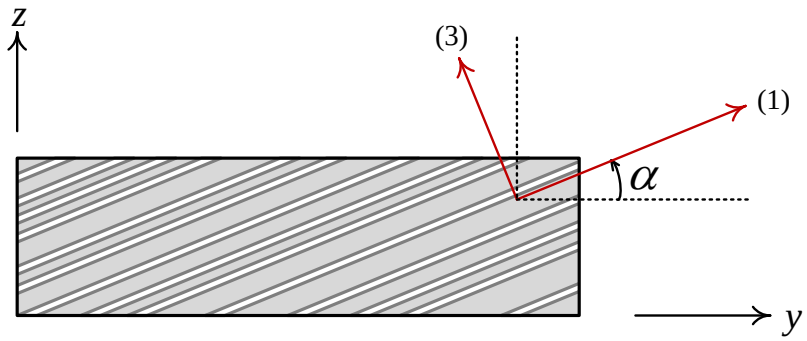

Figure 6.2: View along the x-axis of a 90°-ply with an inclination, where the individual fibres are shown with the white lines.

Figure 6.3 shows the relative axial strains and absolute shear strains as function of α. For a 90°-ply, the (2)-axis coincides with the x-axis. For a load N_{xx}, the lateral contraction in the global y- and z-direction will differ since the corresponding Poisson's ratios and elastic moduli are rotated over an angle α. This will affect the strains in y- and z-direction, as can be seen from figure 6.3a. A significant increase of ε^0_{yy} is observed, since the Poisson's ratio ν_{23}, which is higher compared to the other relevant Poisson's ratio ν_{12}, will become more dominant in y-direction as α increases, causing more lateral contraction. Correspondingly, ε^0_{zz} shows a small decrease as α increases, since the Poisson's ratio ν_{12} will become less dominant in z-direction as α increases, causing less

lateral contraction and thus a decrease in relative strain. Due to the high differences in relative axial strain shown in figure 6.3a, it can be stated that the inclination has a very high influence on the strains for a 90°-ply with the used material properties loaded by N_{xx}. It should be noted that the relative strains are highly dependent on the used material properties. If, for example, the Poisson's ratios are altered in such a way that $\nu_{12} > \nu_{23}$, ε^0_{yy} will show a decrease and ε^0_{zz} will show an increase, instead of the other way around as showed in figure 6.3a where $\nu_{12} < \nu_{23}$ was used.

The shear strain γ^0_{yz} also changes as α increases for a load in x-direction, which coincides with the (2)-direction for a 90°-ply. This is caused by the difference in lateral contraction in the (1)- and (3)-direction. For $\alpha = 90°$, the out-of-plane shear strain is zero again, since the local directions coincide with (positive or negative) global directions so no out-of-plane shear strain can occur. Correspondingly, the maximum γ^0_{yz} occurs for $\alpha = 45°$. The other two shear strains γ^0_{xz} and γ^0_{xy} are not affected by α when a load N_{xx} is applied.

For a load N_{yy}, all three axial strains will change as α increases. The relative strain ε^0_{xx} increases significantly, again due to the rotation of lateral contraction as explained for ε^0_{yy} and ε^0_{zz} when a load N_{xx} was applied. The axial strain in y-direction also increases as α increases. From figure 6.3c it can be seen that the relative strain ε^0_{yy} is about 4.5 times higher for $\alpha = 90°$, due to the fact that the lower elastic modulus E_2 will become more dominant as α increases. The relative strain ε^0_{zz} is also affected by the difference in lateral contraction, causing an increase until $\alpha = 45°$ and a decrease to one between $\alpha = 45°$ and $\alpha = 90°$.

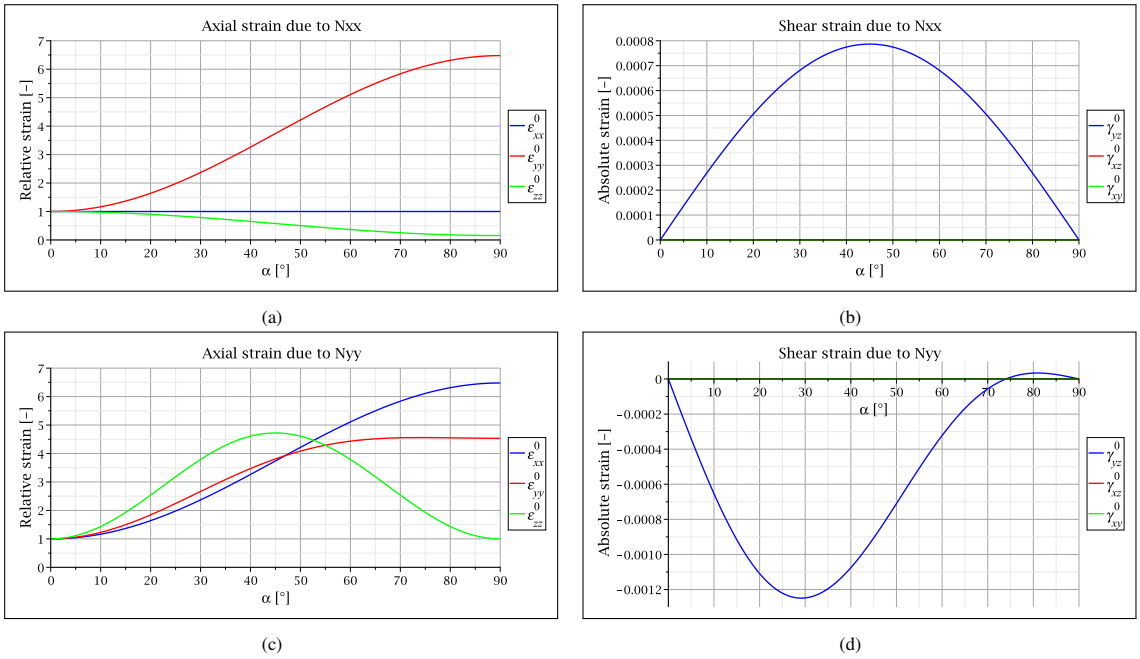

Figure 6.3: Strains due to an axial load N_{xx} and N_{yy} for a 90°-ply.

Finally, figure 6.3d shows that the absolute out-of-plane shear strain γ^0_{yz} strongly depends on α for a load in y-direction. For the chosen material properties, a negative out-of-plane shear strain will occur for α's up to ~70° due to the difference in elastic moduli E_1 and E_2. At some value, the absolute shear strain reaches its maximum value. Next, γ^0_{yz} starts to decrease again and even shows a positive value for a large α. It should be noted that the out-of-plane shear strain is strongly affected by the material properties. For example, figure 6.4a shows the absolute shear strain for $E_1 = E_2 = 39$ GPa. Here, it can be seen that the figure is rotational symmetric around $\alpha = 45°$. In that case, the out-of-plane shear deformation is purely caused by the difference between the elastic modulus and the shear modulus. For an isotropic material, the material properties are the same in every direction, meaning the material properties are not affected by an inclination angle α. This means an isotropic material could never cause out-of-plane shear deformations. If the following relation holds for the shear modulus, the material can be assumed to be isotropic (if $E_1 = E_2$ still holds) and no out-of-plane shear deformations should occur:

$$G_{12,\text{iso}} = \frac{E_2}{2\,(1+\nu_{12})} = \frac{39}{2\,(1+0.28)} = 15.23 \text{ GPa} \tag{6.1}$$

The result for the shear modulus corresponding to isotropic material calculated above is shown in figure 6.4b. Originally, the shear modulus was 3.8 GPa, thus much lower than the shear modulus for which the out-of-plane shear strain is zero. If the shear modulus exceeds the value for the shear modules corresponding to isotropic material derived above, the figure flips and shows first a positive shear strain for small α. Figure 6.4c shows the absolute shear strain when $G_{12} = 25$ GPa is used. Again for all figures shown, the out-of-plane shear strain γ^0_{xz} and the in-plane shear strain γ^0_{xy} are equal to zero.

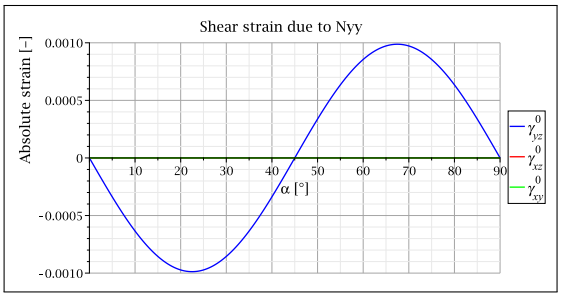

(a) Shear strain for a 90°-ply loaded by N_{yy} with $E_1 = E_2$ and $G_{12} < G_{12,\text{iso}}$.

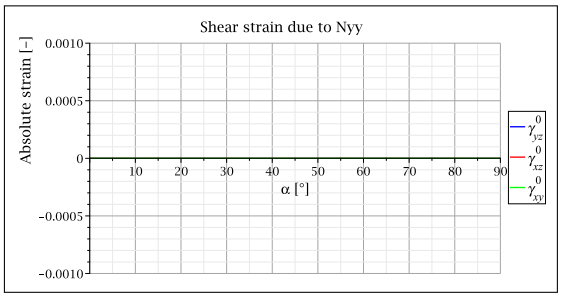

(b) Shear strain for a 90°-ply loaded by N_{yy} for isotropic material properties.

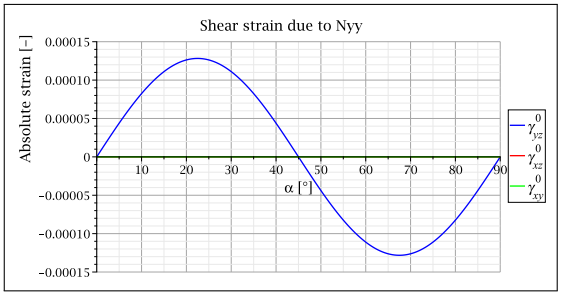

(c) Shear strain for a 90°-ply loaded by N_{yy} with $E_1 = E_2$ and $G_{12} > G_{12,\text{iso}}$.

Figure 6.4: Shear strains of a 90°-ply for various material properties.

6.2. Equivalent stiffness

In section 3.4, the derivation of engineering constants for the regular CLT was given, which included the equivalent stiffnesses E_x and E_y. For the modified CLT, the engineering constants can be derived similarly, where it should be noted that the ABD-matrix is increased to a 12×12 matrix. The equations for the in-plane equivalent stiffnesses ($E_{x,\text{ip}}$ and $E_{y,\text{ip}}$) are not affected by this increase and are the following:

$$E_{x,\text{ip}} = \frac{\det[ABD]}{\mathrm{M}_{1,1}\, t_{\text{tot}}} \qquad \text{and} \qquad E_{y,\text{ip}} = \frac{\det[ABD]}{\mathrm{M}_{2,2}\, t_{\text{tot}}} \tag{6.2}$$

Here, the minor is now applicable to the complete 12×12 ABD-matrix, as well as the determinant of the ABD-matrix. Because the ABD-matrix is increased in size, different minors should be taken to obtain the flexural engineering constants. When for example $E_{x,\text{f}}$ is derived, a bending moment T_x is applied and the corresponding curvature κ_{xx} is determined. This κ_{xx} corresponds now to the seventh entry in row and column instead of the fourth entry in row and column for the original ABD-matrix. This results in the following equations for the flexural equivalent stiffnesses:

$$E_{x,\text{f}} = \frac{12\det[ABD]}{\mathrm{M}_{7,7}\, t^3_{\text{tot}}} \qquad \text{and} \qquad E_{y,\text{f}} = \frac{12\det[ABD]}{\mathrm{M}_{8,8}\, t^3_{\text{tot}}} \tag{6.3}$$

For the reduced modified CLT with the 8×8 ABD-matrix, the engineering constants will be the same as for the modified CLT with the 12×12 ABD-matrix. However, different minors should be used in the determination of the flexural equivalent stiffnesses:

$$E_{x,\text{f}} = \frac{12\det[ABD]}{\mathrm{M}_{6,6}\, t^3_{\text{tot}}} \qquad \text{and} \qquad E_{y,\text{f}} = \frac{12\det[ABD]}{\mathrm{M}_{7,7}\, t^3_{\text{tot}}} \tag{6.4}$$

First, the equivalent stiffnesses for a 0°-ply and a 90°-ply are derived. For a single ply, there is no difference between the in-plane engineering constants and the flexural engineering constants so no distinction needs to be made. Next, several laminate lay-ups will be used to derive the corresponding equivalent stiffnesses.

Every plot contains the relative equivalent stiffnesses. These are obtained by dividing the equivalent stiffness by the elastic modulus in the fibre direction of a ply (E_1). All the plots are given for $0° < \alpha < 90°$.

6.2.1. 0°-ply

As mentioned in section 6.1.1, the material properties for a 0°-ply are not affected for any α. This should also not affect the equivalent stiffnesses. Figure 6.5 shows both the relative equivalent stiffness in x- and y-direction. It can be seen that indeed the relative equivalent stiffnesses are both constant for any α, confirming that the equivalent stiffnesses remain the same when an inclination is added to a ply. The equivalent stiffness in x-direction is equal to E_1 for a 0°-ply, so a ratio of 1 is obtained. The relative E_y is equal to the ratio $\frac{E_2}{E_1}$.

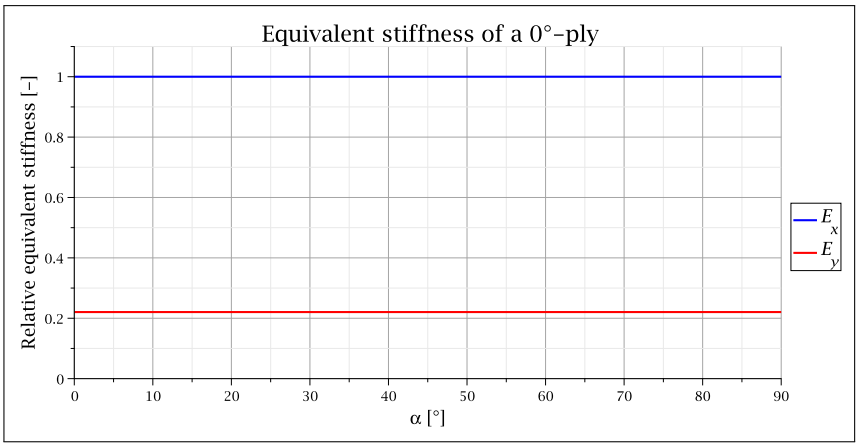

Figure 6.5: Equivalent stiffnesses of a 0°-ply as a function of the inclination angle.

6.2.2. 90°-ply

Figure 6.6 shows the relative equivalent stiffnesses for a 90°-ply as a function of α. It can be seen that E_x is constant and does not depend on the inclination. E_x is derived by evaluating the axial strain in x-direction ε^0_{xx} for a load in x-direction. This corresponds to the axial strain ε^0_{xx} for a 90°-ply with a load N_{xx} as plotted in figure 6.3a, which shows a constant value for the strain. Since the strain was also constant for any α, the relative equivalent stiffness E_x is also constant and is equal to the ratio $\frac{E_2}{E_1}$.

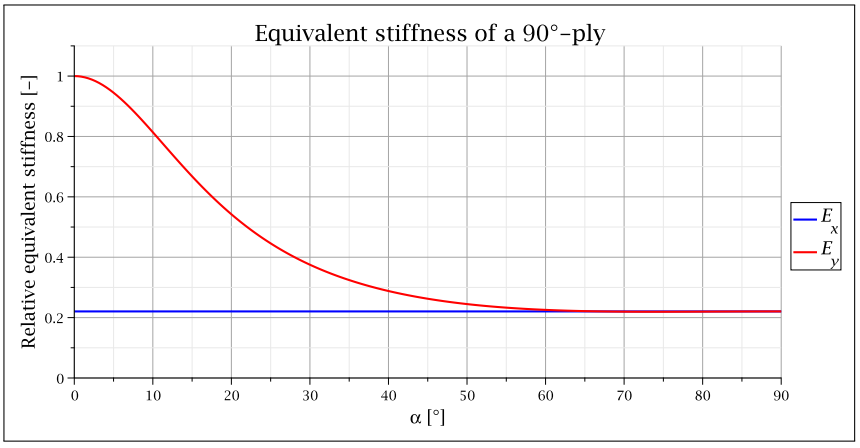

Figure 6.6: Equivalent stiffnesses of a 90°-ply as a function of the inclination angle.

The equivalent stiffness in y-direction is significantly affected by α. When $\alpha = 0°$, E_y is equal to E_1 for a 90°-ply, hence the ratio of 1 in figure 6.6. As α increases, the elastic modulus perpendicular to the fibres will become

more important. Since this E_2 is lower than E_1, the equivalent stiffness will decrease, which is confirmed by figure 6.6. When $\alpha = 90°$, E_y is equal to E_2 since all the fibres are now parallel to the z-axis (figure 6.7). The relative equivalent stiffness E_y is therefore equal to the ratio $\frac{E_2}{E_1}$ for $\alpha = 90°$.

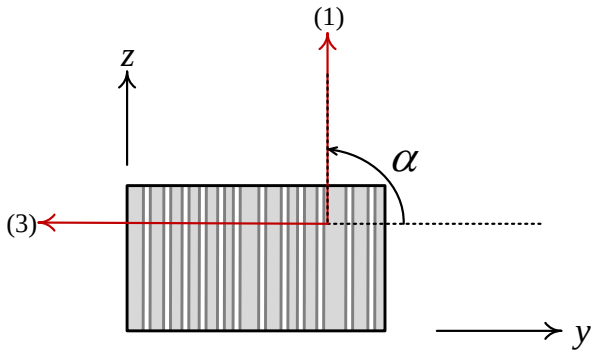

Figure 6.7: 90°-ply with an inclination of 90°. The fibres are oriented parallel to the z-axis.

6.2.3. Balanced and symmetric four-ply laminates

A balanced and symmetric laminate without inclination shows no coupling effects. When an inclination is added to the plies, the **B**-matrix is still zero, so there are again no coupling effects between forces and curvatures, and no coupling effects between moments and strains. However, extra terms do appear in the 12×12 ABD-matrix, for example the terms in the **A**-matrix that relate the out-of-plane shear deformations to in-plane forces (A_{14}, A_{24} and A_{34}). This means the equivalent stiffnesses of balanced and symmetric laminates will also depend on the inclination angle α.

Two four-ply laminates are chosen. Both contain two 0°-plies and two 90°-plies, but their lay-up differs. The first laminate has the two 90°-plies in the middle ($[0/90]_s$) and the second laminate has the two 90°-plies at the edges ($[90/0]_s$). Figure 6.8 shows a cross section of the yz-plane of both laminates.

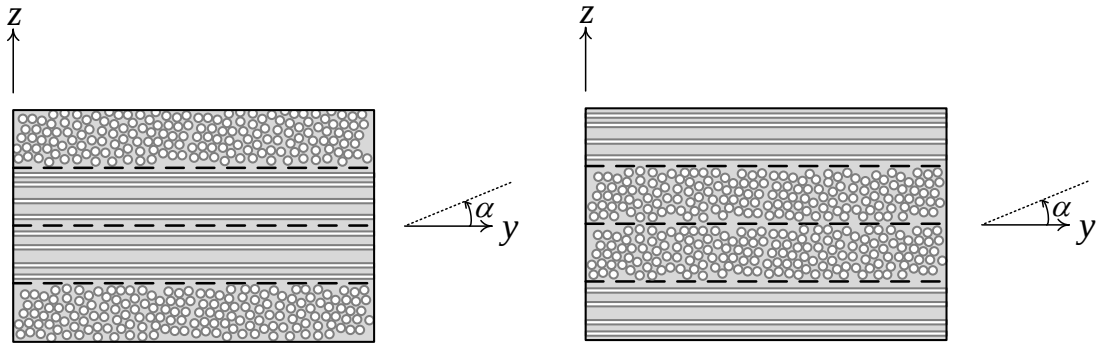

(a) $[0/90]_s$ laminate. (b) $[90/0]_s$ laminate.

Figure 6.8: Two balanced and symmetric laminates.

For both laminates, the in-plane equivalent stiffnesses will be the same for any α since the same number of plies has been used for every fibre direction. The flexural equivalent stiffnesses will differ per laminate, since the location of the stiffest plies differs per laminate. However, for $\alpha = 0°$, the flexural equivalent stiffness in x- and y-direction for the $[0/90]_s$ laminate will be equal to the flexural equivalent stiffness in y- and x-direction for the $[90/0]_s$ laminate respectively.

For both laminates, the relative equivalent stiffnesses as function of α are shown in figure 6.9. As was shown in the sections 6.2.1 and 6.2.2, the equivalent stiffnesses in x-direction of 0°- and 90°-plies do not depend on the inclination angle α. This holds for both the in-plane and flexural equivalent stiffness. Both laminates are composed of 0°- and 90°-plies, so $E_{x,\text{ip}}$ and $E_{x,\text{f}}$ are also constant for the two balanced and symmetric laminates and thus independent of α.

In y-direction, the in-plane and flexural equivalent stiffnesses will differ as α changes. When the inclination increases, the stiffness perpendicular to the fibre direction (E_2) will become more dominant in the determination of the equivalent stiffness. This means a reduction in relative equivalent stiffness will be observed, as indicated in figure 6.9. The in-plane equivalent stiffness does not depend on the location of plies within a laminate for any α. This means $E_{y,\text{ip}}$ is the same for both laminates. For $\alpha = 90°$, the equivalent stiffness $E_{y,\text{ip}}$ is exactly equal to E_2 if the lateral contraction is not taken into account, since all the fibres are parallel to the z-axis, meaning the stiffness in the (3)-direction of every ply coincides with the stiffness along the global y-axis.

The flexural relative equivalent stiffness $E_{y,\text{f}}$ is not the same for both laminates. When an inclination is added, individual 90°-plies show a reduction in equivalent stiffness in y-direction, as mentioned before in section 6.2.2. For the $[90/0]_s$ laminate, the stiffest plies with fibres parallel to the y-axis are located at the top and bottom of the laminate, thus it has the highest $E_{y,\text{f}}$ when $\alpha = 0°$, compared to the $[0/90]_s$ laminate. The outer plies dominate the value for $E_{y,\text{f}}$, so if an inclination is added to a laminate, the laminate with stiffer outer plies will be affected the most by that inclination. Therefore, the relative flexural equivalent stiffness in y-direction for the $[0/90]_s$ laminate in figure 6.9a shows a smaller decrease than the flexural relative equivalent stiffness in y-direction for the $[90/0]_s$ laminate in figure 6.9b. However, the $E_{y,\text{f}}$ for both laminates is the same for $\alpha = 90°$.

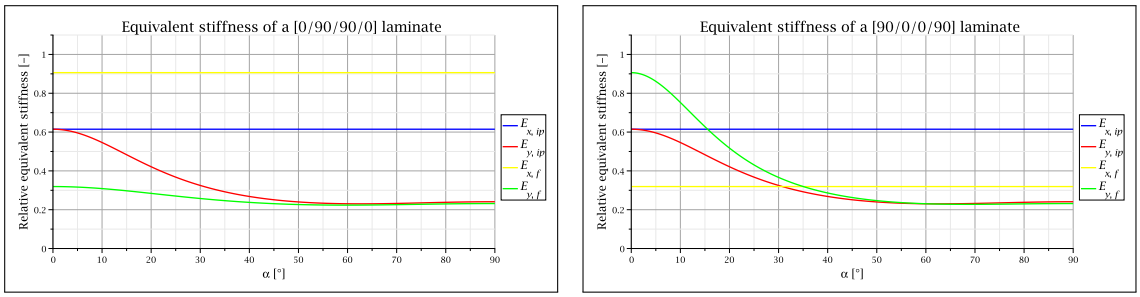

(a) Equivalent stiffness of a $[0/90]_s$ laminate.

(b) Equivalent stiffness of a $[90/0]_s$ laminate.

Figure 6.9: Equivalent stiffnesses of two balanced and symmetric laminates.

6.2.4. Non-balanced and non-symmetric four-ply laminate

A non-balanced and non-symmetric laminate with an inclination will not contain any zero terms in the 12×12 ABD-matrix. The relative equivalent stiffnesses for a $[0/-45/0/90]$ laminate are shown in figure 6.10. Again, the in-plane and flexural equivalent stiffness in x-direction are not affected by the inclination, resulting in a constant $E_{x,\text{ip}}$ and $E_{x,\text{f}}$ for any α. In y-direction, both the in-plane and flexural equivalent stiffness depend on α. The exact values of the reduction of $E_{y,\text{ip}}$ and $E_{y,\text{f}}$ due to the inclination strongly depend on the laminate lay-up and are therefore not further elaborated.

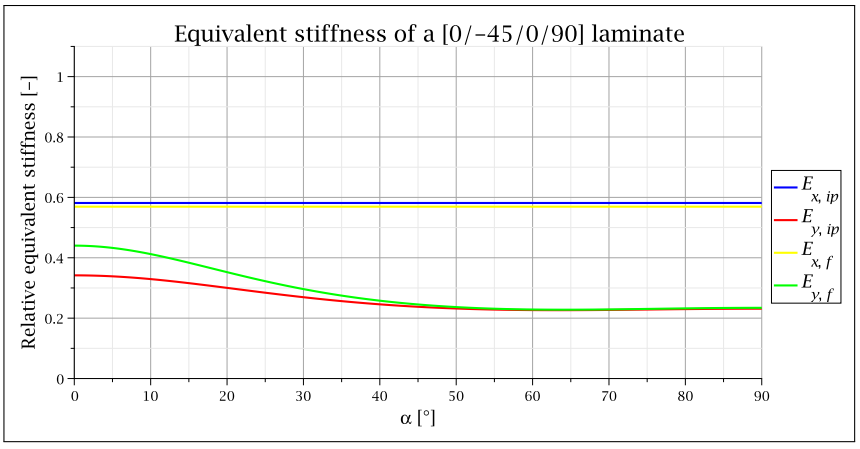

Figure 6.10: Equivalent stiffnesses of a four-ply laminate as a function of the inclination.

7

Lay-up differences due to the ply inclination

Due to the inclination in the plies within a laminate, the lay-up of that laminate will differ along the y-axis, as was described in section 4.4.1. Correspondingly, the results from the modified CLT will also differ along the y-axis. This means the equivalent stiffnesses $E_{x,\text{ip}}$, $E_{y,\text{ip}}$, $E_{x,\text{f}}$ and $E_{y,\text{f}}$ will also be affected. The equivalent stiffnesses of a $[0/90]$ laminate and a $[0/-45/0/90]$ laminate are checked. These two cases will provide insight in the elastic behaviour of inclined laminates with respect to their equivalent stiffnesses along the y-axis.

The material input for the two cases is given in table 2.3. Furthermore, an inclination angle of $\alpha = 10°$ is chosen. It is also assumed that at $y = y_0$, the laminates only contain plies with full thickness. This means that the total laminate thickness measured in the global coordinate system (or $t_{\text{tot},\alpha}$ in figure 4.6) is equal to nt_α, where n represents the number of plies and t_α is the ply thickness measured perpendicular to the plane of the laminate.

7.1. Two-ply laminate

Figure 7.1 shows a cross section of the yz-plane of a $[0/90]$ laminate with an inclination. The lay-up at y_0 and y_2 are the same, and in between those locations at y_1, the laminate lay-up is mirrored. The laminate thickness depends on the inclination angle α, the number of plies and the ply thickness measured perpendicular to the plane of the ply (equation 4.19):

$$t_{\text{tot},\alpha} = n\frac{t_{\text{ply}}}{\cos\alpha} = 2\frac{0.0005}{\cos(10)} = 0.001015 \text{ m} \tag{7.1}$$

The difference between two consecutive full lay-ups depends on the ply thickness and the inclination angle α, and is referred to as the ply width and is indicated with y_{ply}:

$$y_{\text{ply}} = \frac{t_{\text{ply}}}{\sin\alpha} = \frac{0.0005}{\sin(10)} = 0.002879 \text{ m} \tag{7.2}$$

This means that every 0.002879 m, a new ply will appear at the bottom of the two-ply laminate and at the same time a ply will disappear at the top of the laminate. The ply width can also be expressed in terms of y-coordinates:

$$y_{\text{ply}} = y_i - y_{i-1} \qquad \text{with:} \qquad i = 1,2 \tag{7.3}$$

For a two-ply laminate, it is sufficient to determine result up to y_2, since for a larger y-coordinate, the same lay-up will repeatedly be observed.

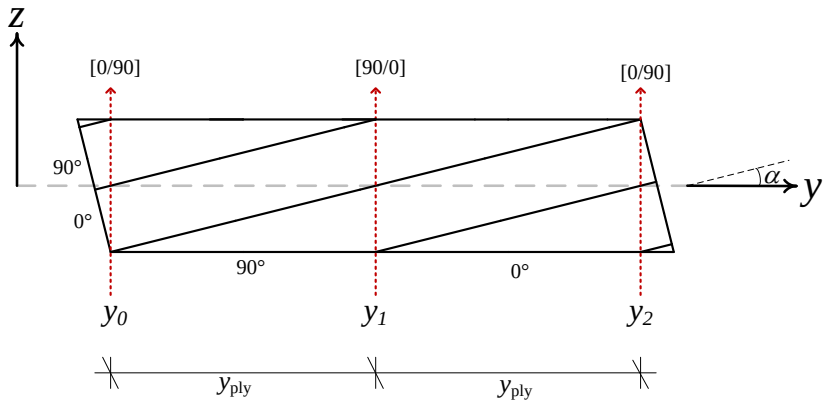

Figure 7.1: Cross section of a two-ply laminate with inclination.

Figure 7.2 shows the equivalent stiffnesses of a $[0/90]$ laminate as a function of the y-coordinate. Due to the same lay-up at y_0 and y_2, and the mirrored lay-up at y_1, the equivalent stiffnesses of these three exact locations along the y-axis are the same. This means for every ply width y_{ply}, the graphs of the equivalent stiffnesses are symmetric around the middle of that same ply width. For example, the graphs plotted between y_0 and y_1 are symmetric around $\frac{y_1+y_0}{2}$. The total number of fibres in one direction does not change along the y-axis. For example halfway between the first ply width at $\frac{y_1+y_0}{2}$, a symmetric lay-up is observed. The 0°-ply is located in the middle and a half 90°-ply is located at both the top and bottom of the laminate. In total, the number of fibres in the 90°-direction is exactly equal to one complete 90°-ply.

From figure 7.2, it can also be seen that the in-plane equivalent stiffnesses in x- and y-direction are different along the y-axis. These differences can completely be assigned to the differences in coupling effects, since the total number of fibres in one direction does not change. Halfway each ply width, a symmetric lay-up is present, so the **B**-matrix will be zero and coupling effects are not present. This means $E_{x,\text{ip}}$ has the same value halfway each ply width (at $\frac{y_i+y_{i-1}}{2}$). The same holds for $E_{y,\text{ip}}$. Since coupling effects reduce the equivalent stiffness, it can also be stated that the $E_{x,\text{ip}}$ and $E_{y,\text{ip}}$ are maximum halfway each ply width (at $\frac{y_i+y_{i-1}}{2}$) and minimal at y_i since the coupling effects are the largest at these locations.

The flexural equivalent stiffnesses strongly depend on the location of the plies within a laminate. When the plies with the stiffest fibre direction are located on the outside, the flexural equivalent stiffness will be the highest along the direction of those stiff fibres. This is confirmed by the graphs for $E_{x,\text{f}}$ and $E_{y,\text{f}}$ in figure 7.2. The flexural equivalent stiffness in x-direction is the lowest for $y = \frac{y_1+y_0}{2}$ since the plies with the stiffest fibre direction are at the center in the 0°-ply and all the weak fibre direction in the 90°-ply are at the top and bottom of the laminate. Correspondingly, $E_{x,\text{f}}$ is the highest for $y = \frac{y_2+y_1}{2}$, where the stiffest 0°-fibres are located at the top and bottom of the laminate. For the flexural stiffness in y-direction it is the other way around. For the y-direction, the 90°-plies are considered as the stiffest plies. At $y = \frac{y_1+y_0}{2}$, these 90°-fibres are located on the outside of the laminate, causing the highest flexural stiffness in y-direction. For $y = \frac{y_2+y_1}{2}$, the lowest $E_{y,\text{f}}$ will be observed.

When no inclination is present in the plies of a laminate, $E_{y,\text{f}}$ of a $[90/0]_s$ laminate will be equal to $E_{x,\text{f}}$ of a $[0/90]_s$ laminate. These laminates correspond to the two-ply laminate presented in figure 7.1 at $y = \frac{y_1+y_0}{2}$ and $y = \frac{y_2+y_1}{2}$ respectively. However, figure 7.2 does not show the same values for the corresponding equivalent stiffnesses at these locations. This comes from the fact that the equivalent stiffness of a 0°-ply is not affected by an inclination and a 90°-ply is affected . This means when the 0°-plies dominate the value for the flexural equivalent stiffness of the $[0/90]$ laminate with an inclination, which is the case for $E_{x,\text{f}}$ at $y = \frac{y_2+y_1}{2}$, the result will be the highest.

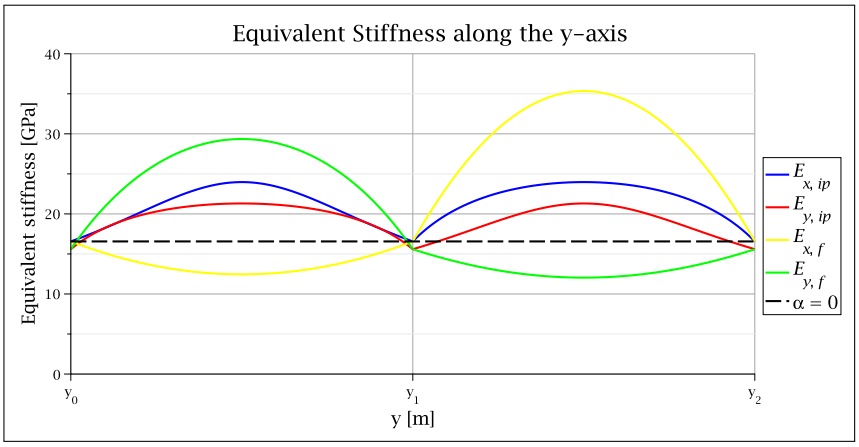

Figure 7.2: Equivalent stiffnesses of a [0/90]-laminate as a function of the y-coordinate.

In figure 7.2, the black dashed line indicates the equivalent stiffness when no inclination is present. All four equivalent stiffnesses are the same for a [0/90] laminate. The equivalent stiffness graph for $\alpha = 0°$ for $y_{i-1} < y < y_i$ is obtained by evaluating the corresponding equivalent stiffness for $\alpha = 0°$ at $y = y_{i-1}$. This means that the lay-up difference is not taken into account. At y_0, y_1 and y_2, $E_{x,\text{ip}}$ and $E_{x,\text{f}}$ are exactly equal to the non-inclined result, since the equivalent stiffnesses in x-direction do not depend on the inclination angle α, as was shown in section 6.2. $E_{x,\text{ip}}$ and $E_{x,\text{f}}$ do differ from the non-inclined result at these locations, since these equivalent stiffnesses depend on the inclination angle α. At $y = \frac{y_i + y_{i-1}}{2}$, large differences are observed between the non-inclined result and the four equivalent stiffnesses due to the symmetric lay-up at those locations for the inclined results. This symmetric lay-up is not taken into account in the non-inclined result.

7.2. Non-balanced and non-symmetric four-ply laminate

The same four-ply laminate with a lay-up of $[0/-45/0/90]$ will be chosen. Figure 7.3 shows a cross section of this laminate, where it can be seen that four different lay-ups occur along the y-axis. The total laminate thickness will be the following:

$$t_{\text{tot},\alpha} = n\frac{t_{\text{ply}}}{\cos\alpha} = 4\frac{0.0005}{\cos(10)} = 0.002031 \text{ m} \tag{7.4}$$

Since the inclination angle α and the ply thickness t_{ply} are not altered compared to the [0/90] laminate, the same ply width is applicable ($y_{\text{ply}} = 0.002879$ m). Again, the ply width can also be expressed in terms of y-coordinates:

$$y_{\text{ply}} = y_i - y_{i-1} \qquad \text{with:} \qquad i = 1,2,3,4 \tag{7.5}$$

For a four-ply laminate, results need to be derived for $y_0 < y < y_4$. For $y > y_4$, the same lay-up will repeatedly be observed and the results will be the same.

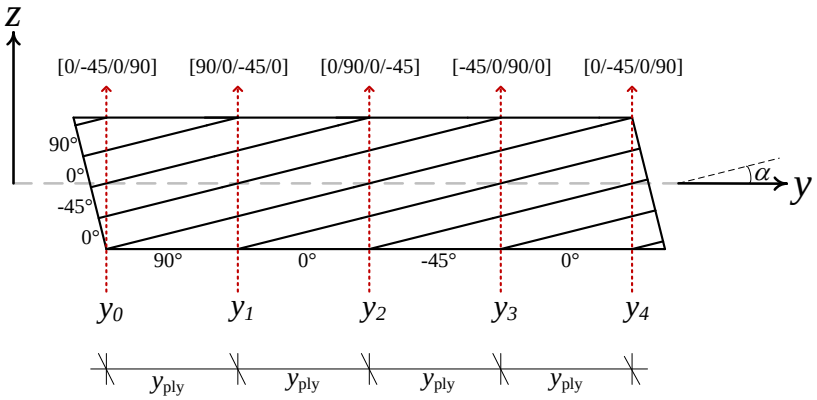

Figure 7.3: Cross section of a four-ply laminate with inclination.

Figure 7.4 shows all the equivalent stiffnesses for the four-ply laminate. The lay-ups at y_0 and y_1 are mirrored, which means the values for all four equivalent stiffnesses are equal at y_0 and y_1. It can therefore be stated that the graphs for the equivalent stiffnesses are symmetric around $\frac{y_1+y_0}{2}$ between y_0 and y_1. The lay-ups at y_2 and y_3 are also mirrored, so the equivalent stiffness graphs between these two locations must be symmetric around $\frac{y_3+y_2}{2}$. At y_4, the same lay-up is obtained as for y_0, meaning the equivalent stiffnesses will be the same. So in total, the equivalent stiffnesses at y_0, y_1 and y_4 are the same. Furthermore, the lay-ups at y_2 and y_3 lead to the same equivalent stiffnesses. Due to all these similarities in equivalent stiffnesses, it can be deduced that when the equivalent stiffness graphs between y_1 and y_2 are mirrored around $y = \frac{y_3+y_2}{2}$, the equivalent stiffness graphs between y_3 and y_4 are obtained.

This laminate is non-balanced and non-symmetric for all five y_i-coordinates, so coupling effects are present at these locations. The in-plane equivalent stiffnesses in x- and y-direction will differ along the y-axis due to the difference in coupling effects between all the locations y_i. At $y = \frac{y_1+y_0}{2}$ the lay-up is symmetric, namely $[90_{0.5}/0/-45/0/90_{0.5}]$, where the 0.5 in the subscript indicates the ply has half the thickness of the other plies. The same holds for $y = \frac{y_3+y_2}{2}$, where the lay-up is equal to $[-45_{0.5}/0/90/0/-45_{0.5}]$. The in-plane equivalent stiffnesses will be the highest at the corresponding locations, due to the absence of coupling effects for these symmetric laminates. Note that this symmetry in the non-balanced, non-symmetric four-ply laminate is only possible since two plies with the same fibre orientation are present. This means the former is not applicable to all non-balanced and non-symmetric laminates.

It is remarkable that both $E_{y,\text{ip}}$ and $E_{y,\text{f}}$ show approximately evenly curves between three times the ply width, namely between y_1 and y_4. As mentioned before, the in-plane equivalent stiffness in y-direction is the highest at $y = \frac{y_3+y_2}{2}$ due to the absence of coupling effects. At this location, the plies with the least stiff fibre direction (from a 0°-ply) are located on the outside of the laminate. Therefore, the flexural equivalent stiffness at this location will be the lowest. At y_1, the stiffest 90°-ply is still located on the outside of the laminate, which is not the case any more at y_2. This is the reason $E_{y,\text{f}}$ is decreasing between y_1 and y_2. Correspondingly, the in-plane equivalent stiffness $E_{y,\text{ip}}$ is increasing between these two locations, since the coupling effects decrease.

The differences in lay-up are not large enough to affect the equivalent stiffnesses in x-direction as significantly as in y-direction. However, $E_{x,\text{ip}}$ is larger at y_2 and y_3 compared to y_1 and y_4. The differences are very limited, thus the curved shape is still obtained for every ply width. The flexural stiffness $E_{x,\text{f}}$ also shows a small increase, meaning $E_{x,\text{f}}$ is larger at y_2 than at y_1, which is not in correspondence with the graph of $E_{y,\text{f}}$, which showed a significant decrease between y_1 and y_2. This small increase comes from the fact that at y_1 a 0°-ply and a 90°-ply are located on the outside and at y_2 a 0°-ply and a −45°-ply are located on the outside. The −45°-ply has a higher stiffness in x-direction compared to a 90°-ply, thus the flexural stiffness $E_{x,\text{f}}$ is also larger.

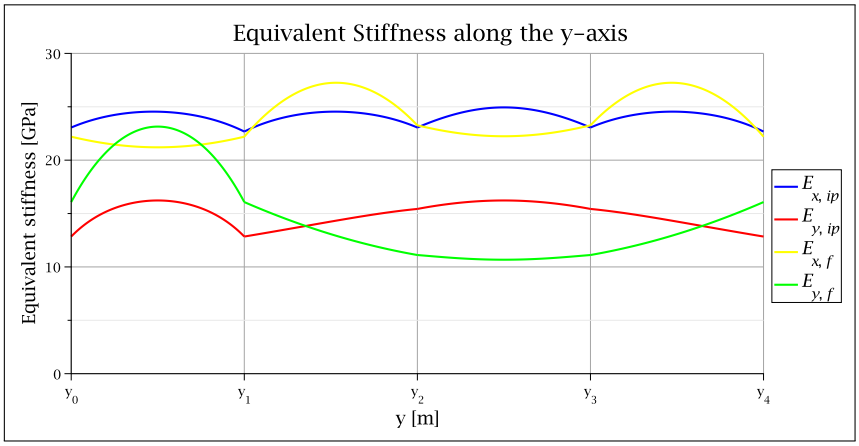

Figure 7.4: Equivalent stiffnesses of a $[0/-45/0/90]$-laminate as a function of the y-coordinate.

7.2.1. Comparison with the non-inclined result

Figure 7.5 shows all four equivalent stiffnesses as a function of the y-coordinate where the non-inclined results are included with dashed lines. The non-inclined result for $y_{i-1} < y < y_i$ is obtained by evaluating the equivalent stiffness for $\alpha = 0°$ at $y = y_{i-1}$. This means the lay-up differences are not taken into account between y_{i-1} and y_i, meaning a constant equivalent stiffness is found.

Since the lay-ups at y_0 and y_1 are mirrored, the same equivalent stiffnesses are obtained at these locations. This means that the non-inclined results are constant between y_0 and y_2. Correspondingly, the non-inclined equivalent stiffnesses are constant between y_2 and y_4 since the lay-ups at y_2 and y_3 are mirrored.

As described in section 6.2, the equivalent stiffnesses in x-direction do not depend on the inclination angle α. This means the non-inclined result at $y = y_i$ is always equal to the inclined result at $y = y_i$. The differences in $E_{x,\text{ip}}$ and $E_{x,\text{f}}$ can completely be assigned to the lay-up differences and not to the inclination angle α. The equivalent stiffnesses in y-direction do depend on the inclination angle. Therefore, at $y = y_i$, $E_{y,\text{ip}}$ and $E_{y,\text{f}}$ are not equal to the non-inclined result at $y = y_i$.

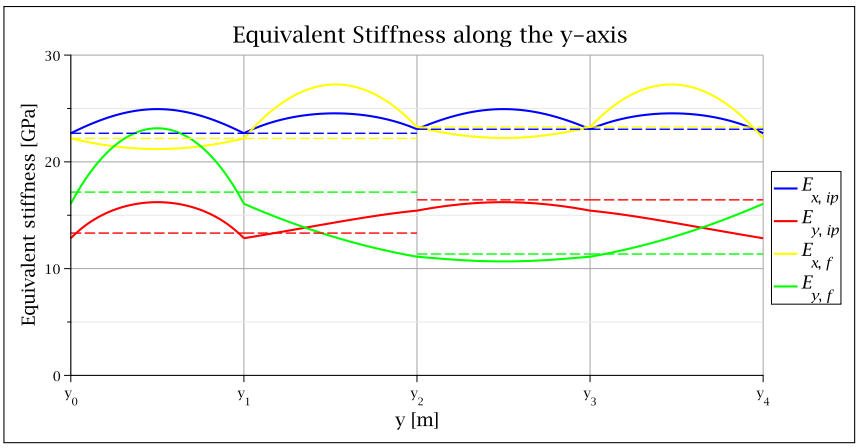

Figure 7.5: Equivalent stiffnesses of a $[0/-45/0/90]$-laminate as a function of the y-coordinate including the non-inclined results with dashed lines.

It should be noted that the non-inclined result does not have a practical meaning. The lay-up differences are only evaluated at four locations, which results in jumps in the lay-up, as indicated in figure 7.6. Since no inclination is present, the y_{ply} cannot be evaluated. However, the same y_{ply} obtained for an inclination of $\alpha = 10°$ is used to determine the locations of the lay-up jumps. In figure 7.6, it can also be seen that the lay-up between y_1 and y_2 is the same, but mirrored, compared with the lay-up between y_0 and y_1. Therefore, the non-inclined equivalent stiffnesses are constant between y_0 and y_2. The same holds for the non-inclined equivalent stiffnesses between y_2 and y_4, since the lay-up between y_3 and y_4 is the same, but mirrored, as the lay-up between y_2 and y_3.

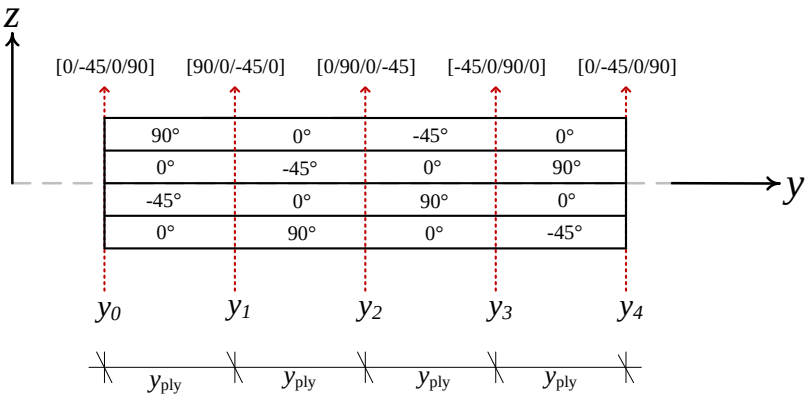

Figure 7.6: Cross section of a four-ply laminate without inclination, but with lay-up jumps.

8

Modified CLT with respect to InfraCore

InfraCore panels contain plies that start at the bottom skin, continue in the web and end at the top skin, as described in section 2.3.2. This causes the plies to be inclined in the skins of the InfraCore panel. The skins can be evaluated using the modified CLT, where the inclination has been included. In this chapter the influence of the inclination angle α on InfraCore skins will be determined.

First, the input for the modified CLT must be defined. The five transversely isotropic material are given in table 2.3 and are used as material parameters for each individual ply. The lay-up of an InfraCore skin might differ per design. The following ply configuration is common for InfraCore skins [5]:

$$\text{Lay-up:} \quad [0_2/-45/45]_N \tag{8.1}$$

Here, N indicates the number of repetition, which can differ per design of InfraCore, but N=3 is a common number of repetition. Furthermore, the thickness of each ply is needed as input. A common ply thickness lays between 800 and 900 µm, where the resin layer in between the plies has a thickness between 50 and 90 µm [5]. In total, the ply thickness will be between 850 and 990 µm. For all the results presented in this chapter, a ply thickness of 900 µm (=0.0009 m) is assumed. Finally, the inclination angle α is needed as input for the modified CLT. It should be mentioned that the inclination angle in InfraCore skins strongly depends on the dimensions of a panel, such as the distance between the webs and the total number of plies. It can be assumed that an angle $\alpha = 2°$ is representative for InfraCore skins [5].

8.1. Influence of the inclination on the equivalent stiffnesses

The inclination angle α is constant for an InfraCore skin and depends on the distance between the webs and the ply thickness. Since these parameters can differ per InfraCore panel design, the inclination can also differ. It is therefore necessary to determine the influence of the inclination angle α. This will be done with respect to the equivalent stiffnesses in x- and y-direction. Distinction is made between the complete laminate input of the InfraCore skin and a simplification of the skin with one homogeneous layer, where the material properties are determined using engineering constants.

8.1.1. Complete laminate input of the InfraCore skin

As described in section 6.2, the 0°-plies will not be affected by the inclination. However, the ±45°-plies are affected by α, thus the total InfraCore skin for any N will be affected by the inclination. It should be noted that an InfraCore skin is balanced for any N, which will cause zero terms in the 12×12 ABD-matrix.

The equivalent stiffnesses in x-direction ($E_{x,\text{ip}}$ and $E_{x,\text{f}}$) do not change for any laminate for any α, as was found in section 6.2.4. Here it was shown that the relative equivalent stiffness in x-direction for a non-balanced and non-symmetric laminate was constant and equal to one. However, the absolute $E_{x,\text{ip}}$ is not equal to the absolute $E_{x,\text{f}}$, except for single plies. The same holds in y-direction, with the difference that $E_{y,\text{ip}}$ and $E_{y,\text{f}}$ do depend on α. It is expected that as the number of repetition N in the InfraCore panels increases, the values of the in-plane equivalent stiffnesses will be closer to the flexural equivalent stiffnesses in the corresponding direction. As N increases, the laminate will become more homogeneous and can better be approximated as a single ply. To check this presumption, two absolute equivalent stiffness plots are given for N=1 and N=3 in figure 8.1.

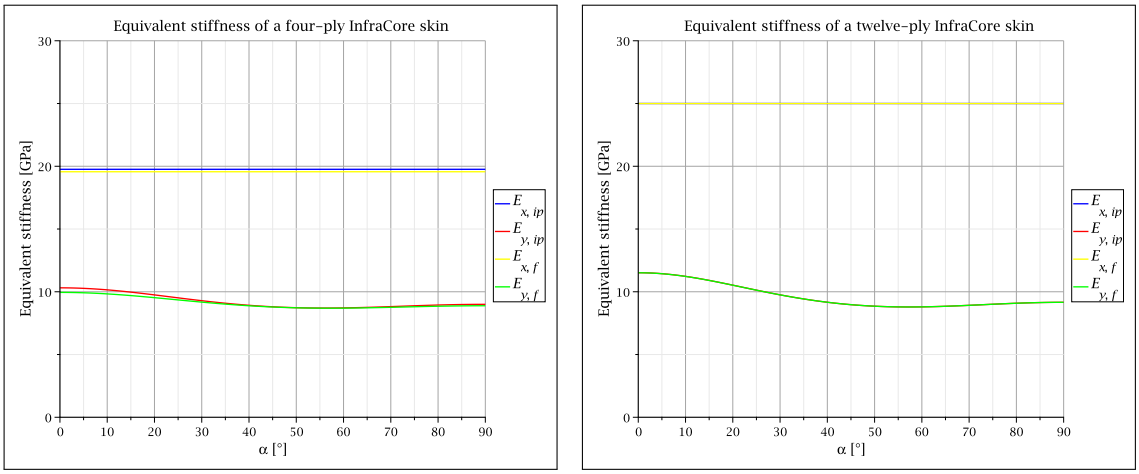

(a) N=1. (b) N=3.

Figure 8.1: Equivalent stiffness of two InfraCore skins.

For N=1, very small differences between the in-plane stiffnesses and the flexural stiffnesses are observed for both the x- and y-direction. Since the equivalent stiffnesses in x-direction are not affected by the inclination α, the differences between $E_{x,\text{ip}}$ and $E_{x,\text{f}}$ are the same for any α. In y-direction, it can be seen that the differences between $E_{y,\text{ip}}$ and $E_{y,\text{f}}$ decrease as α increases until a minimum value of approximately $\alpha \approx 60°$ has been reached. After that value, the differences between $E_{y,\text{ip}}$ and $E_{y,\text{f}}$ increase again. For N=3, all the differences are decreased and it is hard to distinguish different lines for the in-plane stiffnesses and the flexural stiffnesses. To check at what rate the differences between the in-plane stiffnesses and flexural stiffnesses decrease, the ratio between $E_{x,\text{ip}}$ and $E_{x,\text{f}}$ has been determined, as well as the ratio between $E_{y,\text{ip}}$ and $E_{y,\text{f}}$. This has been done for N ranging from 1 to 5. The equivalent stiffnesses in x-direction do not depend on α, so only one graph is necessary. The equivalent stiffnesses in y-direction do depend on α. For this reason, the ratio between $E_{y,\text{ip}}$ and $E_{y,\text{f}}$ has been determined for an inclination equal to 0°, 30°, 60° and 90°. The results can be found in figure 8.2.

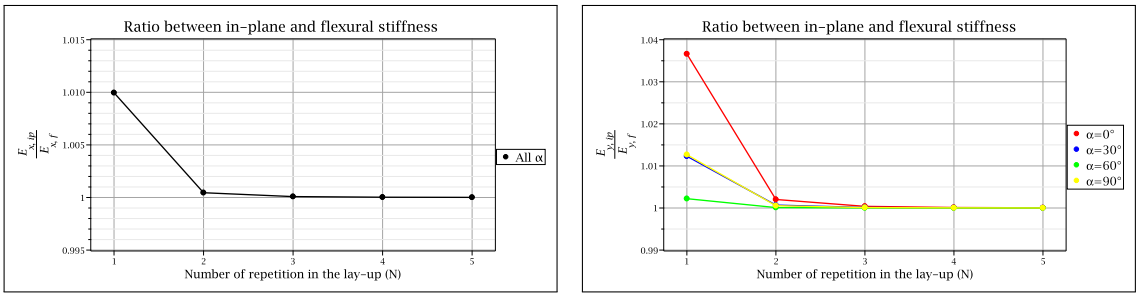

(a) x-direction. (b) y-direction.

Figure 8.2: Ratio between the in-plane and flexural equivalent stiffness of a $[0_2/-45/45]_N$ InfraCore skin.

It can be seen that the ratio between the in-plane equivalent stiffness and the flexural equivalent stiffness converges to 1 as N increases. This holds for both the x-direction and the y-direction. For the y direction, the ratio is the closest to 1 for $\alpha = 60°$. This is in correspondence with the result plotted in figure 8.1a, where it can be seen that $E_{y,\text{ip}}$ and $E_{y,\text{f}}$ are the closest to each other for $\alpha \approx 60°$. The largest ratios are observed for $\alpha = 0°$ for the equivalent stiffnesses in y-direction. From the figures 8.2a and 8.2b it seems that for N=3 it is safe to assume that the in-plane equivalent stiffnesses are equal to the flexural equivalent stiffnesses in the corresponding direction. The largest ratio is equal to 1.0004, which is assumed to be close enough to 1 to conclude that $E_{\text{ip}} = E_{\text{f}}$ for both the x- and y-direction.

As mentioned before, the inclination angle α can differ per InfraCore design. An angle of 2° is very common in InfraCore skins. It is therefore more useful to plot the relative equivalent stiffness for angles much smaller than 90°, as had been done up to now. A plot for $0° < \alpha < 10°$ will provide practical insight of the effect of the inclination on the relative equivalent stiffness of InfraCore panels, and can be found in figure 8.3. Since

the equivalent stiffness in x-direction is independent of α for any laminate, it does not need to be plotted. In this case, the relative equivalent stiffness E_y has been determined by dividing the equivalent stiffness with the corresponding equivalent stiffness for $\alpha = 0°$. This will provide better insight in the reduction of E_y with respect to its value for $\alpha = 0°$, meaning the influence of α can be better evaluated. It can be seen that the reduction in stiffness is limited. For $\alpha = 2°$, a relative equivalent stiffness of 0.9985 is obtained, meaning E_y of an InfraCore skin reduces 0.15%, so it can be concluded that the inclination of 2° has a very small effect on elastic behaviour of an InfraCore skin with material properties and a lay-up as presented in this section.

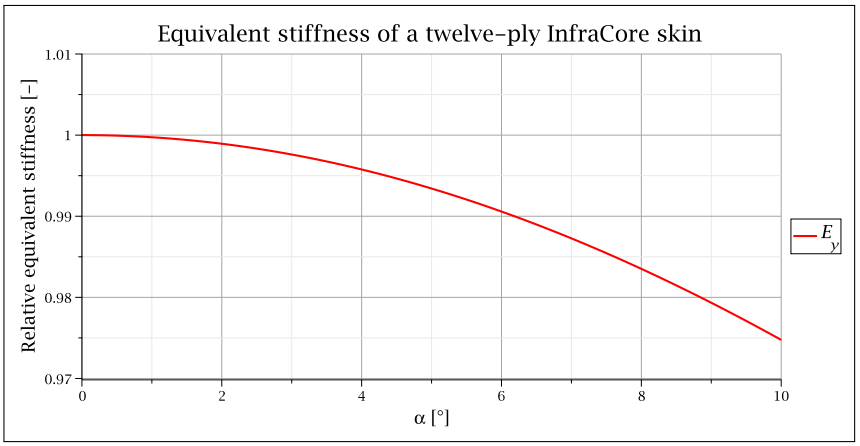

Figure 8.3: Relative equivalent stiffness of a twelve-ply InfraCore skin.

8.1.2. Single-layer simplification of the InfraCore skin

In a preliminary design phase, it is desirable to use a single homogeneous layer to perform a first design check. As mentioned before, the behaviour of a single ply with inclined properties is much easier to predict and explain compared to a complete laminate. Engineering constants can be derived for an InfraCore skin using the regular CLT. The result can be used as input in the modified CLT for an equivalent 0°-ply. In chapter 6 it was shown that a 0°-ply was not affected by the inclination angle α. However, when the engineering constants are used as input, a general orthotropic material should be used instead of a transversely isotropic material since it no longer holds that the (2,3)-plane is a plane of isotropy. This means nine independent material parameters are needed and the 0°-ply will be affected by α. Since $E_2 \neq E_3$, out-of-plane shear deformations can occur when an inclination is present in the 0°-ply.

Four material parameters can be determined using the engineering constants from the regular CTL. Distinction can be made between in-plane and flexural engineering constants. For the InfraCore lay-up $[0_2/-45/45]_N$, the values of the engineering constants are not the same. Figure 8.4 shows the ratio between the in-plane engineering constants and the flexural engineering constants. It can be seen that as the number of repetition N increases, the ratios all converge to 1. For N=3, the largest ratio occurs for G_{xy} and is equal to 1.001. It is assumed that this ratio is close enough to 1 to assume that the in-plane engineering constants are equal to the flexural engineering constants for N=3. When the regular CLT with transversely isotropic material parameters from table 2.3 is used, engineering constants are obtained as given in table 8.1. Here, E_1, E_2, G_{12} and ν_{12} correspond to engineering constants for E_x, E_y, G_{xy} and ν_{xy} respectively.

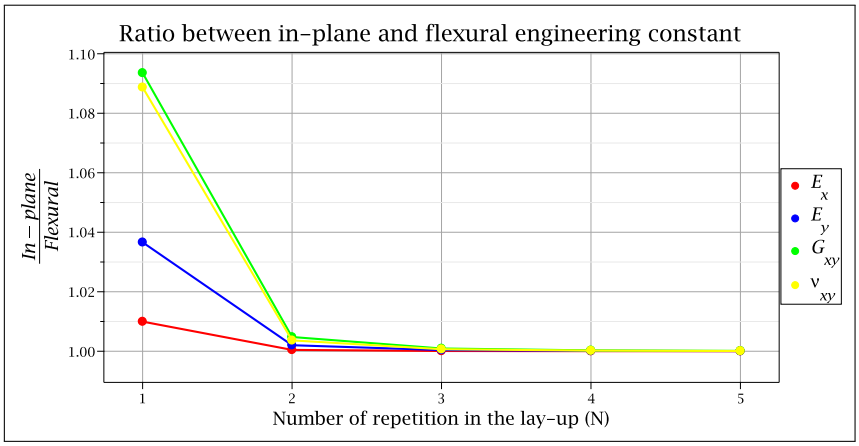

Figure 8.4: Ratio between the in-plane and flexural engineering constants from the regular CLT of a $[0_2/-45/45]_N$ InfraCore skin.

The axial stiffness E_3 represents the stiffness perpendicular to the ply. When the regular CLT is considered, E_3 is the same for every ply and thus also the same for the complete laminate. According to the rules for transversely isotropic material, the out-of-plane ply stiffness E_2 can be used for E_3 in the single-layer simplification of the InfraCore skin.

The two additional Poisson's ratios ν_{13} and ν_{23} are determined by the strain in the (3)-direction when a load in the (1)- or (2)-direction is applied respectively. Since it is assumed that the stiffness in the (3)-direction is the same for the complete laminate, it is also assumed that the lateral contraction in the (3)-direction is the same. Therefore, it is assumed that the Poisson's ratios ν_{13} and ν_{23} do not need to be changed. For a transversely isotropic material, ν_{13} is equal to ν_{12} while ν_{23} is an independent material parameter.

The shear stiffness G_{13} is assumed to remain unchanged when an orthotropic material is used. Therefore, G_{13} will be equal to the original G_{12}. The remaining shear stiffness G_{23} was determined by using the isotropic relation due to the plane of isotropy in the plies (equation 3.10). If this is done in this case with the new E_2, which is the E_y from the engineering constants, a value of 4.11 GPa is obtained for G_{23}. The resulting equivalent stiffness for the single-layer simplification of the InfraCore skin for this value of G_{23} is plotted in figure 8.5 with the yellow line. It can be seen that for $0 < \alpha < 10$, the value of the relative E_y increases, which indicates the shear stiffness estimate is too high compared to the used E_2. This can be explained by the fact that for the complete laminate, the (2,3)-plane is not a plane of isotropy.

A lower value of G_{23} must be chosen. The original value for G_{12} can also be used (G_{12}=3.8 GPa). The result is plotted with the green line in figure 8.5. The dashed black line indicates the result for the complete twelve-ply input of an InfraCore skin. It can be seen that for G_{12}=3.8 GPa, the relative equivalent stiffness in y-direction is lower than 1, but still too high compared to the original result with the twelve-ply input. A lower value could also be chosen, for example G_{12}=2 GPa. This result is plotted in blue and shows that the relative E_y decreases too fast compared to the original result, indicating the shear stiffness is too low compared to E_2.

Originally, E_3 was equal to E_2 for the transversely isotropic material input. Since this is not the case any more, the shear stiffness G_{23} can be estimated by the following relation:

$$G_{23} = \frac{E_3}{2\,(1+\nu_{23})} = \frac{8.6}{2\,(1+0.4)} = 3.07 \text{ GPa} \tag{8.2}$$

The relative E_y for the single-layer InfraCore skin simplification is plotted in red in figure 8.5 and is close to the original result. It should be stressed that it is hard to determine a correct value for G_{23}, and that this shear stiffness is highly influential on the equivalent stiffness in y-direction. For now, the value presented in equation 8.2 will be chosen and used to compare the single-layer InfraCore skin simplification with the twelve-ply input. All nine independent orthotropic material parameters are presented in table 8.1.

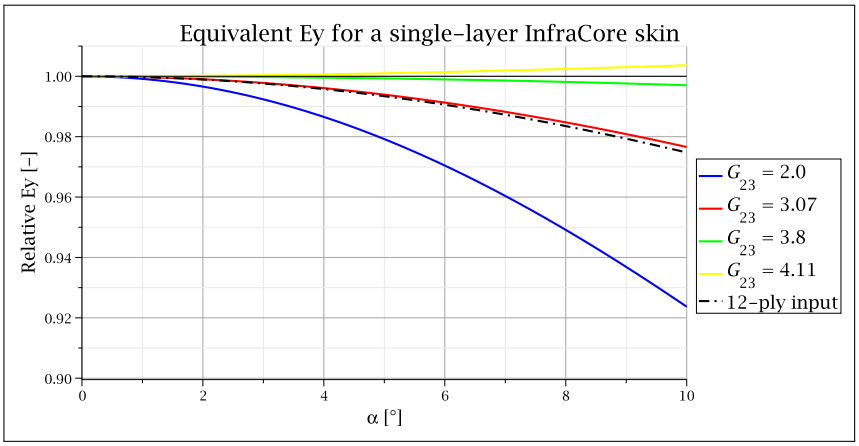

Figure 8.5: Equivalent stiffness in y-direction for a single-ply InfraCore skin simplification for different G_{23} (in GPa).

The relative equivalent stiffness in x-direction is still independent of α and has therefore not been plotted. From figure 8.5, it can be seen that the difference between the original twelve-ply input and the single-ply simplification with G_{23}=3.07 GPa increases as α increases. For $\alpha = 10°$, the difference between the two is 0.2%, which is assumed to be small enough to conclude that the single-ply simplification of the InfraCore skin with G_{23}=3.07 GPa is a good estimate.

Table 8.1: Orthotropic material parameters for the single-layer InfraCore skin simplification.

Property	Value	Origin
E_1	25 GPa	Engineering constant: $E_{x,\text{laminate}}$
E_2	11.5 GPa	Engineering constant: $E_{y,\text{laminate}}$
E_3	8.6 GPa	Out-of-plane ply stiffness: $E_{3,\text{ply}}$
G_{12}	7.2 GPa	Engineering constant: $G_{xy,\text{laminate}}$
G_{13}	3.8 GPa	Assumed to remain unchanged
G_{23}	3.07 GPa	Calibrated
ν_{12}	0.46	Engineering constant: $\nu_{xy,\text{laminate}}$
ν_{13}	0.28	Assumed to remain unchanged
ν_{23}	0.4	Assumed to remain unchanged

8.1.3. Approximation of stiffness reduction

All the equivalent stiffness plots provided in this report strongly depend on the number of plies, laminate lay-up and material properties. The equations that are plotted are very complex due to the fact they contain very many sine and cosine terms and are therefore not presented in this report, but can be obtained using the Maple script presented in appendix A. In practice, it is desirable to use a simple formula to determine the stiffness reduction as a function of α. Since the equivalent stiffness in x-direction is independent of α, only E_y will be considered. Furthermore, it will be assumed that inclination angles up to 10° are relevant for InfraCore panels. The simplified formulas will therefore only be derived for $0° < \alpha < 10°$.

Several types of formulas can be chosen to approximate the relative equivalent stiffness E_y. From figures 8.3 and 8.5, it seems that all the lines can be approximated by a parabola (second-order polynomial):

$$f_k(\alpha) = C_1 + C_2\alpha + C_3\alpha^2 \tag{8.3}$$

To determine the constants C_1, C_2 and C_3 of the parabola, several values are chosen for α. The corresponding E_y is determined for each α using the complex formula obtained with the modified CLT for a twelve-ply InfraCore skin. Next, a parabola $f_k(\alpha)$ is fitted through all the points using the `PolynomialFit` function in Maple. This function fits a polynomial of a specified order to data points by minimising the least-squares error [13]. The quality of the parabola fit is evaluated considering the coefficient of determination (R-squared) and the average difference between the original result and the fitted result.

The number of points used to evaluate the original E_y is indicated with k. For example, when k=3, 3 equidistant points are taken on the interval of $0° < \alpha < 10°$. This results in 0°, 5° and 10° as the 3 values for α used to fit

the parabola. Since a parabola contains 3 constants that need to be determined (C_1, C_2 and C_3), 3 is the lowest possible value for k. When k increases, the distance between the points decreases since the total interval remains the same. In this case, 21 is taken as the highest value for k. This leads to 20 intervals of $\Delta\alpha = 0.5°$ each.

When a polynomial fit is obtained, the average difference is determined. This is done by evaluating the absolute difference between E_y and $f_k(\alpha)$ for 201 points ($\Delta\alpha = 0.05°$), and taking the average of the absolute differences of all those points. It does not matter how many points are taken, since the average is taken over all those points. The number of points should however be large enough in order to obtain a correct value for the average difference. In this case, it is assumed that 201 points is enough, since the largest value for k is almost a factor 10 smaller.

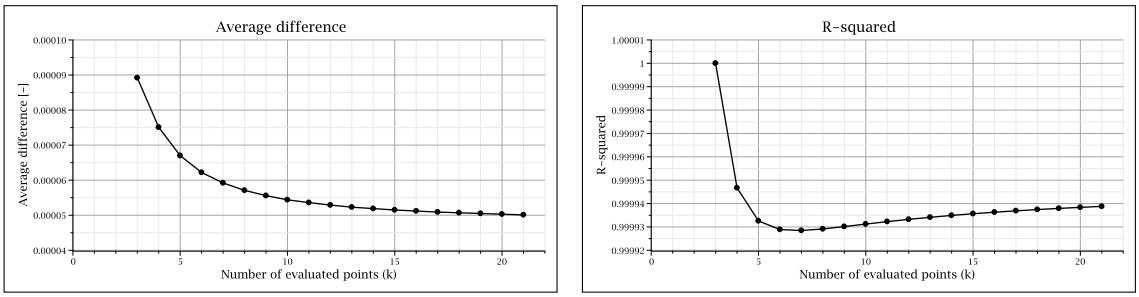

(a) Average difference.

(b) R-squared.

Figure 8.6: Quality of the fit as a function of the number of evaluated points k.

Figure 8.6a shows the average difference for all the k-values. It can be seen that the average difference decreases as k increases. The highest average difference between the original relative equivalent stiffness and the fitted result is equal to 0.00009 and occurs for k=3. This difference is very low, meaning the fit for k=3 will match the original result quite good. The fit f_3 is shown in figure 8.7 where the original has also been shown. Due to the quality of the fit, hardly any differences can be observed.

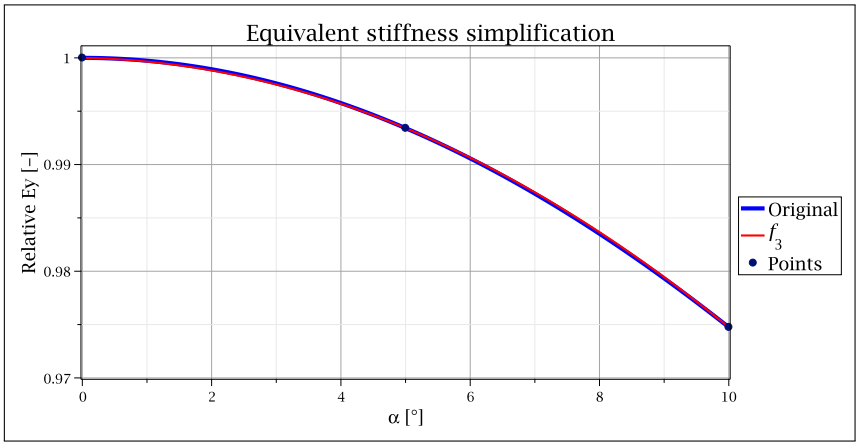

Figure 8.7: Fitted parabola for k=3.

Figure 8.6b shows the R-squared value for $3 < k < 21$. For k=3, R-squared is equal to 1, since the number of points used to determine the parabola is equal to the number of constants in a parabola. It is also shown that the R-squared value decreases and reaches a minimum at k=7. For $k > 7$, the R-squared value increases, indicating the fit becomes closer to the point results. It should be noted that even the lowest value for R-squared is very close to 1, meaning even the worst fit is quite good. This is confirmed by the graph in figure 8.8, where hardly any differences can be seen between the fitted result and the original result.

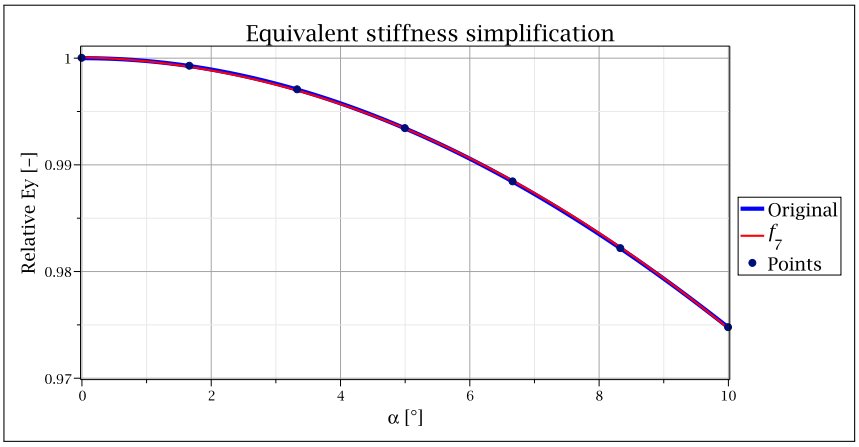

Figure 8.8: Fitted parabola for k=7.

In conclusion, for $0° < \alpha < 10°$ all the fits are very good and approximate the original result very well. The reduction in equivalent stiffness in y-direction of a twelve-ply InfraCore skin can be approximated by the parabola presented in equation 8.4. Here, the values for C_1, C_2 and C_3 are taken for $k = 21$, since the average difference of the polynomial fit is the lowest for $k = 21$, considering all values of k considered in this section.

$$f_{21}(\alpha) = 1 - 0.00013\alpha - 0.00024\alpha^2 \tag{8.4}$$

When an angle of 2° is considered, which is a representative value for the ply inclination in an InfraCore skin, a relative equivalent stiffness of 0.99897 is obtained. This means the reduction in stiffness due to the inclination in the plies in an InfraCore skin is only 0.122%, which is in the same order of magnitude as the 0.15% obtained with the complete result presented in section 8.1.1.

8.2. Influence of the inclination on the out-of-plane shear strains

Due to the inclination in the plies of an InfraCore skin, out-of-plane shear strains occur. The local axes of the ±45°-plies in the InfraCore skin with an inclination do not coincide with any axis in the global coordinate system. This means both γ^0_{yz} and γ^0_{xz} will be observed. The influence of the ply inclination on the out-of-plane shear strains of an InfraCore skin is given in figure 8.9, where the out-of-plane shear strains are plotted as a function of α for angles between 0° and 10°. Distinction is made between an axial load N_{xx} and an axial load N_{yy}, where both have a value of 10000 N/m. Furthermore, the out-of-plane shear strains are obtained for both a four-ply InfraCore skin ($N = 1$) and a twelve-ply InfraCore skin ($N = 3$), which will provide insight in the dependence of the number of repetition on the out-of-plane shear strains. The total thickness of the laminate is kept the same, meaning the ply thickness of the twelve-ply InfraCore skin is one third of the ply thickness of the four-ply InfraCore skin.

The figures 8.9a and 8.9b give the out-of-plane shear strains that occur when a load in x-direction is applied. The same scale on the vertical axis has been used. It can be seen that in absolute terms both γ^0_{yz} and γ^0_{xz} increase as α increases. The same holds for a load N_{yy}, which is shown in the figures 8.9c and 8.9d. When the values on the vertical axes are compared, it can be concluded that for an InfraCore skin, the out-of-plane shear strains are larger for a load N_{yy} compared to a load N_{xx}.

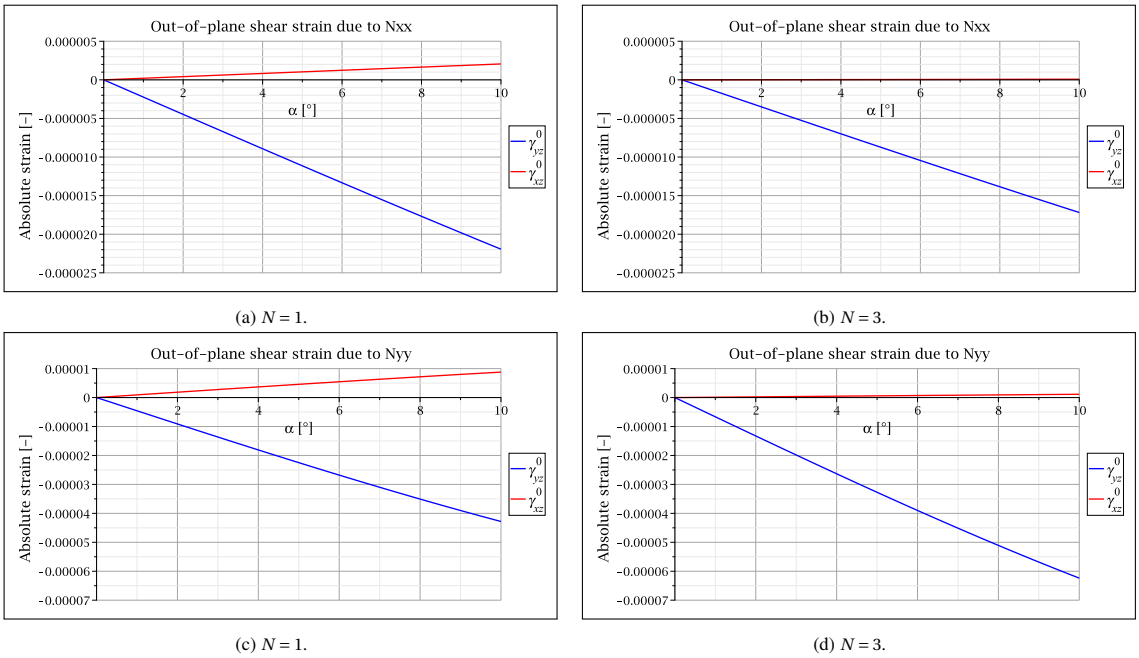

(a) $N = 1$. (b) $N = 3$.

(c) $N = 1$. (d) $N = 3$.

Figure 8.9: Out-of-plane shear strains due to an axial load N_{xx} and N_{yy} for an InfraCore skin with $N = 1$ and $N = 3$.

As the number of repetition increases, the values of the out-of-plane shear strains change. From figure 8.9, it can be seen that γ^0_{yz} increases for a load N_{yy} and γ^0_{yz} decreases for a load N_{xx} as the number of repetition increases. The shear strain γ^0_{xz} decreases for both loading cases for a higher N. It can be stated that the out-of-plane shear strains depend on the number of repetition, thus the out-of-plane shear strains also depend on the laminate lay-up.

The dependence of the number of repetition on the out-of-plane shear strain is shown in figure 8.10. Here, both out-of-plane shear strains have been determined for an inclination angle of 2° for both loading cases. It can be seen that all four graphs converge to a certain value. It can be concluded that as the homogeneity of the InfraCore skin increases, the out-of-plane shear strain does not change any more.

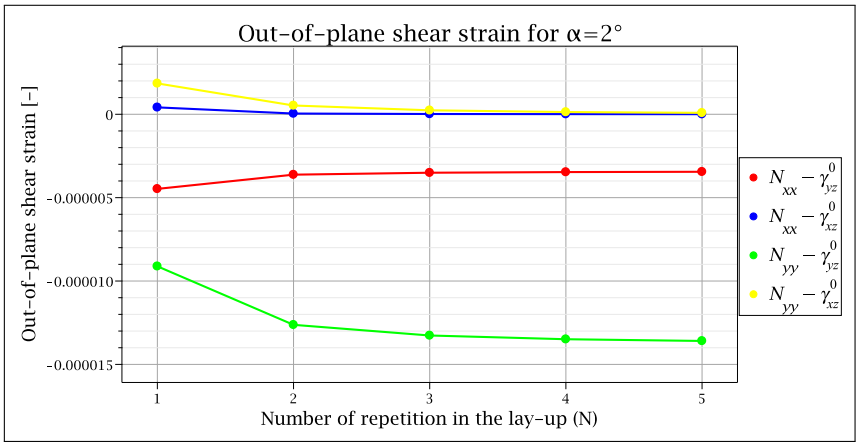

Figure 8.10: Out-of-plane shear strains as a function of the number of repetition (N).

8.3. Lay-up differences in InfraCore due to the inclination

The inclination in the plies in the skin of an InfraCore panel causes changes in the lay-up along the y-axis. Correspondingly, the equivalent stiffnesses of the InfraCore skin change along the y-axis. For InfraCore skins, it is assumed that an inclination of $\alpha = 2°$ is present and that the ply thickness is equal to 0.0009 m. This results in the following ply width:

$$y_{\text{ply}} = \frac{t}{\sin\alpha} = \frac{0.0009}{\sin(2)} = 0.0258 \text{ m} \tag{8.5}$$

Figure 8.11 shows a cross section of a twelve-ply InfraCore skin (N=3). When N=1, only one third of the laminate in z-direction is present.

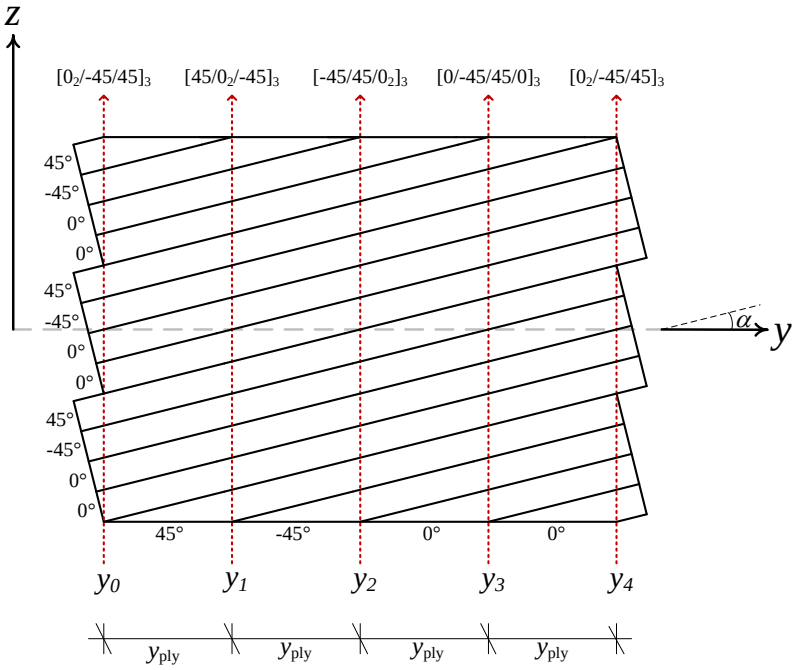

Figure 8.11: Cross section of a twelve-ply InfraCore skin.

Due to the repetition in the lay-up of InfraCore, only four different total lay-ups are possible. Therefore, the equivalent stiffness plots only need to be plotted for $y_0 < y < y_4$. For y-coordinates larger than y_4, the same equivalent stiffness plots will be obtained. The dependence on the y-coordinate is plotted for N=1 in figure 8.12.

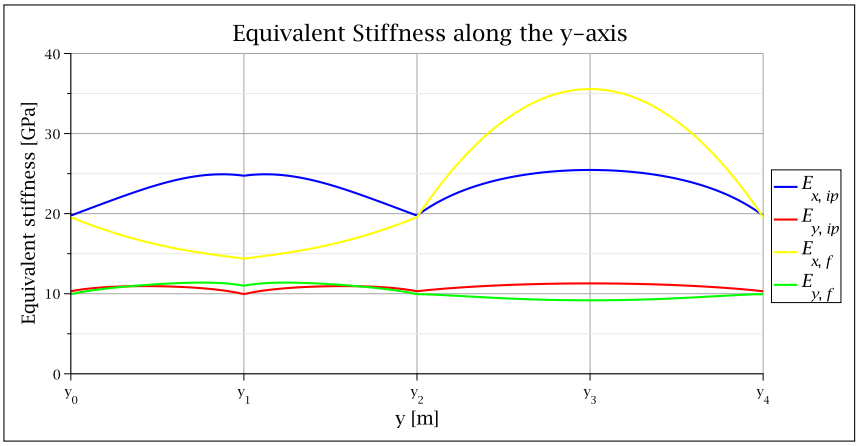

Figure 8.12: Equivalent stiffnesses as a function of the y-coordinate for an InfraCore skin with N=1.

It can be seen that the equivalent stiffnesses in y-direction do not differ much along the y-axis. In x-direction, $E_{x,\mathrm{ip}}$ and $E_{x,\mathrm{f}}$ do change significantly due to the differences in lay-up. The flexural equivalent stiffness in x-direction has the highest value at y_3, since the stiffest 0°-plies are located on the outside of the laminate at that location. Correspondingly, $E_{x,\mathrm{f}}$ is the lowest at y_1, due to the fact that the stiffest 0°-plies are at the center of the laminate.

Next, the equivalent stiffnesses can be plotted for an InfraCore skin with N=3. This has been done in figure 8.13, where it can be seen that the in-plane equivalent stiffnesses are closer to the flexural equivalent stiffnesses compared to the results for N=1. This confirms the results presented in section 8.1, where it was shown that as

the number of repetition N increases, the in-plane equivalent stiffnesses will approach the values of the flexural equivalent stiffnesses due to the more homogeneous lay-up when N increases.

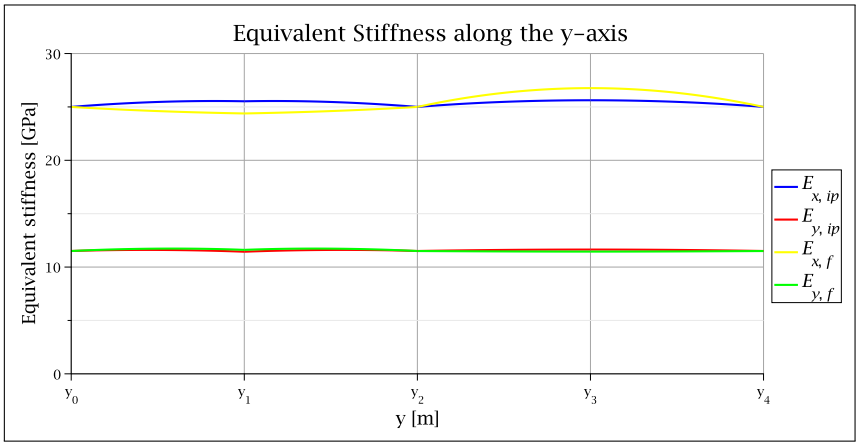

Figure 8.13: Equivalent stiffnesses as a function of the y-coordinate for an InfraCore skin with N=3.

It should be mentioned that in practice, an InfraCore skin is not a plate with a constant total thickness. In reality, the plies have a sudden termination rather than the gradual tapering assumed here, as can be seen from figure 8.11. The results presented in this section do assume a plate with a constant total thickness, so the results should be handled with care. The simplifications made in the modified CLT with respect to InfraCore are dealt with in section 4.4.3.

8.3.1. Comparison with the non-inclined result

The non-inclined equivalent stiffnesses of an InfraCore skin are shown in figure 8.14 together with equivalent stiffnesses when a ply inclination of 2° is present. The non-inclined results for $y_{i-1} < y < y_i$ are determined by evaluating the equivalent stiffnesses at y_{i-1} for $\alpha = 0°$ and are shown with a dashed line. Since the equivalent stiffnesses in x-direction do not depend on the inclination angle, the non-inclined result between y_{i-1} and y_i is exactly equal to the inclined result at $y = y_{i-1}$. The reduction in equivalent stiffness in y-direction of an InfraCore skin is very limited, as was shown in section 8.1. Therefore, hardly any differences can be distinguished between the inclined and non-inclined $E_{y,\text{ip}}$ and $E_{y,\text{ip}}$ in figure 8.14.

Furthermore, it can be stated that the equivalent stiffnesses for $\alpha = 2°$ are closer to the non-inclined equivalent stiffnesses as the homogeneity of the InfraCore skin increases. In figure 8.14b, hardly any differences can be observed between the inclined and non-inclined results for the equivalent stiffnesses in y-direction, which is in accordance with the results presented in section 8.1 where it was shown the in-plane and flexural equivalent stiffnesses are closer to each other as the number of repetition increases.

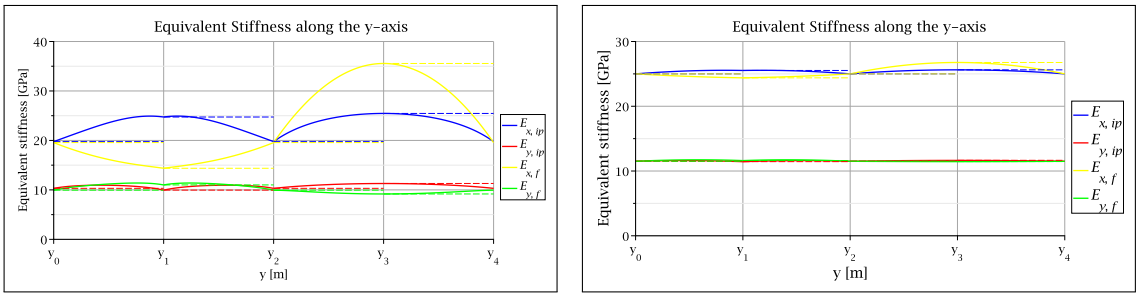

(a) $N = 1$. (b) $N = 3$.

Figure 8.14: Non-inclined equivalent stiffnesses as a function of the y-coordinate for both a four- and twelve-ply InfraCore skin.

9

Conclusions and recommendations

The Classical Laminate Theory (CLT) describes the elastic behaviour of laminates. The properties of individual plies within a laminate are stacked in order to create a stiffness matrix for the complete laminate. Certain types of Fibre Reinforced Polymer (FRP) structures could include laminates where the plies are under an inclination. These inclined plies occur for example in the skin of InfraCore panels, which is a special type of sandwich panel where the skins are connected with webs. The current CLT does not account for the extra rotation in the plies of such a laminate. It is therefore unknown to what extend the extra rotation affects the behaviour of laminates, which results in the following research question:

In what way does an inclination in the plies of a laminate affect the elastic behaviour of that laminate?

The CLT has been modified in order to take the inclination in the plies into account. This modified CLT is used to answer the main research question.

9.1. Conclusions

In order to obtain the modified CLT, the regular CLT is revised and adjusted where necessary. First of all, the regular CLT makes use of plane stress conditions in the plies. The laminate constitutive equations are used to derive the CLT, meaning the plane stress conditions are also applicable to the complete laminate. Due to the plane stress conditions, only in-plane stresses need to be taken into account. This results in a reduction of the stiffness matrix of a transversely isotropic material applicable to a ply with fibres all oriented in the same direction on mesoscale. A 6×6-matrix that relates all six independent strain components to the six independent stress components is reduced to a 3×3-matrix that only relates the in-plane strains to the in-plane stresses. When an inclination is added in the plies, it can no longer be stated that the out-of-plane stress components in the plies are equal to zero, meaning plane stress conditions are no longer applicable. This means no reduction of the stiffness matrix is possible for the modified CLT.

The stiffness matrix of an individual ply is translated from the local coordinate system of that ply to the global coordinate system of the complete laminate. In the regular CLT, this is done using transformation equations that depend on the fibre orientation in a ply. The extra rotation that occurs due to the inclination of the plies is implemented in the transformation equations to obtain the correct global stiffness matrix of each ply in the modified CLT. The transformation equations are written in matrix shape, and must match in dimensions with the stiffness matrix, leading to a 6×6 transformation matrix for the modified CLT.

Furthermore, Kirchhoff assumptions are applicable to both the individual plies and the complete laminate when no inclination is present, meaning straight lines perpendicular to the mid-surface remain both straight and perpendicular to the mid-surface after deformation. The inclination in the plies could cause an out-of-plane shear deformation due to the difference in stiffness parallel and perpendicular to the fibre direction in a ply. Out-of-plane shear deformations indicate that lines perpendicular to the mid-surface do not remain perpendicular to the mid-surface after deformation. This means the Kirchhoff assumptions are not applicable to the laminate when a ply inclination is present. In the derivation of the laminate constitutive equations for the modified CLT, it is however assumed that straight lines of a laminate remain straight after deformation. This remains a valid assumption, since the thickness of a laminate is small compared to the other laminate dimensions.

The modified CLT has been verified using Finite Element (FE) analyses. Several laminates have been modelled and axial loads are applied. The resulting strains and curvatures have been evaluated and compared with the results from the modified CLT. The results of individual plies with inclined properties matched perfectly. For a non-symmetric and non-balanced four-ply laminate, the average difference was 2%. These differences were assigned to the limitations of the FE model, but were still small enough to conclude the modified CLT has a correct implementation of the inclination in the plies.

The main research question can be answered using the modified CLT. Due to the inclination in the plies, a reduction in equivalent stiffness along the inclination direction is observed for a laminate. For every ply within a laminate, the out-of-plane elastic modulus is the same and it is lower compared to the elastic modulus of the ply measured along the fibre direction. As the inclination angle increases, this lower stiffness becomes more dominant in the determination of the equivalent stiffness of a laminate. When the inclination angle reaches its maximum of 90°, all the plies are placed vertically next to each other. This leads to an equivalent stiffness of the laminate equal to the out-of-plane elastic modulus perpendicular of the ply.

An important limitation of the modified CLT is that the result is only applicable at one location of the laminate. Due to the inclination, a ply starts at the bottom in a laminate, but ends at the top of a laminate. This causes lay-up differences within the laminate, since it is assumed the total thickness of a laminate does not change. Due to the lay-up differences, the equivalent stiffnesses of the laminate will also differ along the inclination direction. The equivalent stiffnesses strongly depend on the lay-up of a laminate. Distinction is made between in-plane and flexural equivalent stiffnesses. The in-plane equivalent stiffnesses are applicable when a laminate is loaded by normal forces in its plane. When the lay-up is symmetric, the in-plane equivalent stiffnesses will be the highest due to the absence of coupling effects, meaning no out-of-plane deformations can occur when the laminate is loaded in its plane. Flexural equivalent stiffnesses are used when a laminate is predominantly loaded in bending. It can be concluded that the flexural equivalent stiffness is the highest when the plies with the stiffest fibre direction are located at the outside of the laminate.

Finally, the main research question has been answered for InfraCore panels. These specific type of sandwich panels contain inclined plies in the top and bottom skin. The exact lay-up may differ per design, but usually a repetition of four plies is observed, namely two 0°-plies, a -45°-ply and a +45°-ply. As the repetition in lay-up increases, a more homogeneous laminate is created. When the four plies are three times repeated, creating a twelve-ply laminate, the InfraCore skin has become homogeneous enough to assume the in-plane equivalent stiffnesses are equal to the flexural equivalent stiffnesses. As the inclination angle increases, the equivalent stiffness in the inclination direction decreases for an InfraCore skin. A reduction in stiffness of 0.15% is observed for a twelve-ply InfraCore skin with a ply inclination of 2°. Due to the homogeneity in the lay-up for the twelve-ply InfraCore skin, the differences in equivalent stiffness along the inclination direction are very limited.

9.2. Recommendations for future research

Given the results presented in this report, several future research topics can be suggested:

- The modified CLT only deals with the stiffness behaviour of laminates with inclined plies. Failure is not dealt with in the modified CLT. Several failure modes are possible in FRP structures, delamination being a main problem in laminates. A mode 1 delamination indicates a split between plies, causing an opening in the direction perpendicular to the plane of the ply. The modified CLT does take the relevant stress in this direction into account, where the regular CLT does not. This means the modified CLT could be used to determine the sensitivity of an inclined laminate to mode 1 delamination due to in-plane loading.

- Structural linear static FE analyses have been performed on several laminates to verify the modified CLT. The behaviour of a laminate with inclined plies could have out-of-plane shear deformations. These type of deformations cannot occur in axially loaded laminates where no ply inclination is present. The value of the out-of-plane shear deformation could be checked with experiments. A single-ply laminate with the fibre direction under an angle with respect to the plane of the laminate could be used. In the test, an axial load should be applied in the inclination direction. This will lead to an out-of-plane shear deformation that could be compared with the modified CLT result.

- The verification of the modified CLT could be further elaborated. For example, the influence of the limitations of the FE model could be reduced when a larger plate size is assumed, but the thickness is kept

the same. This will mean the FE model better approximates the assumptions made in the derivation of the modified CLT.

- Several FE packages include the possibility to assign an ABD-matrix obtained with the regular CLT to plate finite elements. The ABD-matrix obtained with the modified CLT could also be implemented in finite elements. Plate elements that take shear deformations into account should be used in order to be able to account for the out-of-plane shear strain. This means Mindlin-Reissner plate theory must be applicable to the finite elements.
- The interlaminar shear strength of a laminate with inclined plies will depend on the inclination angle. For a small angle, the shear crack will occur in the matrix material, meaning fibres within a ply will not break. As the inclination angle increases, the possibility of a crack passing through the fibres will increase. The failure due to interlaminar shear depends on the in-plane shear strength and depends on the inclination angle. The modified CLT can be used to determine the relevant shear stress, since it takes the inclination angle into account.
- In this report, it has been assumed that the inclination angle is the same for all the plies within a laminate. However, this input variable can also be varied per ply. For example, an InfraCore skin with inclined plies is finished with a 0°-ply on top of the skin. This top ply does not have an inclination and is not taken into account in this research. The top ply can also be implemented in the modified CLT when the inclination angle is defined per individual ply and not constant for the complete laminate.
- The influence of the inclination has been checked for the InfraCore skin. The whole InfraCore panel has not been considered. It can be checked how the ply inclination affects the elastic behaviour of the complete InfraCore panel, where the webs should also be taken into account.

Bibliography

[1] Honeycombs and honeycomb materials information. Website, 2018. URL https://www.globalspec.com/learnmore/materials_chemicals_adhesives/composites_textiles_reinforcements/honeycombs_honeycomb_materials.

[2] Halm Altenbach, Johannes Altenbach, and Wolfgang Kissing. *Mechanics of Composite Structural Elements*. Springer, 2018.

[3] J. Blaauwendraad. Plate analysis, theory and application. volume 1, theory. Technical report, Faculty of Civil Engineering and Geosciences, 2006.

[4] Wouter de Corte, Arne Jansseune, Wim van Paepegem, and Jan Peeters. Structural behaviour and robustness assessment of an infracore inside bridge deck specimen subjected to static and dynamic local loading. *Proceedings of the 21st International Conference on Composite Materials*, 2017.

[5] Wouter de Corte, Arne Jansseune, Wim van Paepegem, and Jan Peeters. Elastic properties and failure behavior of tiled laminate composites. *Key Engineering Materials*, 774:564–569, August 2018. ISSN 1662-9795.

[6] *Diana User's Manual Element Library*. DIANA FEA BV.

[7] Herbert Goldstein. *Classical Mechanics*. Addison Wesley, 1980.

[8] C. Hartsuijker and J.W. Welleman. Spanningsleer en bezwijkmodellen. Technical report, TU Delft, January 2018.

[9] Zheng-Ming Huang and Ye-Xin Zhou. *Strength of Fibrous Composites*. Springer, 2011.

[10] Laszlo P. Kollar and Georges S. Springer. *Mechanics of Composite Structures*. Cambridge University Press, 2003.

[11] Allan Malano, Thiru Aravinthan, Amir Fam, and Brahim Benmokrane. State-of-the-art review on frp sandwich systems for lightweight civil infrastructrure. *Journal of Composites for Construction*, 21(1), 2017.

[12] P.K. Mallick. *Fiber-Reinforced Composites*. Taylor & Francis Inc, 2007.

[13] Maplesoft. *Statistics PolynomialFit*. Maplesoft.

[14] A.T. Nettles. Basic mechanics of laminated composite plates. Nasa reference publication, NASA, 1994.

[15] R.P.L. Nijssen. *Composieten Basiskennis*. Hogeschool Inholland, 2013.

[16] J.N. Reddy. *Mechanics of Laminated Composite Plates and Shells: Theory and Analysis*. CRC Press, 2004.

[17] David Roylance. Laminated composite plates. Technical report, Massachusetts Institute of Technology, 2000.

[18] David Roylance. Transformation of stresses and strains. Technical report, Massechusetts Institute of Technology, 2001.

[19] SAND.CORe. *Best Practice Guide for Sandwich Structures in Marine Applications*. Sandcore, 2007.

[20] P.D. Soden, M.J. Hinton, and A.S. Kaddour. Lamina properties, lay-up configurations and loading conditions for a range of fibre-reinforced composite laminates. *Composites Science and Technology*, 1998.

[21] *Data sheet Strenx 1100*. Strenx, 2017.

List of Figures

List of Tables

A

Maple appendix

The modified Classical Laminate Theory (CLT) presented in this report is modelled using Maple. The great advantage of Maple compared to other programming languages is that Maple allows an analytic derivation of the results. This means the dependence on the inclination angle α of a laminate with inclined plies can be determined in an analytic fashion. The code used to obtain the ABD-matrix in the modified CLT is given on the following pages. The determination of the equivalent stiffnesses is also given, as well as an equivalent stiffness plot example.

```
> restart; with(linalg) : with(LinearAlgebra) : with(Statistics) : with(ArrayTools) : with(plots) :
      with(CurveFitting) : interface(rtablesize = 12) :
```

----------INPUT PLIES----------

Number of plies:

```
> n := 4 :
```

Input ply properties:

```
> E1 := 39·10^9 :
> E2 := 8.6·10^9 :
> nu12 := 0.28 :
> nu23 := 0.4 :
> G12 := 3.8·10^9 :
```

Input ply dimensions and orientation:

```
> ply_thickness := 0.0005 :
> theta[x] := vector([0, -Pi/4, 0, Pi/2]) :
> alpha := a·Pi/180 :
```

----------END INPUT PLIES----------

Ply properties needed as vector for loop input:

```
> E[1] := vector(n, E1) :
> E[2] := vector(n, E2) :
> nu[12] := vector(n, nu12) :
> nu[23] := vector(n, nu23) :
> G[12] := vector(n, G12) :
> t := vector(n, ply_thickness) :
```

Additional dimensional properties:

```
> t_tot := add(t[i], i = 1..n) :
> zcoor := Matrix([[0, CumulativeSum(t)]]) - Matrix(1, n + 1, t_tot/2) :
```

Loop to determine the global stiffness matrix per ply:

```
> for i from 1 to n do
  E1[i] := E[1][i]: E2[i] := E[2][i]: nu12[i] := nu[12][i]: nu23[i] := nu[23][i]:
      G12[i] := G[12][i]: theta[i] := theta[x][i]:

  #Stiffness matrix of a transversely isotropic material in the local coordinate system:
  Cbar[i] := inverse(Matrix([
  [1/E1[i], -nu12[i]/E1[i], -nu12[i]/E1[i], 0, 0, 0],
  [-nu12[i]/E1[i], 1/E2[i], -nu23[i]/E2[i], 0, 0, 0],
  [-nu12[i]/E1[i], -nu23[i]/E2[i], 1/E2[i], 0, 0, 0],
  [0, 0, 0, 2·(1 + nu23[i])/E2[i], 0, 0],
  [0, 0, 0, 0, 1/G12[i], 0],
  [0, 0, 0, 0, 0, 1/G12[i]]
  ])):

  #Transformation matrix:
  Tthetaalpha := Matrix([
  [cos(theta[i])^2, sin(theta[i])^2, 0, 0, 0, -2·cos(theta[i])·sin(theta[i])],
  [cos(alpha)^2·sin(theta[i])^2, cos(theta[i])^2·cos(alpha)^2, sin(alpha)^2, -2·cos(theta[i])
      ·sin(alpha)·cos(alpha), -2·cos(alpha)·sin(theta[i])·sin(alpha), 2·cos(alpha)^2
      ·sin(theta[i])·cos(theta[i])],
  [sin(theta[i])^2·sin(alpha)^2, cos(theta[i])^2·sin(alpha)^2, cos(alpha)^2, 2·cos(theta[i])·sin(alpha)
      ·cos(alpha), 2·cos(alpha)·sin(theta[i])·sin(alpha), 2·sin(theta[i])·sin(alpha)^2
      ·cos(theta[i])],
  [sin(theta[i])^2·sin(alpha)·cos(alpha), cos(theta[i])^2·sin(alpha)·cos(alpha), -cos(alpha)
      ·sin(alpha), cos(alpha)^2·cos(theta[i]) - sin(alpha)^2·cos(theta[i]), cos(alpha)^2
      ·sin(theta[i]) - sin(alpha)^2·sin(theta[i]), 2·cos(alpha)·sin(theta[i])·sin(alpha)
      ·cos(theta[i])],
  [cos(theta[i])·sin(alpha)·sin(theta[i]), -cos(theta[i])·sin(alpha)·sin(theta[i]), 0, -cos(alpha)
      ·sin(theta[i]), cos(alpha)·cos(theta[i]), cos(theta[i])^2·sin(alpha) - sin(theta[i])^2
      ·sin(alpha)],
  [cos(theta[i])·cos(alpha)·sin(theta[i]), -cos(theta[i])·cos(alpha)·sin(theta[i]), 0, sin(alpha)
      ·sin(theta[i]), -sin(alpha)·cos(theta[i]), cos(theta[i])^2·cos(alpha) - sin(theta[i])^2
      ·cos(alpha)]
  ]):
```

#Stiffness matrix in the global coordinate system:

$Cnobar[i] := Tthetaalpha \cdot Cbar[i] \cdot transpose(Tthetaalpha)$:

#A-, B- and D-matrix per ply:

$Ai[i] := Cnobar[i].(zcoor[1, i+1] - zcoor[1, i])$:

$Bi[i] := Cnobar[i].\left(zcoor[1, i+1]^2 - zcoor[1, i]^2\right) \cdot \frac{1}{2}$:

$Di[i] := Cnobar[i].\left(zcoor[1, i+1]^3 - zcoor[1, i]^3\right) \cdot \frac{1}{3}$:

end do:

Adding the A-, B- and D-matrices of each ply:

> $A := add(Ai[i], i = 1..n)$: $B := add(Bi[i], i = 1..n)$: $D\_ := add(Di[i], i = 1..n)$:

ABD-matrix:

> $M := Matrix([[A, B], [B, D\_]])$:

> $DetM := Determinant(simplify(M))$:

Relative equivalent stiffness plot:

In-plane equivalent stiffnesses:

> $E[ip, x] := \frac{DetM}{Minor(simplify(M), 1, 1) \cdot t\_tot}$: $E[ip, y] := \frac{DetM}{Minor(simplify(M), 2, 2) \cdot t\_tot}$:

Flexural equivalent stiffnesses:

> $E[f, x] := \frac{DetM \cdot 12}{Minor(simplify(M), 7, 7) \cdot t\_tot^3}$: $E[f, y] := \frac{DetM \cdot 12}{Minor(simplify(M), 8, 8) \cdot t\_tot^3}$:

Equivalent stiffnesses for alpha=0:

> $a := 0$:

> $E[ip, x0] := evalf(E[ip, x])$: $E[f, x0] := evalf(E[f, x])$:

> $E[ip, y0] := evalf(E[ip, y])$: $E[f, y0] := evalf(E[f, y])$:

Plot of the relative equivalent stiffness with respect to E1:

> $a :=$'a': alpha :='alpha':

> $plot\left(\left[\frac{E[ip, x]}{E1[1]}, \frac{E[ip, y]}{E1[1]}, \frac{E[f, x]}{E1[1]}, \frac{E[f, y]}{E1[1]}\right], a = 0..90, y = 0.0..1.1, gridlines, axesfont = ["Times", "Roman", 15], labelfont = ["Times", "Roman", 20], legend = [E_{x, ip}, E_{y, ip}, E_{x, f}, E_{y, f}], legendstyle = [font = ["Times", 20], location = right], color = ['blue','red','yellow', 'green'], thickness = 3, labels = ["α [°]","Relative equivalent stiffness [-]"], labeldirections = ["horizontal", "vertical"], size = [1200, 600], title = "Equivalent stiffness of a [0/-45/0/90] laminate", titlefont = ["Times", "Roman", 25]\right)$:

>